Oxidative Medicine and Cellular Longevity

The Role of Epigenetic Modifications in Oxidative Stress

Lead Guest Editor: Qianqian Wang
Guest Editors: Ying Li and Xing-Xing Fan

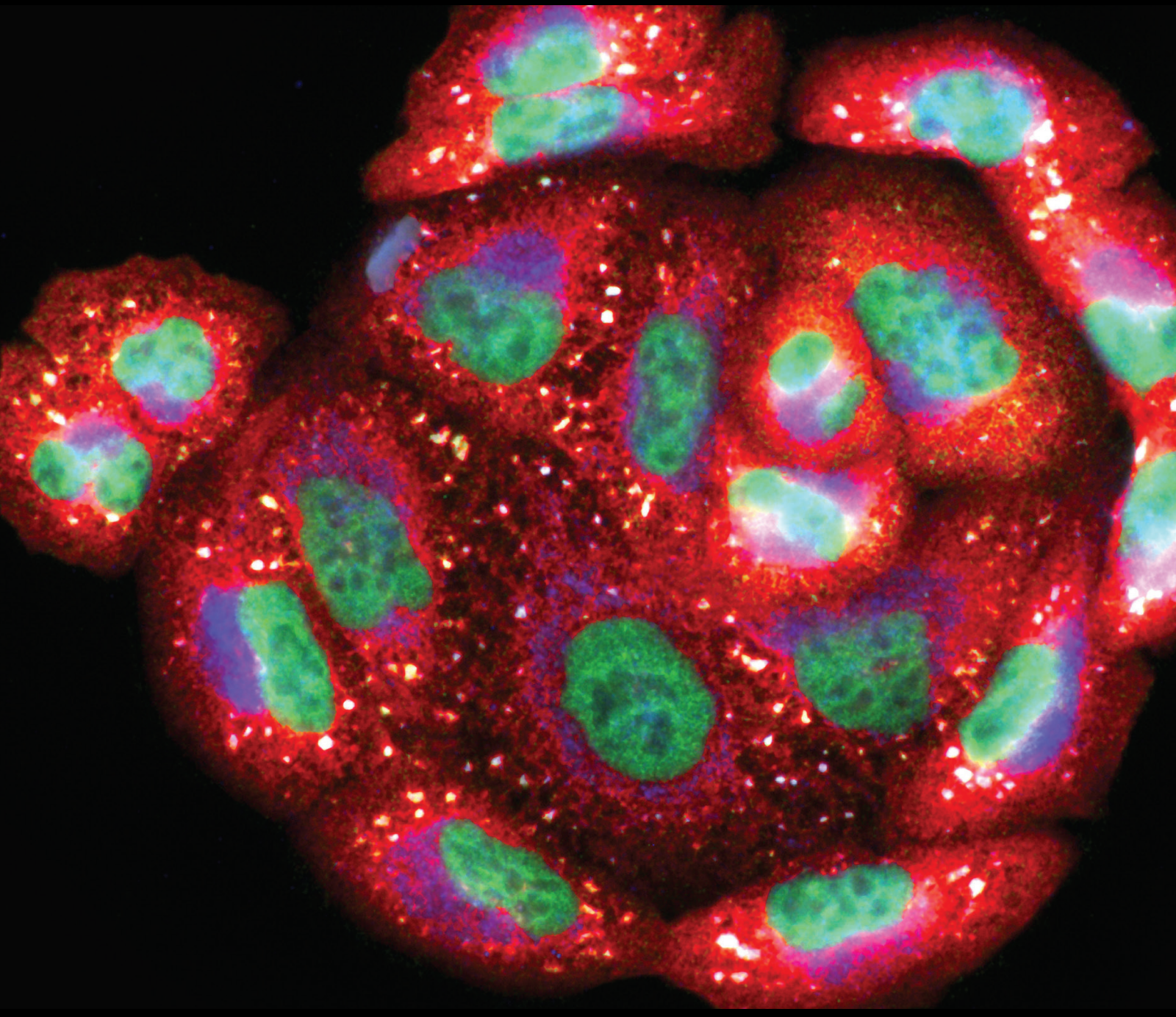

The Role of Epigenetic Modifications in Oxidative Stress

Oxidative Medicine and Cellular Longevity

The Role of Epigenetic Modifications in Oxidative Stress

Lead Guest Editor: Qianqian Wang
Guest Editors: Ying Li and Xing-Xing Fan

Contents

Hindawi
Oxidative Medicine and Cellular Longevity
Volume 2022, Article ID 3243647, 19 pages
https://doi.org/10.1155/2022/3243647

Research Article

High Glucose Promotes Pancreatic Ductal Adenocarcinoma Gemcitabine Resistance and Invasion through Modulating ROS/MMP-3 Signaling Pathway

Junyuan Deng,[1] Yujie Guo,[1] Xiaomu Hu,[2] Jiali Du,[1] Jichun Gu,[1] Lei Kong,[1] Baian Tao,[1] Deliang Fu,[1] Tianlei Ying,[3] and Ji Li[1]

[1]*Department of Pancreatic Surgery, Pancreatic Disease Institute, Huashan Hospital, Fudan University, 12 Wulumuqi Middle Road, Shanghai 200040, China*
[2]*Department of Pathology, Huashan Hospital, Fudan University, Shanghai 200040, China*
[3]*MOE/NHC/CAMS Key Laboratory of Medical Molecular Virology, School of Basic Medical Sciences, Fudan University, Shanghai 200032, China*

Correspondence should be addressed to Deliang Fu; surgeonfu@163.com, Tianlei Ying; tlying@fudan.edu.cn, and Ji Li; liji@huashan.org.cn

Received 21 March 2022; Revised 2 May 2022; Accepted 1 July 2022; Published 29 September 2022

Academic Editor: Qianqian Wang

Pancreatic ductal adenocarcinoma (PDA) is often concomitant with diabetes mellitus, which mainly manifests as an increased blood glucose level. Previous studies revealed that diabetic status reduced the survival and blunted gemcitabine sensitivity in PDA patients. This study is aimed at analyzing the mechanism of elevated gemcitabine resistance and cancer invasion ability under high glucose environment. We selected 129 patients with 22 surgical resected samples from 2015 to 2021, who underwent pancreatic surgery in Huashan Hospital. The gene expression and clinical data of PDA were obtained from The Cancer Genome Atlas (TCGA) website and were analyzed by R software. Cell viability assays and flow cytometry were applied to detect gemcitabine sensitivity and apoptosis levels in pancreatic cancer cells. Wound healing and Transwell tests were used to analyze the invasion and metastasis of cancer cells. Streptozotocin (STZ) was used to establish a hyperglycemic mouse model for the *in vivo* study. In this study, diabetic PDA gemcitabine users showed reduced survival compared to euglycemic PDA gemcitabine users. Clinical samples and laboratory studies revealed that MMP-3 expression was associated with glucose concentration and diabetic status. Elevated MMP-3 expression was positively related to cancer invasion and gemcitabine resistance in PDA cells and gemcitabine resistant PDA cells. Blocking MMP-3 expression inhibited gemcitabine resistance and cancer progression in cellular and animal models. MMP-3 was closely related to the expression of RRM1, a gemcitabine metabolism-related gene. Reactive oxygen species (ROS) level increased under higher glucose concentrations and was mediated by NOX4. ROS determined the MMP-3 expression in pancreatic cancer cells. Inhibiting NOX4 expression effectively suppressed MMP-3 expression, gemcitabine resistance, and cancer invasion. In conclusion, a high glucose environment induces gemcitabine resistance and cancer invasion via ROS/MMP-3 signaling pathway. MMP-3 can be a potential novel target for suppressing gemcitabine resistance and invasion in PDA.

1. Introduction

Pancreatic ductal adenocarcinoma (PDA), often referred to as pancreatic cancer, is a devastating disease that ranks the fourth leading cause of cancer-related death and is projected to be the second leading cause of death by 2030 in the United States [1]. Currently, the 5-year survival of PDA patients is lower than 10%, and over 80% of cases were unresectable when diagnosed. Currently, chemotherapy is a crucial method for prolonging PDA patients' survival. Gemcitabine (GEM), a nucleoside analog of deoxycytidine, inhibits pancreatic cancer through interfering DNA

synthesis. After being treated with gemcitabine, increased cell apoptosis and decreased cell viability were observed in pancreatic cancer cells. Since its approval by the FDA in 1996, gemcitabine has been extensively used to treat various solid tumors and currently in certain lymphomas [2, 3]. At present, as no alternative therapeutic options exist, gemcitabine is vital for neoadjuvant, adjuvant, and palliative therapy in PDA. However, the problem is that the relatively low gemcitabine response rate (less than <30%) is consistently disturbing PDA patients [4].As a chronic disease, diabetes mellitus (DM) is often concomitant with PDA. Epidemiological evidence revealed that over 50% of PDA patients had DM, and over 75% of PDA cases reported were hyperglycemia. Unlike typical type 2 diabetes mellitus (T2DM), diabetes in PDA patients manifests as hyperglycemia with normal or relatively lower insulin levels caused by the removal of normal pancreatic tissue. Aside from this, diabetic patients showed a significant reduction in overall survival compared with euglycemic patients, especially those who received gemcitabine-based chemotherapy. Currently, the mechanism of how high glucose initiates tumorigenesis and PDA development is well studied. However, unfortunately, a systematic understanding of how diabetes interferes with gemcitabine sensitivity in pancreatic cancer is still not clear at present.

This study is aimed at clarifying the potential mechanism of how high glucose induces gemcitabine resistance and metastasis in pancreatic cancer. And we also delivered a novel target for suppressing PDA progression and chemoresistance induced by hyperglycemia.

2. Materials and Methods

2.1. Public Database Data Download. The Cancer Genome Atlas (TCGA), sponsored by National Cancer Institute, is a publicly available database containing multidimensional cancer genomics and clinical data sets. We downloaded pancreatic adenocarcinoma (PAAD) clinical information and RNA sequence data from the Broad Firehose Website (http://gdac.broadinstitute.org). In the TCGA-PAAD cohort, patients that had a history of diabetes were regarded as having pancreatic cancer with diabetes (the diabetic cohort). In contrast, pancreatic cancer individuals without a history of diabetes were considered as PAAD without diabetes (the normal cohort). Cases with no clear diabetes history were excluded from our study. The RNA sequence data of GSE50931 was downloaded from the GEO (Gene Expression Omnibus) database to evaluate the downstream effectors of MMP-3 involved in PDA gemcitabine resistance.

2.2. Identification of Differentially Expressed Genes (DEGs). The DEGs analysis was performed on two categories of samples according to the diabetes history (the normal cohort and the diabetic cohort) or the MMP-3 expression (the high MMMP-3 expression cohort and the low MMP-3 expression cohort). Limma R package was used to identify the differentially expressed genes between the normal and diabetic cohorts, which were defined as those with a false discovery rate <0.05 and a $|\text{fold change}| > 1$. The heat map analysis of the mRNA expression pattern was performed using R software with the "edgeR" package.

2.3. Univariate Cox Analysis and LASSO Regression Analysis. We applied survival-related univariate Cox analysis and LASSO regression analysis to determine the critical factor in PDA patients' survival. After eliminating the patient data with no survival time, the DEGs with positive prognosis in the TCGA cohort were determined by univariate Cox analysis. After screening the DEGs with survival univariate Cox analysis, LASSO regression analysis was performed to examine the key factors furtherly. The algorithm of LASSO regression was conducted with the Glmnet R package to select and shrink variables by excluding the variables with a regression coefficient equal to 0. Then, an interpretable model was established according to the nonzero regression coefficients in the TCGA cohort, and the optimum λ was selected in 10-fold cross-validation. We calculated the risk scores of each DEGs and its corresponding regression coefficient based on risk scores in the TCGA cohort.

2.4. ROC Model Construction. A time-dependent ROC analysis (1 year, 3 years, and 5 years) was conducted to measure the MMP-3 survival prediction effect using the survival and time ROC R package to assess the prediction accuracy. The sequence data and clinical information were obtained from the TCGA database. Areas under the curve (AUC) were used to measure the survival predicting the efficacy of the prognostic model of MMP-3.

2.5. Functional Enrichment Analysis. Functional enrichment analysis, including Gene Set Enrichment Analysis (GSEA), Gene Ontology (GO), and Kyoto Encyclopedia of Genes and Genomes (KEGG) analyses, were used to identify gene sets and pathways correlated with diabetic cohort and high MMP-3 expression cohort. The GSEA software was downloaded from the Broad Institute Website (http://software.broadinstitute.org/gsea/index.jsp), and GSEA analysis was performed according to the manufacturer's instructions. The GO and KEGG analyses based on DEGs were conducted by "clusterProfiler" in R software.

2.6. Case Selection and Diabetes Evaluation. The study protocol was authorized by the Ethics Committee of Huashan Hospital, Fudan University. Officially written informed consent was acquired from all patients involved in this study. We strictly selected 129 patients who underwent surgical resection from October 2015 to December 2021, in a high-volume pancreatic center, and all of them had a clear diabetes history or nondiabetic diagnosis. The assessment of diabetes was based on American Diabetes Association (ADA) guidelines and clinical records. The major criteria of DM diagnosis were preoperative fasting plasma glucose ≥12.6 mg/dL, random plasma glucose ≥200 mg/dL, or hemoglobin A1c (HbA1c) ≥6.5%. Patients who had a DM history were also concluded in the DM group [5]. Pancreatic surgery was performed based on malignant signs and patients' decisions. Two independent pathologists made pathological stage evaluations from Huashan Hospital, Fudan University.

2.7. Cell Culture. The pancreatic cancer cell lines, BxPc-3, PANC-1, PANC-2, HPDE6-C7, and MiaPaCa-2, were obtained from the National Collection of Authenticated Cell Culture Bank (Shanghai, China). The gemcitabine-resistant BxPc-3 cell line (BxPc-3(GemR)) and its normal control (BxPc-3(Normal)) were obtained from YBR Bioscience, Shanghai, China. All cancer cells were cultured in a DMEM medium containing 10% fetal bovine serum with 1% 100 U/mL penicillin/streptomycin mixture (Beyotime, Shanghai, China). All pancreatic cancer cells were cultured at 37°C with 5% CO_2. The glucose concentration was 25 mM for normal cell culture, and to evaluate the influence of different glucose environments, two relatively lower glucose concentration levels (5 mM and 15 mM) were created. In this study, 5 mM, 15 mM, and 25 mM glucose concentration group was defined as the Low Glucose Group (LG), Medium Glucose Group (MG), and High Glucose Group (HG), respectively.

2.8. Cell Viability Assay. The cells in each group (1×10^4 cells/well) were cultured in 96-well plates with different agents for different times (24 h and 48 h). At each time point, 10 μL of Cell Counting Kit-8 (CCK-8) solution (Beyotime, Shanghai, China) was supplemented into each well and incubated for 1.5 h. Next, the absorbance of each well at 450 nm (OD450 value) was measured by a microplate reader (BioRad Laboratories, Inc., Hercules, CA, United States). The proliferative rate (PR) was measured by: PR = OD450 value (treated group)/OD450 value (normal control group). To adjust the influence of proliferative advantages by high glucose concentration, the normal control groups of HG, MG, and LG were cultured in different glucose levels DMEM.

2.9. Western Blotting Assay. After 3 times of PBS washing, all cell lysates were extracted with RIPA lysis buffer (Beyotime, Shanghai, China). 15 μL of each sample was used for SDS-PAGE electrophoresis and transferred to PVDF membranes (Millipore, Billerica, MA, USA). The membranes were blocked in 5% nonfat milk for 1 h and incubated with primary antibody at 4°C overnight. After washing the samples with PBST (fifteen min/time) three times, the membranes were incubated with a second antibody at room temperature for 1.5 h. After washing three times with PBST, they were visualized with enhanced chemiluminescence (Tanon 3500R, China).

2.10. ROS Measurement Assay. ROS assay was purchased from Beyotime, Shanghai, China (S0033S). Intracellular ROS was detected employing an oxidation-sensitive fluorescent probe (DCFH-DA). After being treated with different glucose concentrations DMEM for 24 h, cancer cells were washed three times in phosphate-buffered saline (PBS). They were then incubated with 10 μmol/L DCFH-DA at 37°C for 20 min according to the manufacturer's instructions. DCFH-DA was deacetylated intracellularly by nonspecific esterase, which ROS further oxidized to the fluorescent compound 2,7-dichlorofluorescein (DCF). DCF fluorescence was detected by a microplate reader (BioRad Laboratories, Inc., Hercules, CA, United States).

2.11. Transient Transfection Assay. Transient transfection was applied to construct the MMP-3 overexpression cell model and MMP-3 silencing pancreatic cell model. MMP-3 overexpression cDNA (MMP3-GFP-Puro) vector and empty vector cDNA (GAPDH-NC) were designed and synthesized by Mohan (Shanghai, China). The MMP3 siRNAs used for inhibiting MMP-3 expression were designed and synthesized by Ribobio (Guangzhou, China). Lipofectamine™2000 (Invitrogen, California, U.S.A.) was used in the transient transfection process of cDNA and the siRNAs according to the manufacturer's protocol. After transfecting for 16 h, the medium was replaced with 10% FBS High Glucose DMEM, and the transfected cell lines were used for further research.

2.12. Apoptosis Detection (Flow Cytometry Assay). Cell apoptosis and necrosis were determined by Annexin V-FITC/PI double staining and quantified by flow cytometry. Briefly, 1×10^6 cells were harvested and resuspended in 500 μL binding buffer containing 10 μL Annexin V-FITC and 5 μL PI from the Annexin V-FITC/PI Apoptosis Detection Kit (Yeasen, Shanghai, China) for 30 min at room temperature in the dark environment. Then the samples were analyzed using FACSCalibur (BD Biosciences). The living cells were disseminated in Annexin V-FITC−/PI− area (lower left quadrant), early apoptotic cells in Annexin V-FITC+/PI− area (upper left quadrant), late-stage apoptotic cells in Annexin V-FITC+/PI+ area (upper right quadrant), and necrotic cells as Annexin V-FITC−/PI+ (upper left quadrant). Annexin V-FITC/PI Apoptosis Detection Kit was purchased from the Yeasen Corporation, Shanghai, China.

2.13. Cell Migration and Invasion Assays. Wound healing and Transwell assays were performed to assess the cell migration and invasion in PDA cells. For wound healing assay, 6-well plates were seeded with 5×10^5 cells and incubated in a humidified atmosphere of 37°C. Until 100% confluence was reached, the layer of cells was scratched with a 100 μL pipette tip (sigma) and washed by PBS three times. Cells were then incubated in fresh serum-free DMEM for an additional 12 hours. The wound closure extent was measured by microscopy. For the Transwell invasion assay, the upper chamber inserts were precoated with 50 μL Matrigel (1 : 4 ratio in high glucose DMEM without FBS) and 3×10^3 cells in 100 μL of serum-free medium were seeded into the upper chamber of each well. Each lower chamber was filled with 600 μL DMEM supplemented with 10% FBS. After 24 h, pancreatic cancer cells were fixed, stained with 500 μL, 4% paraformaldehyde, and 1% crystal violet (Beyotime, Shanghai), respectively. Next, ImageJ software was used to evaluate the number of invasion cells of the corresponding group, and the average of those fields was utilized as a result.

2.14. Immunohistochemistry (IHC) Assay and Measurement. Written informed consent of the sample usage was acquired from all patients involved in this study. 22 surgical resected pancreatic cancer samples subjected to antigen were retrieved through incubation in EDTA antigen retrieval

buffer (pH 9.0) for 15 min at 100°C. Endogenous peroxidase was blocked by incubation with 3% H_2O_2 for 25 min, followed by washes in PBS solution for 5 minutes/3 times. Incubation with 3% bovine serum albumin (BSA) was performed to block other antigens. Incubation with the primary MMP-3 antibody (SantaCruz sc21732 (1 : 100)) was performed overnight at 4°C. After washing three times, the samples were incubated with a secondary antibody labeled with HRP (GB23303, 1 : 200, Servicebio) for 50 min at room temperature, followed by wash and incubation with the diaminobenzidine substrate (DAKO) for a period controlled under the microscope. Counterstaining was performed with diluted Harris hematoxylin (KIGENE, China). Microscopic results were scanned with the CaseViewer system.

The IHC result was determined by two independent pathologists from Huashan Hospital, Fudan University, Shanghai, China. The pathological section observed a brown-stained area or region for MMP-3 positive granules. Each slice was observed via the CaseViewer system, and the number of positive cells was observed. The MMP-3 expression was graded as negative, weakly positive, medium positive, and strong positive. The point of each grade was: negative (0): lower than 10%; weak positive (1): 11%-40%; medium positive (2): 41%–70%; strong positive (3): higher than 70%.

2.15. In Vivo Study Assays. 10 nude mice (6-8 weeks, male) were randomly divided into 2 groups: 5 in the single gemcitabine (GEM) group and 5 in cordycepin plus gemcitabine (CG) group. The procedure of *in vivo* study is shown in Figure 1(d). In the first, GEM and CG groups were injected with STZ 175 mg/kg after fasting for 12 hours. All mice were injected with $5^{*}10^{6}$ BxPC-3 pancreatic cancer cells subcutaneously a week later. The fast blood glucose level of the two groups was measured using a glucometer purchased from Yuyue, Shanghai, China. Only when the fasting blood glucose of the mice is over 20 mmolo/L can they be regarded as diabetic mice. Mice in the GEM group were injected abdominally with 50 mg/kg gemcitabine (MCE, Shanghai, China) twice a week. Mice in the CG group were abdominally injected with 50 mg/kg gemcitabine + 30 mg/kg cordycepin twice a week. All animals were sacrificed two weeks after the first injection of drugs. The timeline and schematic diagram of the animal experiment are shown in Figure 1(d).

3. Results

3.1. Diabetic Status Affects Clinical Outcomes in Pancreatic Cancer Patients. In the TCGA cohort (Figure 2(a)), the diabetic PDA cases had a relatively lower OS level than normal cases in advanced pathological grade patients (median survival: 224 days vs. 652 days, $P = 0.0075$). Similarly, in Figure 2(b), the median overall survival (OS) in the diabetic group and normal group was 501 days and 414 days ($P = 0.0298$) in patients who accepted adjuvant therapy of gemcitabine plus paclitaxel therapy after surgery in Huashan Hospital (Huashan cohort). All patients in the Huashan cohort did not accept neoadjuvant treatment previously. Additionally, in Table 1, diabetic status showed little relationship with gender, age, cancer pathological stages, and metastasis but was positively related to the tumor volume in the Huashan cohort (3.44 cm^3 vs. 4.407 cm^3, $P = 0.003$). This result indicated that diabetic patients had a larger tumor volume.

3.2. High Glucose Status Promotes Invasion and Gemcitabine Resistance in PDA Cells. We performed laboratory experiments based on the previous clinical findings to ascertain whether high glucose status promotes gemcitabine resistance and cancer invasion *in vitro*. We defined three groups according to different glucose concentrations in cell mediums: 25 mmol/L glucose as the high glucose (HG) group, 15.5 mmol/L as the medium glucose (MG) group, and 5.5 mmol/L as the low glucose (LG) group. We validated the gemcitabine resistance at first. Firstly, after being treated with 10 μmol/L gemcitabine for 24 h, the HG group showed higher cell viability in all pancreatic cancer cell lines than MG and LG (BxPc-3, PANC-1, MiaCaPa-2, PANC-2, and HPDE6-C7) groups (Figure 3(d)). Moreover, after being treated with 10 μmol/L gemcitabine for 24 h, BxPc-3, PANC-1, and MiaCaPa-2 cell lines showed a statistical difference in cell viability between HG, MG, and LG groups in Figure 3(d) ($P = 0.0069$, 0.0386 and 0.0047). Next, HG and MG groups had a higher cell viability rate than the LD group after being treated with gemcitabine for 24 h and 48 h ($P = 0.0069$ and 0.050) (Figure 3(c)). The cancer cell apoptotic rate in HG, MG, and LG after treated with 10 μmol/L gemcitabine for 24 h was 19.8%, 21.9%, and 26.1% (Figure 3(e)). Next, we assessed cancer invasion ability under the gemcitabine environment via the wound healing test. The invasion ability in the HG group was better than the MG group, and the MG group was better than the LG group in the BxPc-3 cell line (Figure 3(f)).

3.3. MMP-3 Correlates with Survival and Diabetic Status in PDA. Our clinical and experimental study proved the altered gemcitabine resistance and cancer invasion effect under the high glucose environment. Next, in order to clarify the key factors involved in gemcitabine resistance induced by high glucose status, we applied the RNA sequence data downloaded from the TCGA database. We set two groups: the diabetic group ($n = 38$) and the normal group ($n = 108$), according to the diabetes history in the database. Through differentially expressed gene (DEGs) analysis, 119 genes were differentially expressed within these two groups, shown as the volcano plot in Figure 2(d). And the top 30 differentially expressed genes were presented as a heat map in Figure 2(c). Through pathway enrichment analysis (GO and KEGG analysis), digestive function (pancreatic secretion, fat and protein digestion), serine hydrolase activity, and humoral immune response were enriched signal pathways in the diabetic PDA cohort (Figure 2(f)). Moreover, the GSEA results (Figure 2(e)) showed that diabetic samples were associated with the B cell receptor signal pathway, cell adhesion pathway, chemokine signal pathway, and NADPH oxidase pathway. We then performed a univariate Cox regression analysis and found 19 genes statistically related to the overall survival in PDA patients. We finally used the

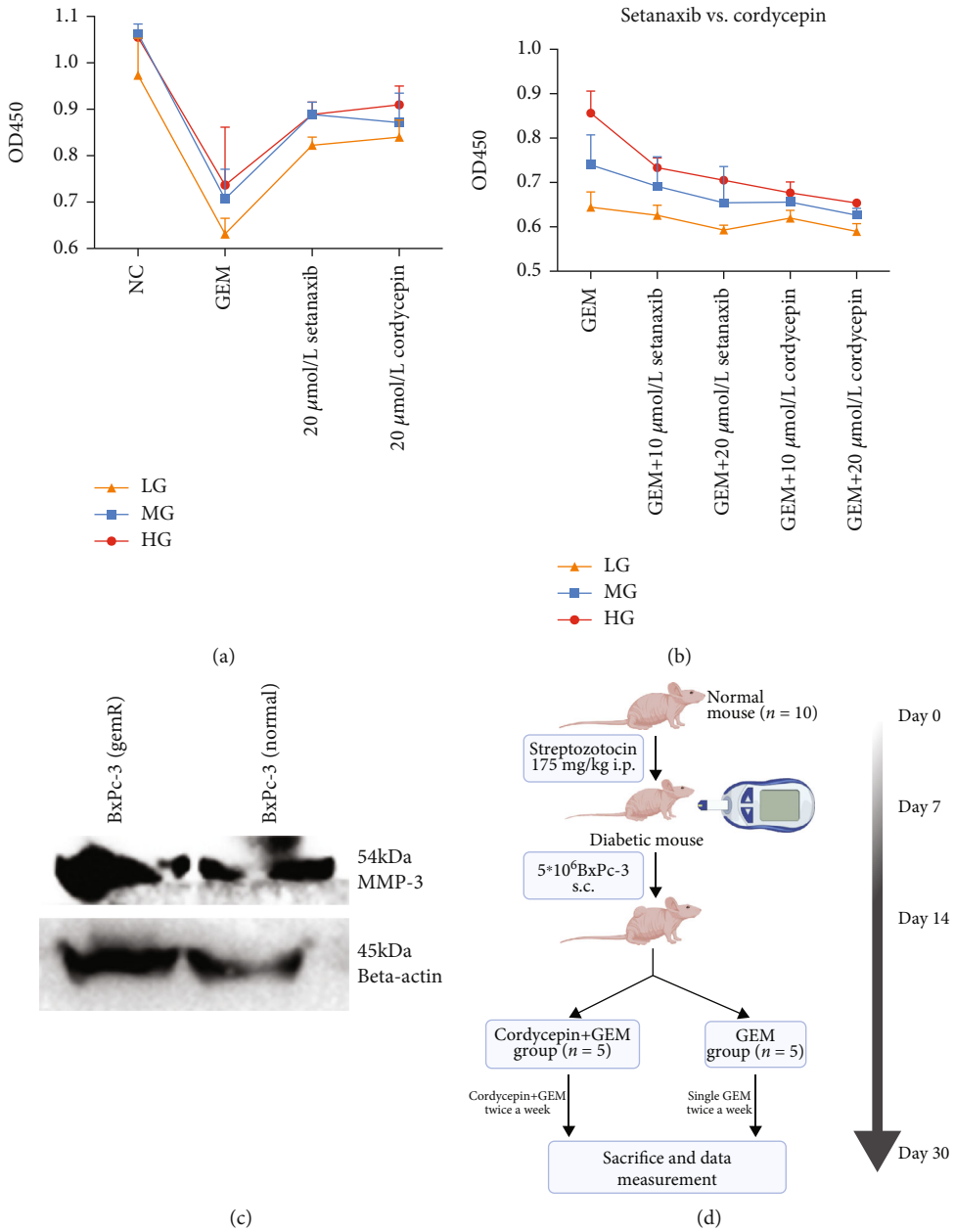

Figure 1: Continued.

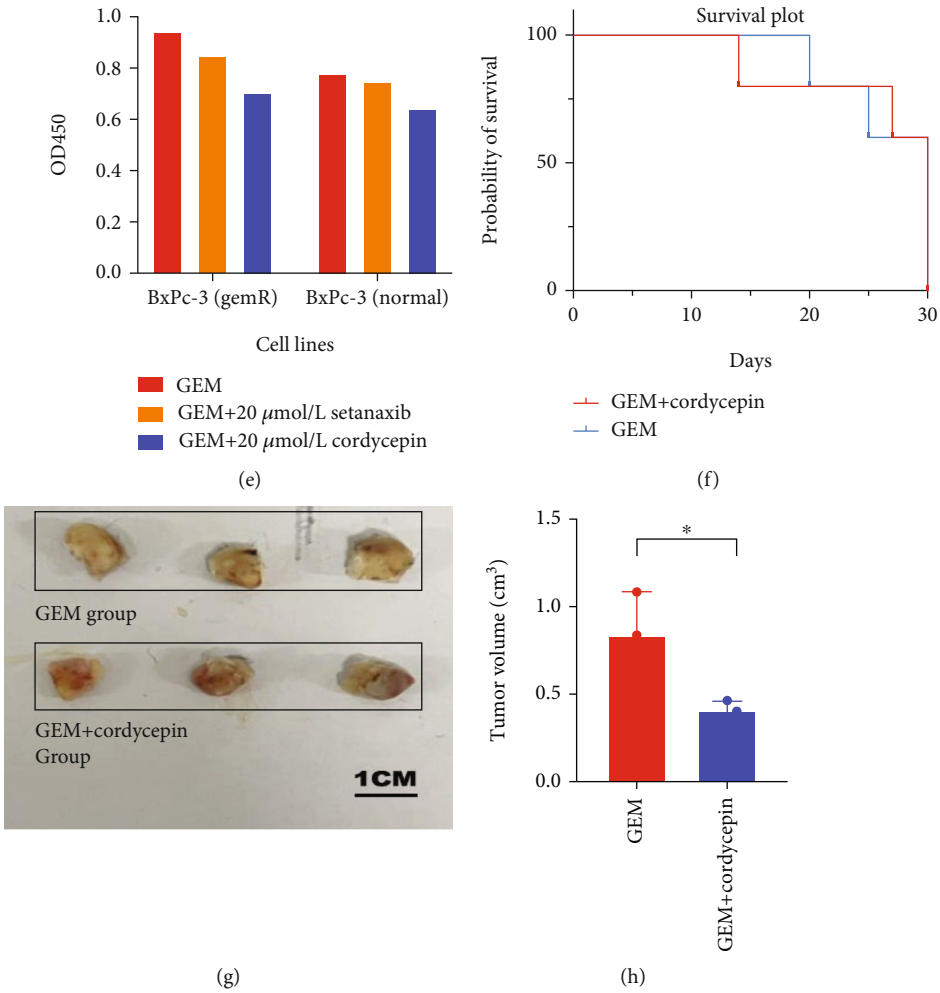

Figure 1: (a) Different glucose groups (HG, MG, and LG) BxPc-3 cells treated with normal control (NC), single 10 μmol/L GEM group, single 20 μmol/L setanaxib, and single 20 μmol/L cordycepin. (b) Different glucose groups (HG, MG, and LG) BxPc-3 cells treated with single 10 μmol/L GEM group, 10 μmol/L setanaxib+10 μmol/L GEM group, and 20 μmol/L setanaxib+10 μmol/L GEM group, 10 μmol/L cordycepin+10 μmol/L GEM group, and 20 μmol/L cordycepin+10 μmol/L GEM group. (c) MMP-3 expression in natural generated gemcitabine resistant cell line (BxPc-3 (GemR)) and in normal control (BxPc-3 (Normal)). (d) The schematic diagram and the timeline of the *in vivo* experiment in nude mouse. (e) The cell viability of BxPc-3 (GemR) and BxPc-3 (Normal) after treated with10 μmol/L GEM, 20 μmol/L setanaxib+10 μmol/L GEM, and 20 μmol/L cordycepin+10 μmol/L GEM for 24 h. (f) The K-M survival plot of the mice in the GEM+cordycepin treated group, and single GEM treated group ($P = 0.9875$). (g, h) Tumor volume comparison between GEM + cordycepin treated diabetic group and single GEM treated group ($^*P < 0.05$).

LASSO regression analysis of these 19 genes and found that MMP-3 had the highest positive coefficient value of 0.11(Figure 3(a)). Based on this, MMP-3 might be an important prognostic factor that participated in the survival reduction of diabetic PDA patients.

We then used clinical resected samples to validate whether MMP-3 was differentially expressed in diabetic PDA samples. Figure 4(a) showed that in PDA patients, MMP-3 expression was significantly increased in tumor tissue than in the normal pancreatic tissue. IHC test based on surgical samples (Figure 5(a)) showed that MMP-3 expression in protein level was higher in tumor tissue. Compared to euglycemic PDA samples, our result showed diabetic PDA samples had higher MMP-3 expression in both mRNA expression and protein expression levels compared to the normal PDA samples (Figures 4(a) and 5(b)). In Figures 5(b) and 5(c), a significantly higher MMP-3 positive value was found in diabetic PDA samples than the positive value in euglycemic PDA samples (mean positive grade: 2.455 vs. 1.727, $P = 0.0189$). In pancreatic cancer cells, MMP-3 expression was higher in the HG group compared to MG and LG groups. And MMP-3 expression was increased with the elevation of glucose concentration in the medium (Figure 5(d)).

After confirming that MMP-3 was closely related to survival and diabetes in PDA models, we next analyzed the role of MMP-3 in PDA gemcitabine resistance and invasion. Firstly, pan-cancer analysis (Figure 2(g)) revealed that MMP-3, a member of the matrix metalloproteinase family, was overexpressed in many types of solid tumors, including breast cancer (BRCA), cervical cancer (CESC), bile duct cancer (CHOL), colon cancer (COAD), esophageal cancer

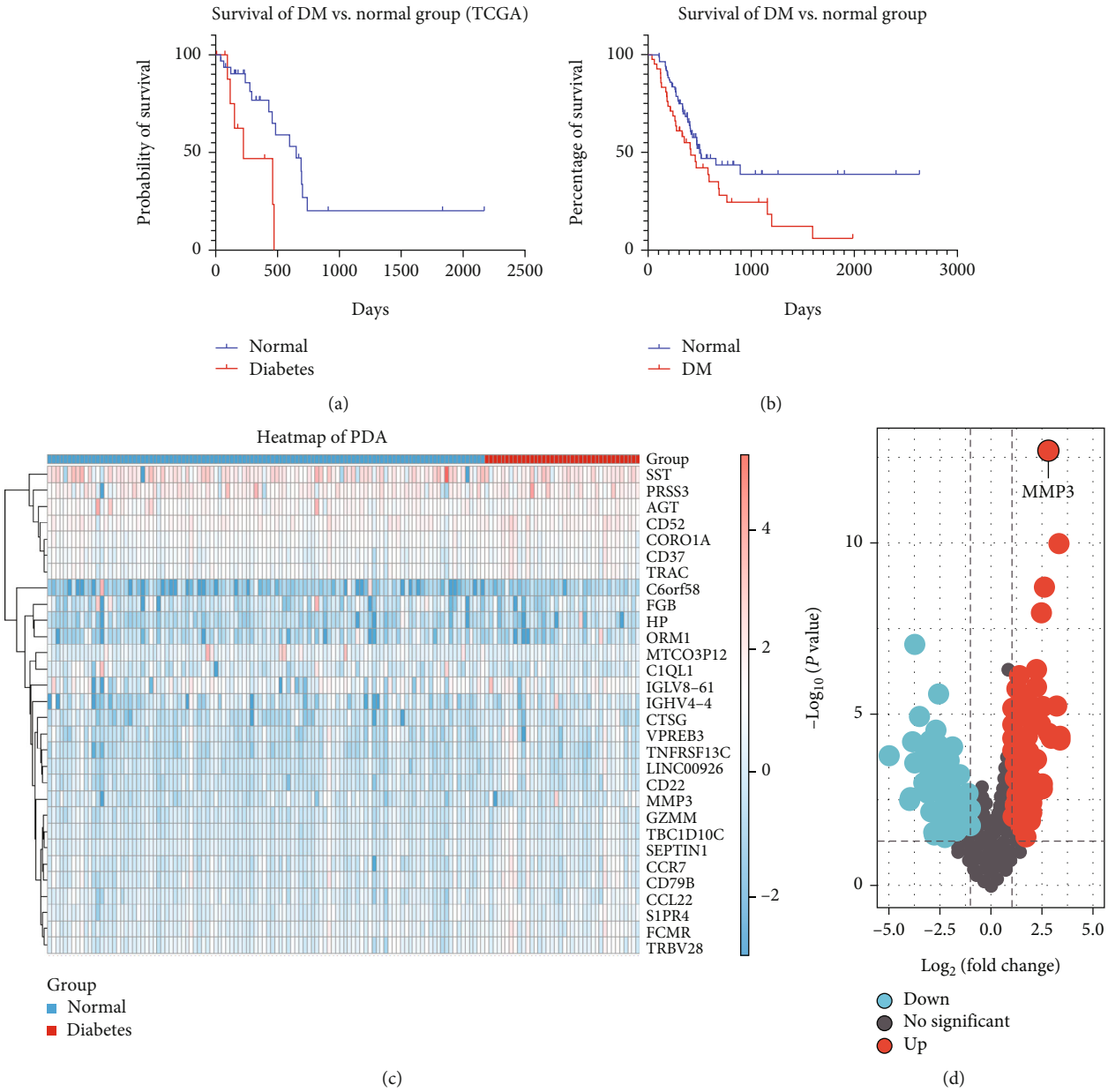

Figure 2: Continued.

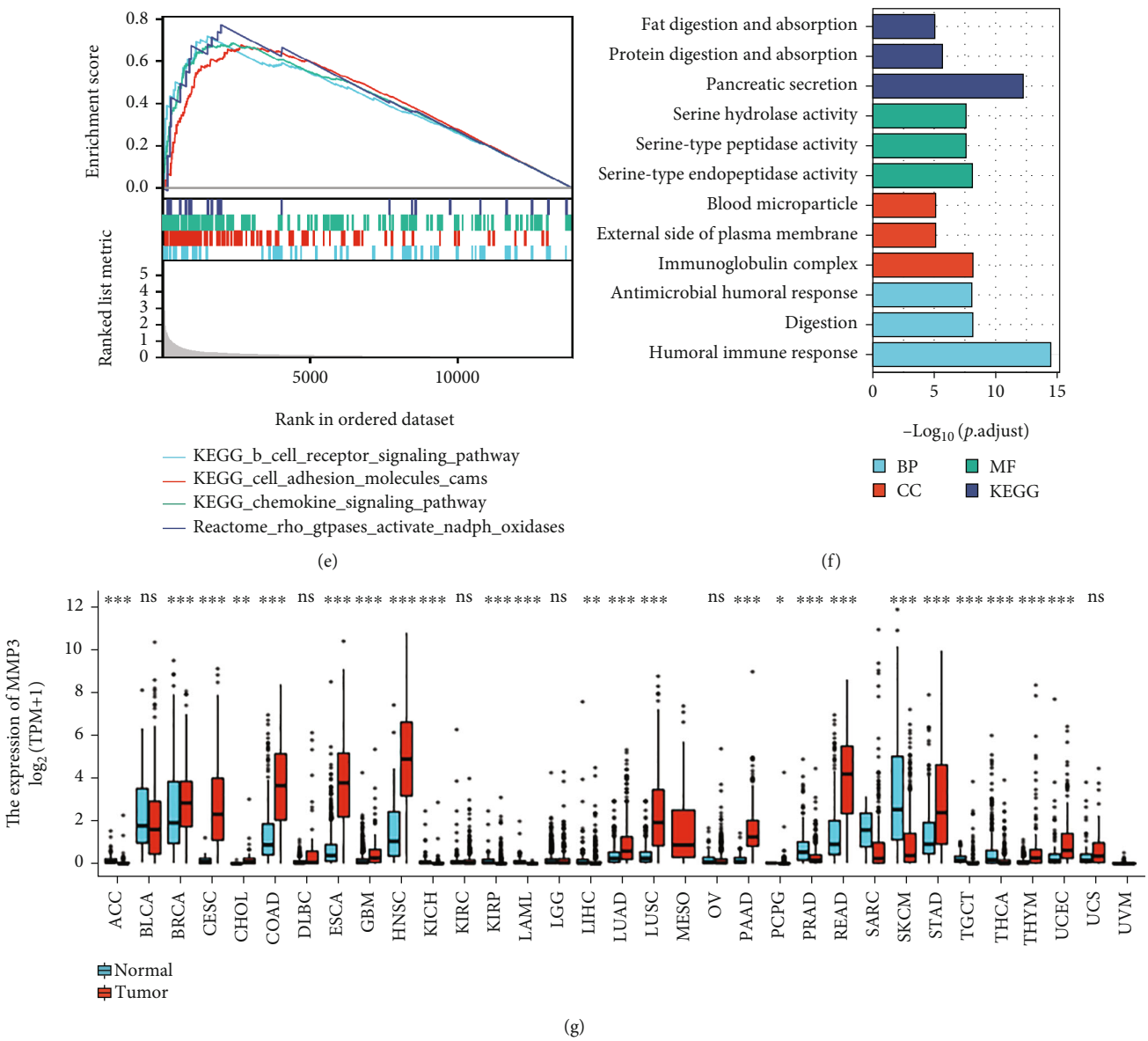

Figure 2: (a, b) K-M survival plots of PDA patients in TCGA cohort (A) and PDA gemcitabine users in Huashan cohort (B). (c) Heat map of the top 30 genes differentially expressed between the normal and the diabetic PDA patients (blue = normal group, red = DM group). (d) Volcano plot of DEGs between normal and diabetic PDA patients in TCGA database (up: upregulated genes, down: downregulated genes). (e) GSEA analysis of pathways enriched in the diabetic group. (f) GO and KEGG analyses of the pathways enriched in the DM group. (g) Pan-cancer analysis of MMP-3 expression between the normal tissue and the cancerous tissue based on the TCGA database ($^{*}P < 0.05$, $^{**}P < 0.01$, $^{***}P < 0.001$).

(ESCA), and pancreatic cancer (PAAD). However, in hematological malignancies, MMP-3 expression was decreased in diffuse large B-cell lymphoma (DLBC) and acute myeloid leukemia (LAML). Next, we set the top 50% MMP-3 expression level in the TCGA-PAAD cohort as the high MMP-3 group and the rest as the low MMP-3 group. In the TCGA database (Figure 4(b)), reduced survival was found in the high MMP-3 group in the whole PDA patients (median survival: 532 days vs.702 days, $P = 0.001$) and gemcitabine users (median survival: 394days vs. 691days, $P = 0.019$). The MMP-3 prognostic prediction efficacy was performed by ROC curve analysis. The area under the curve (AUC) of 1-year, 3-year, and 5-year survival was 0.604, 0.655, and 0.712 (Figure 4(c)). Table 2 was the clinical baseline information in MMP-3 differently expressed groups. MMP-3 was positively related to histological grade ($P = 0.008$) and overall survival ($P < 0.001$). Through DEGs analysis, GO analysis (Figure 4(f)), and GSEA analysis (Figures 4(d) and 4(e)), we found neuronal system, transmission across chemical synapses, drug metabolism, degradation of the extracellular matrix, extracellular matrix organization, matrix metalloprotease, and oxidative stress-related pathways were enriched in the higher MMP-3 expressed group.

3.4. MMP-3 Is Related to Gemcitabine Resistance and Cancer Invasion. We performed a series of laboratory studies to

Table 1: The baseline information of PDA patients ($n = 129$) from Huashan Hospital.

Characteristics	Normal	DM	P value
Overall cases	87	42	
Age	62.91 (39-86)	63.69 (50-77)	0.59
Sex (male)	54	22	0.295
Pathological stage			0.613
I-II	56	22	
III-IV	31	20	
Metastasis	8	6	0.384
Tumour volume	3.44 (0.80-12)	4.407 (1.6-10)	**0.003**

validate the function of MMP-3 in PDA gemcitabine resistance and invasion. We used two MMP-3 siRNAs (MMP-3_Si01 and MMP-3_Si02) and cordycepin, a selective MMP-3 inhibitor, to test the effect of blocking MMP-3 in pancreatic cancer cells. In Figures 5(e) and 5(f), siRNAs (MMP-3_Si01, MMP-3_Si02) and cordycepin significantly inhibited MMP-3 expression compared with normal control (NC_1). And the apoptosis of BxPc-3 cells was higher in MMP-3 siRNAs (MMP-3_Si01, MMP-3_Si02) and 20 μmol/L cordycepin treated groups compared with normal control (NC_1) (Figures 5(g) and 5(h)) under 10 μmol/L gemcitabine environment. Meanwhile, overexpressing MMP-3 (MMP-3_OVER) elevated BxPc-3 cell survival and reduced apoptosis in the 10 μmol/L gemcitabine environment (Figures 5(g) and 5(h)). Compared with normal control, cancer invasion was increased in the MMP-3_OVER group and decreased in the siRNA (MMP-3_Si01) treated group compared with normal control ($P < 0.001$) (Figure 6(a)). In the normal control group, 10 mmol/L cordycepin+10 μmol/L gemcitabine and 20 mmol/L cordycepin +10 μmol/L gemcitabine treated group, the cell viability of pancreatic cancer cells decreased with higher cordycepin concentration (Figure 6(g)). What is more, in Figure 1(b), the difference in cell viability between HG, MG, and LG was also decreased in the 20 mmol/L cordycepin+10 μmol/L gemcitabine treated group than the 10 mmol/L cordycepin+10 μmol/L gemcitabine treated group.

Next, we measured the effect of blocking MMP-3 in the naturally generated gemcitabine-resistant cell line. The MMP-3 expression was elevated in naturally generated gemcitabine-resistant cancer cells than in normal cancer cells (Figure 1(c)). Under single 10 μmol/L gemcitabine treatment, gemcitabine resistant cell line (BxPc-3 (GemR)) showed higher cell viability (0.955 vs. 0.787, $P = 0.0026$) than the normal cell line (BxPc-3 Normal) (Figure 1(e)). However, compared with the single gemcitabine treated group, gemcitabine plus cordycepin and gemcitabine plus setanaxib effectively reduced cell viability (Figure 1(e)). In Figure 1(e), gemcitabine resistant cell line showed a statistically higher cell viability rate than the normal group in the cordycepin plus gemcitabine group (0.7068 vs. 0.6438, $P = 0.0104$) and the setanaxib group (0.8545 vs. 0.7498, $P = 0.0107$). But the difference value between BxPc-3 (GemR) and BxPc-3 (Normal) was reduced in the gemcitabine plus cordycepin treatment group than in the single gemcitabine treated group (0.063 vs. 0.168). In comparison, the difference value was larger in the setanaxib plus gemcitabine group (0.105 vs. 0.168).

Finally, we confirmed our findings *in vivo* using a diabetic pancreatic cancer mouse model. The schematic diagram of the *in vivo* study is shown in Figure 1(d). After constructing the diabetes model, 10 nude mice (6-7 weeks) were randomly divided into 2 groups: GEM (50 mg/kg) group and cordycepin (30 mg/kg) plus GEM (50 mg/kg) (CG) group. The survival plot of these two groups is shown in Figure 1(f). Two mice died on day 20 and day 25 in the GEM group, and two died on day 14 and day 27 in the GEM plus 30 mg/kg cordycepin (CG) group ($P = 0.9873$). The result of tumor volume was 0.8357 ± 0.2483 cm^3 in the GEM group and 0.4093 ± 0.0547 cm^3 in the CG group ($P = 0.0445$) (Figure 1(h)). Obviously, the CG group showed smaller tumor volume and death rate after accepting drug injections.

3.5. Gemcitabine Metabolism-Related Gene RRM1 Is Associated with MMP-3 Expression. Previous studies demonstrated that nucleoside transporters (NTs) family (ENT1 (SLC29A1), CNT1 (SLC28A1), CNT3 (SLC28A3)), ribonucleotide reductase (RR) family (RRM1, RRM2), excision repair cross-complementation 1 (ERCC1), PLK1, and multiple-drug resistant protein 1 (MRP1, ABCB1) were vital in the metabolic process of gemcitabine in pancreatic cancer cells [3]. In the TCGA database, MMP-3 showed a statistical relationship with CNT1, CNT3, RRM1, and RRM2 ($P < 0.05$) in Figure 4(f). Figure 4(h) demonstrated that MMP-3 showed a relatively weaker positive relationship with CNT1 and CNT3, while MMP-3 revealed a stronger relationship with RRM1 and RRM2. We then found that only RRM1 expression (1.156 vs. 0.85, $P = 0.0285$) was significantly increased in the 100 U MMP-3 treated pancreatic cells than the normal control according to the data from GSE50931. Moreover, RRM2 (1.192 vs. 0.879, $P = 0.1415$), CNT1 (0.988 vs. 0.976, $P = 0.4332$), and CNT3 (0.954 vs. 1.009, $P = 0.8548$) expressions showed no statistical difference under the stimulation of 100 U MMP-3 than the normal control group. The results are shown as the heat map in Figure 4(i).

3.6. ROS Is Involved in High Glucose-Induced MMP-3 Overexpression. Next, we tested whether ROS was involved in the mediation of MMP-3. It is generally accepted that high glucose stimulates reactive oxygen species (ROS) to alter a series of cell metabolism. From bioinformatical results, the NADPH oxidase pathway (Figure 2(e)) was enriched in the diabetic cohort, and the oxidative stress (Figure 4(e)) was enriched in the high MMP-3 expression cohort. In Figure 3(b), ROS level was also increased in HG and MG compared to LG ($P < 0.001$). And in Figure 5(d), NOX4 expression was increased with the elevation of glucose concentration. Figure 4(g) revealed that MMP-3 expression was strongly associated with NOX4 rather than NOX1 in pancreatic cancer. And in Figure 6(b), NOX4 showed a positive relationship with NOX in TCGA pancreatic cancer cohort ($r = 0.391$, $P < 0.001$). Taken together, it

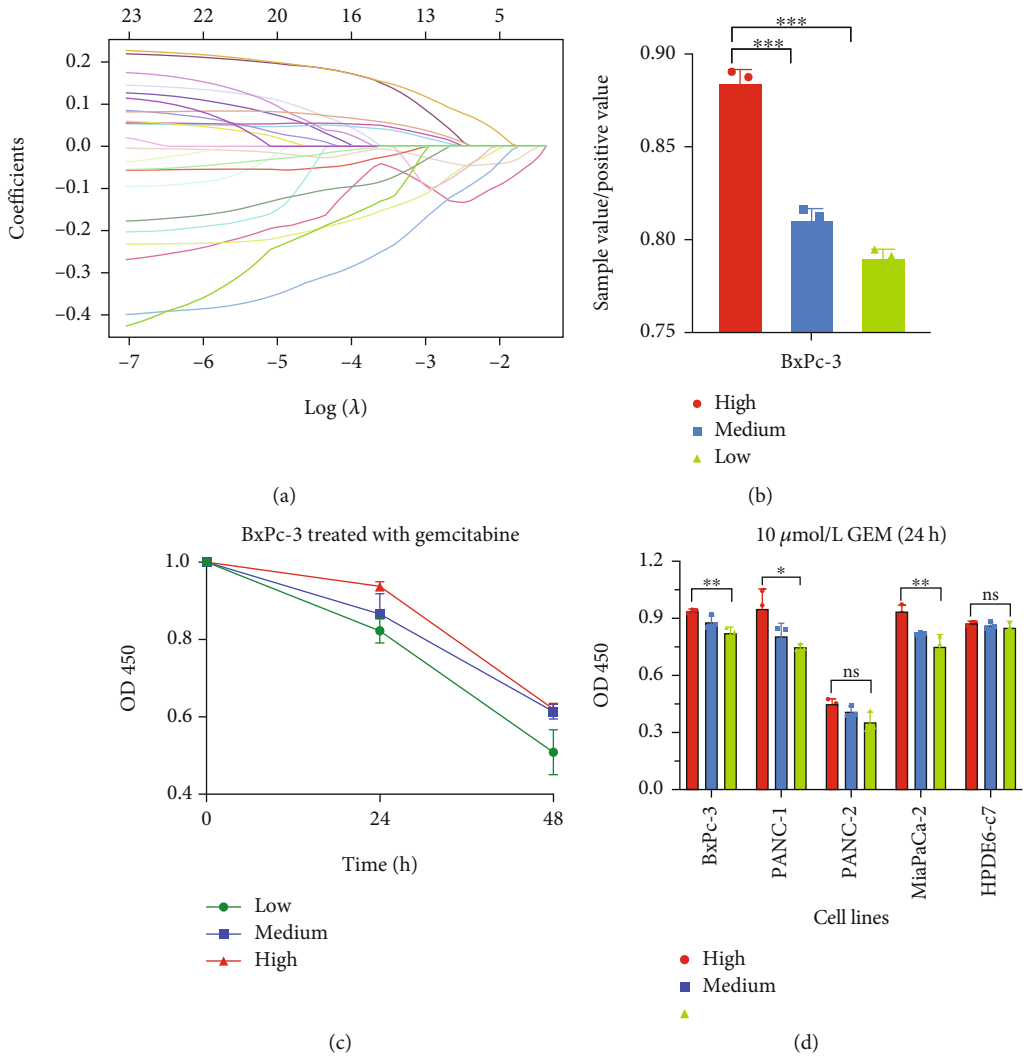

Figure 3: Continued.

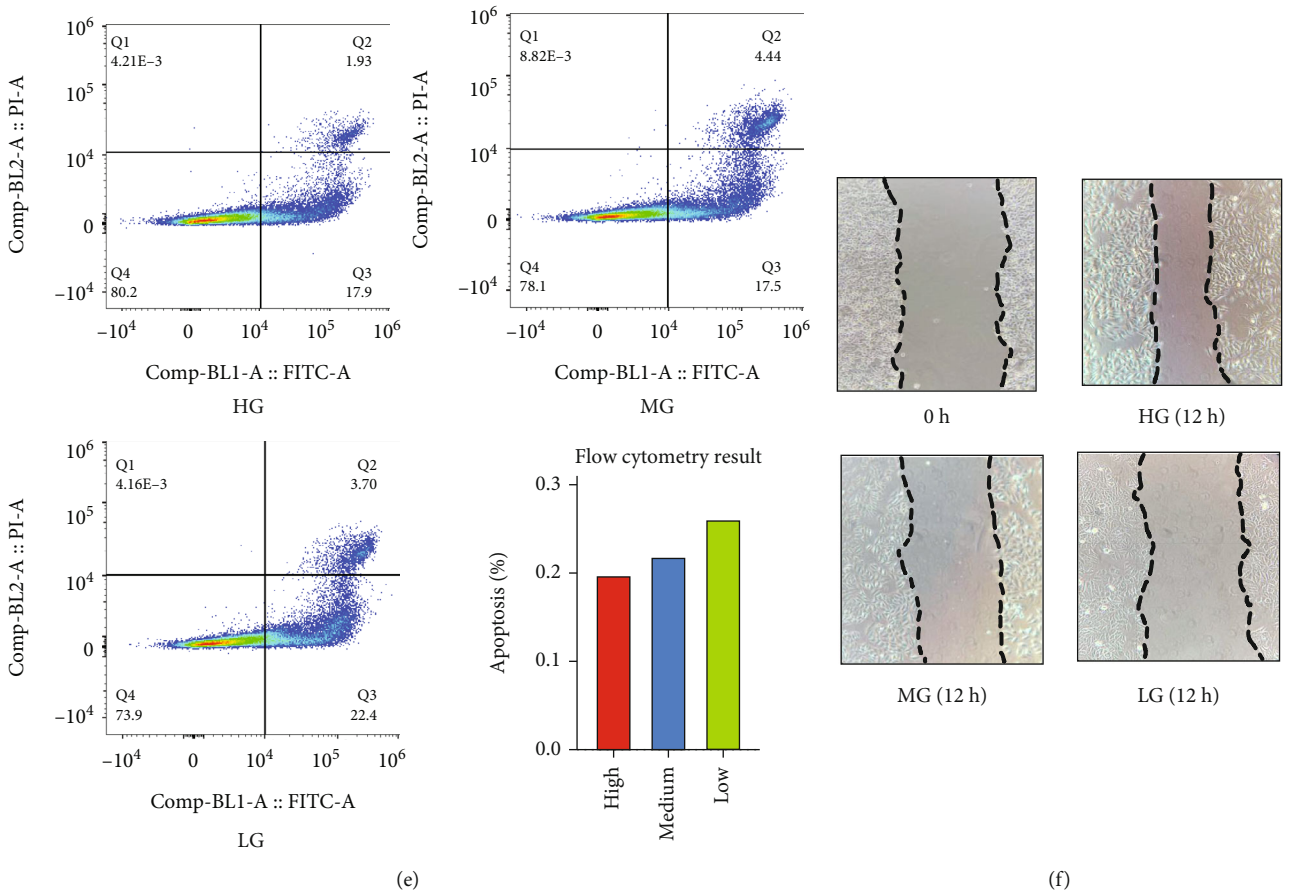

(e) (f)

Figure 3: (a) Lasso regression analysis of DEGs between the normal and the DM groups. (b) ROS level of BxPC-3 cell lines under different glucose levels (HG: high glucose level group, MG: medium glucose level group, LG: low glucose level group). (c) Cell viability of BxPc-3 treated with 10 μmol/L gemcitabine for 24 h and 48 h. (d) Pancreatic cancer cell lines were treated with 10 μmol/L gemcitabine for 24 h under different glucose levels. (e) The apoptosis rate of different glucose groups under 10 μmol/L gemcitabine for 24 h (the lower right is the bar graph concluding the apoptosis between three groups). (f) Wound healing test of different glucose levels.

was logical to suppose that ROS mediated by NOX4 might participate in MMP-3 overexpression regulated by high glucose.

We then performed experiments to prove the role of NOX4-mediated ROS in MMP-3 overexpression. Firstly, in Figure 6(d), the setanaxib, a selective NOX4 inhibitor, effectively suppressed both NOX4 and MMP-3 expression compared to the normal control group in cancer cells. However, in H_2O_2, a potent ROS stimulator, treated group, MMP-3, and NOX4 expression were both increased compared to the normal control. But MMP-3 siRNAs treated groups and the cordycepin treated group did not show an apparent change in NOX4 expression (Figure 5(e)). And MMP-3 overexpression group did not affect the NOX4 expression level (Figure 5(e)). This result indicated that ROS might be an upstream factor in the MMP-3 activation. Moreover, the NOX4 expression in pancreatic cancer cells did not showed an obvious change after being treated with 100 U MMP-3 in the GSE50931 (Figure 4(i)). Finally, after treated with 20 μmol/L setanaxib for 24 h, the MMP-3 and NOX4 expression were similar between the HG, MG, and LG groups compared with the normal group (Figures 6(c) and 6(d)).

3.7. ROS Participates in High Glucose-Induced GEM Resistance and Invasion. We finally confirmed whether ROS was an intermediate factor involved in the gemcitabine resistance and cancer invasion caused by high glucose. Firstly, we observed increased ROS levels in HG and MG compared to LG (0.8855, 0.8115, 0.7910, $P < 0.001$) (Figure 3(b)). In Figure 6(d), H_2O_2 increased NOX4 expression and setanaxib decreased NOX4 expression in BxPc-3 cell lines. Figure 6(f) demonstrated that HG, MG, and LG groups showed increased cell viability after treated with 50 μmol/L and 10 μmol/L H_2O_2 for 24 h compared with the single GEM treated group. Using setanaxib plus GEM, the cell viability was reduced in HG, MG, and LG groups (Figures 1(b) and 6(f)). The cell viability was also decreased with the decrease of H_2O_2 concentration and the increase of setanaxib concentration (Figure 6(f)). The difference between HG, MG, and LG was decreased with the increase with the elevation of H_2O_2 concentration and the senataxib concentration. Secondly, targeting NOX4 mediated ROS also influenced PDA invasion under the gemcitabine environment. In Figure 6(e), BxPc-3 cells treated with 10 μmol/L H_2O_2+10 μmol/L GEM, 20 μmol/L setanaxib+10 μmol/L GEM, and single 10 μmol/L GEM showed statistical

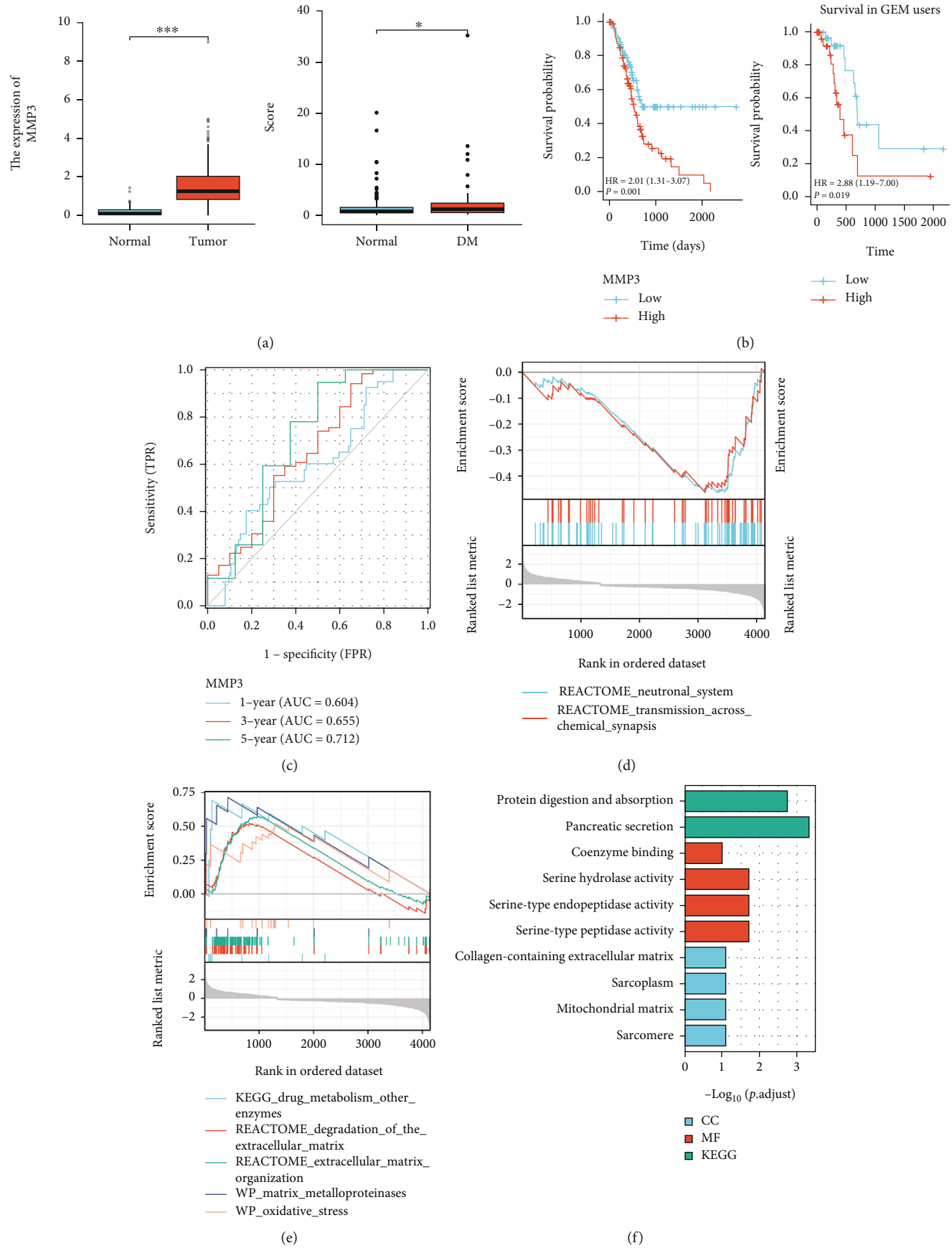

Figure 4: Continued.

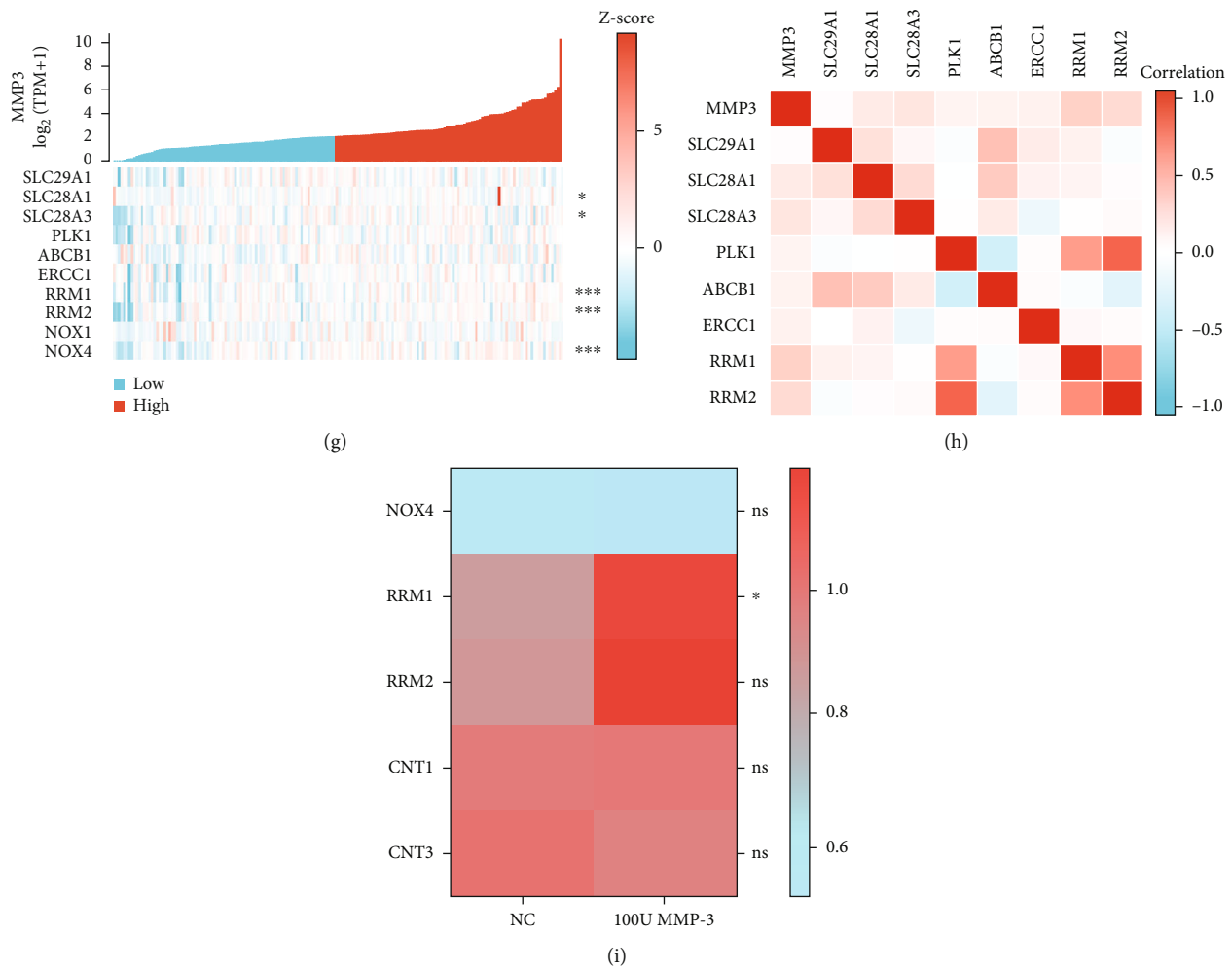

Figure 4: (a) Left: MMP-3 expression between normal tissue and the PDA tissue; Right: MMP-3 expression between normal PDA patients and the person with diabetes (DM) PDA patients ($^{*}P < 0.05$, $^{***}P < 0.001$). (b) ROC curve of MMP-3 predicting the overall survival of PDA patients in 1-year, 3-years, and 5-years. AUC (area under the curve) measures the predicting efficacy of MMP-3 in different time models. (c) K-M survival plot of the high MMP-3 group, and the low MMP-3 group in the TCGA pancreatic cancer cohort (left) and TCGA PDA gemcitabine users (right). (d, e) GSEA analysis of pathways enriched in high MMP-3 group. (f) GO and KEGG analyses of the pathways enriched in high MMP-3 group. (g, h) Heat map of the association between the single genes (ENT1 (SLC29A1), ENT3 (SLC29A3), CNT1 (SLC28A1), CNT3 (SLC28A3), RRM1, RRM2, MRP1 (ABCB1), NOX1, NOX4, and PLK1) expression and the MMP-3 expression in PDA cohort ($^{*}P < 0.05$, $^{***}P < 0.001$). (i) The expression of NOX4, RRM1, RRM2, CNT1, and CNT3 in 100 U MMP-3 treated pancreatic cancer cell line and normal control group from GSE50931 (ns: not significant ($P > 0.05$), $^{*}P < 0.05$).

difference in Transwell study. Interestingly, in Figure 1(a), the tumor-suppressive effect of single cordycepin was similar to the effect of single setanaxib treatment. But in Figure 1(b), 20 μmol/L cordycepin+10 μmol/L gemcitabine group showed better tumor-suppressive effect than 20 μmol/L setanaxib+10 μmol/L gemcitabine. Based on this, the MMP-3 inhibitor may be a better gemcitabine sensitizer compared to the NOX4 inhibitor.

4. Discussion

With the elevation of life quality, it is foreseeable that the incidence of diabetes will continue to rise for a long time in the future. Diabetes mellitus was a signal of poor prognosis found in many studies from American and Asian gemcitabine users [6–10]. Our study elucidated that DM might lead to a worse clinical outcome in Chinese PDA patients. As the main characteristics of diabetes, increased blood glucose level is essential for pancreatic cancer development and resistance to therapies. High glucose cannot only work as a direct energy supply for cancer cells to grow much faster but also stimulate multiple signal pathways, which are essential for pancreatic cancer development [11]. Our study provides a novel insight into that high glucose may directly strengthen gemcitabine resistance and invasion via ROS/MMP-3 signaling pathway.

At first, we confirmed the association between gemcitabine resistance with glucose concentration from clinical data and laboratory experiments. Our clinical retrospective result demonstrated that diabetes signals poor clinical outcomes in PDA patients, especially in PDA gemcitabine users. Gemcitabine is the first-line chemical drug in PDA treatment.

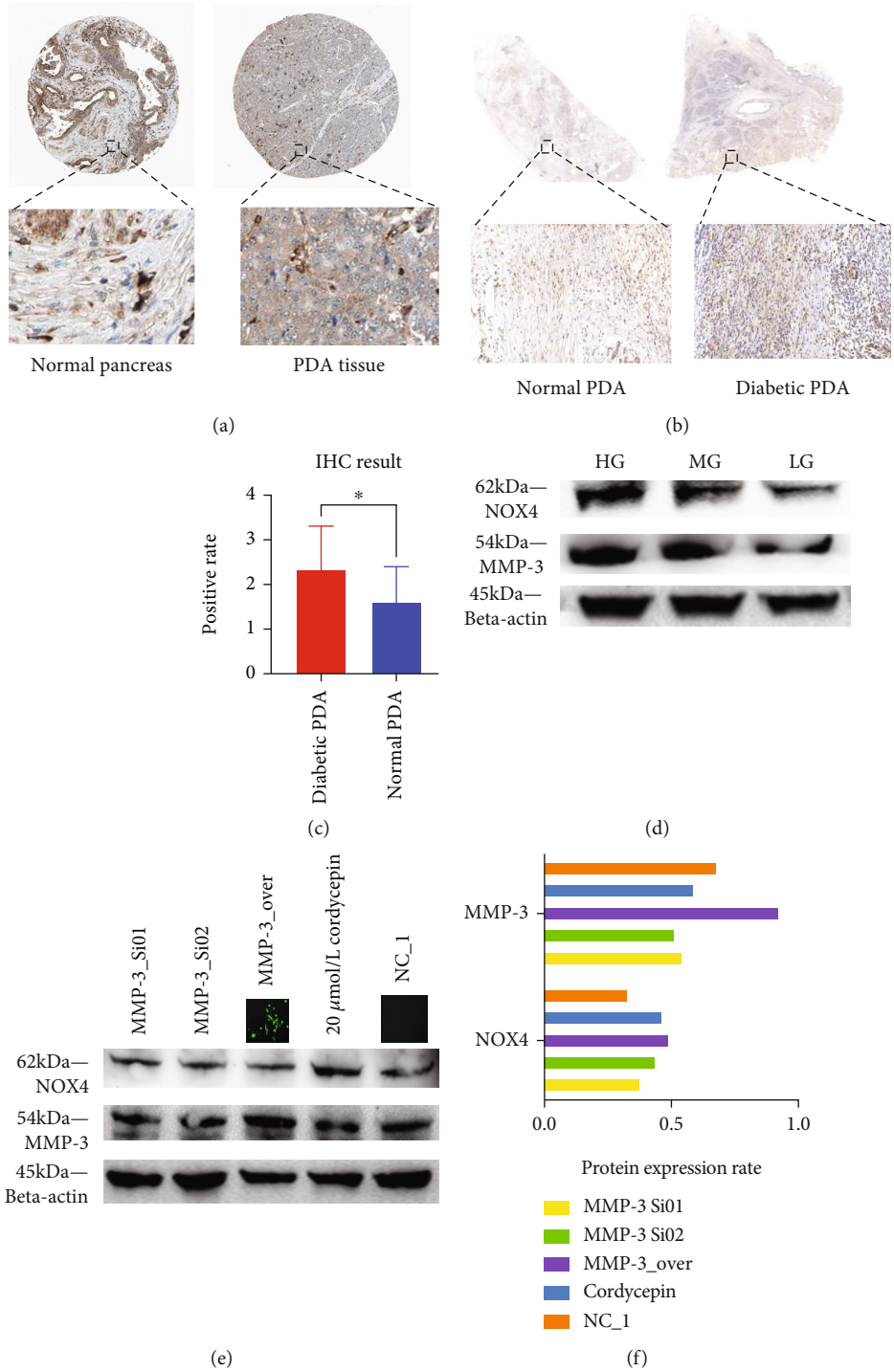

Figure 5: Continued.

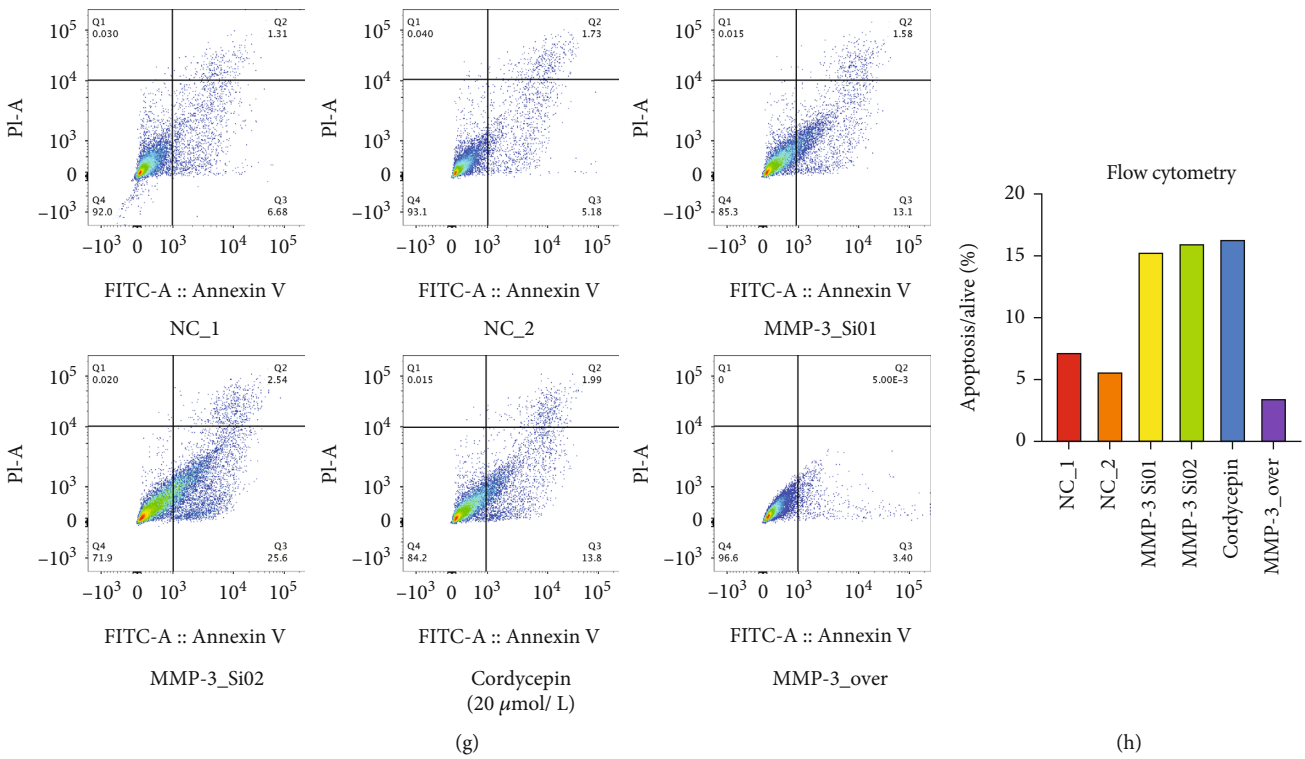

Figure 5: (a) MMP-3 expression in normal pancreas tissue (left) and in PDA tissue (right) (downloaded from https://www.proteinatlas.org). (b, c) MMP-3 expression difference between normal ($n = 11$) (left) and diabetic PDA patients ($n = 11$) (right) ($^{*}P = 0.0198$). (d) MMP-3 expression in high, medium, and low glucose group (e) MMP-3, beta-actin, and NOX4 expression in MMP-3 siRNAs treated group (MMP-3_Si01 and MMP-3_Si02), 20 μmol/L cordycepin, MMP-3 overexpression group (MMP-3_OVER), and normal control (NC_1) ($^{***}P < 0.001$, ns:>0.05). (f) The grey value of MMP-3/beta-actin and NOX4/beta-actin in Figure 1(e). (g) Apoptosis analysis of MMP-3 siRNAs treated group (MMP-3_Si01 and MMP-3_Si02), 20 μmol/L cordycepin, MMP-3 overexpression group (MMP-3_OVER), and normal control (NC_1 and NC_2). (h) The bar plot of the apoptotic rate in MMP-3_OVER, NC_1, NC_2, MMP-3_Si01 MMP-3_Si02, and 20 μmol/L cordycepin treated group.

Gemcitabine mainly interferes with DNA synthesis to induce apoptosis in pancreatic cancer cells to inhibit cancer progression. So, we tested the cell viability, apoptosis, and wound-healing rate to measure the gemcitabine sensitivity and cancer invasion in pancreatic cancer cells under different glucose concentrations. Then, through survival-related univariate study and LASSO regression analysis, we focused our interest on MMP-3, a matrix metalloprotease. And we also found that MMP-3 expression was correlated with high glucose status in PDA through clinical samples, bioinformatical sequencing, and laboratory experiments.

From clinical samples, bioinformatical results and cellular experiments, we found that MMP-3 expression was related to high glucose status in pancreatic cancer. MMP-3, a member of the matrix metalloproteinase family, is well-known as a vital factor in cancer metastasis and invasion. MMP-3 promotes cancer invasion and metastasis through the enzymic breakdown of the basal membrane and extracellular matrix. Our study found that MMP-3 expression was upregulated in many solid malignant tumors. In pancreatic cancer, MMP-3 was reported to be related to cancer invasion and metastasis [12]. This might be the reason why we observed increased PDA invasion under a higher glucose environment. Our study also confirmed that inhibiting MMP-3 expression significantly reduced PDA invasion under the gemcitabine environment. Moreover, MMPs have also been reported to alter cancer cell proliferation and anti-apoptosis through the crosstalk with multiple signal pathways. Our result showed that MMP-3 effectively blunted PDA gemcitabine sensitivity, which presented as reduced apoptosis and promoted proliferation in pancreatic cancer cells. During this process, we furtherly found that cordycepin, a selective MMP-3 inhibitor, had a satisfying effect in suppressing pancreatic cancer gemcitabine resistance. Cordycepin is a derivative from the fungal genus *Cordyceps militaris* and has long been used as an active pharmacological ingredient in traditional Chinese medicine. Cordycepin was reported to inhibit MMP-3 expression in many inflammatory diseases [13–16]. In the *in vivo* study, the GEM+cordycepin group showed a reduced tumor volume than the single gemcitabine treated group. Additionally, MMP-3 was also reported to be closely related to diabetic inflammatory complications. Blocking MMP-3 expression significantly decreased the rate of diabetes-related complications in many animal models. Our study found that diabetic PDA cases were closely related to inflammation. After accepting chemotherapy, reduced mortality in the GEM+cordycepin group indicated that blocking MMP-3 can suppress gemcitabine resistance and increase mice's tolerance to drugs in DM animal models. MMP-3 may be a potential novel target

Table 2: Baseline information of MMP-3 differently expressed groups (TCGA database).

Characteristic	MMP3(low)	MMP3(high)	*P* value
Overall cases	89	89	
T stage, *n* (%)			0.290
T1	4 (2.3%)	3 (1.7%)	
T2	16 (9.1%)	8 (4.5%)	
T3	66 (37.5%)	76 (43.2%)	
T4	1 (0.6%)	2 (1.1%)	
N stage, *n* (%)			0.375
N0	28 (16.2%)	22 (12.7%)	
N1	58 (33.5%)	65 (37.6%)	
M stage, *n* (%)			0.672
M0	38 (45.2%)	41 (48.8%)	
M1	3 (3.6%)	2 (2.4%)	
Pathologic stage, *n* (%)			1.000
I-II	83 (47.4%)	84 (48%)	
III-IV	4 (2.3%)	4 (2.2%)	
Sex (male)	53 (29.8%)	45 (25.3%)	0.292
Histologic grade, *n* (%)			**0.008**
G1	23 (13.1%)	8 (4.5%)	
G2	39 (22.2%)	56 (31.8%)	
G3	25 (14.2%)	23 (13.1%)	
G4	1 (0.6%)	1 (0.6%)	
OS event, *n* (%)			**<0.001**
Alive	55 (30.9%)	31 (17.4%)	
Dead	34 (19.1%)	58 (32.6%)	
Age	67 (58-73)	65 (57-73)	0.448

for suppressing gemcitabine resistance and reducing diabetic complications simultaneously, which may benefit many diabetic PDA victims.

Additionally, we explored the potential downstream signal effectors of MMP-3 in gemcitabine resistance because MMP-3 did not directly participate in gemcitabine metabolism in PDA. CNT1, CNT3, RRM1, and RRM2 were statistically positively related to MMP-3 expression. These four genes were reported to influence gemcitabine metabolism in PDA directly. CNT1 and CNT3 worked as transporter to carry gemcitabine into the cell nucleus. Because of this, increased CNT1 and CNT3 could lead to elevated gemcitabine sensitivity [17, 18]. Reversely, RRM1 and RRM2 were associated with the repairment of DNA structure which is essential for countering the DNA damage effect by gemcitabine. Moreover, data from the GEO database furtherly supported that only RRM1 expression is statistically upregulated by MMP-3 stimulation. RRM1 was found to be upregulated in gemcitabine-resistant pancreatic cancer cells [19]. And it was also reported as an independent prognostic factor in pancreatic cancer patients [20]. RRM1 was reported to accumulate at the DNA damage sites and facilitate damage repairment which helps pancreatic cancer cells to overcome the apoptosis induced by gemcitabine. The silence of RRM1 effectively increased gemcitabine accumulation by enhancing the expression of uptake transporters. Unfortunately, the regulation of RRM1 in pancreatic cancer is still not clear. At present, only the RAS/ERK signaling pathway was reported to regulate the expression of RRM1 [21]. Because of this, it is not clear whether MMP-3 directly promotes RRM1 or indirectly promotes RRM1 expression via signal pathways such as the RAS/ERK signaling pathway. More study on the interaction between RRM1 and MMP-3 in pancreatic cancer is urgently needed in the future.

We also noticed ROS might be an intermediate factor in the high glucose-mediated MMP-3 overexpression. Previous studies found that MMP-3 was regulated by ROS in many models, including pancreatic cancer cell model [22]. Our GSEA result observed an enriched NADPH oxidase pathway in the DM group. The enriched oxidative stress was found in the high MMP-3 expressed group, which indicated NADPH oxidase and ROS might participate MMP-3 related signal pathways. ROS, a group of oxygen-containing chemicals, is an important regulator in many signal pathways. For cancer cells, ROS is essential for tumorigenesis and oncogene initiation. ROS stimulates antioxidation signal pathways to enhance the survival and proliferation of cancer [23].In PDA, ROS level is mainly regulated by NADPH oxidase 4 (NOX4) [24]. The NOX4 expression level directly reflects the ROS level in pancreatic cancer cells and in our study, both elevated ROS and NOX4 expression were found in higher glucose concentration groups [25]. Taken together, it is logical to suppose that MMP-3 may be regulated by ROS, which is initiated by high glucose.

This hypothesis that NOX4-related ROS mediated MMP-3 expression is then validated in our study. Our result indicated that ROS might be the bridge that links a high glucose environment with MMP-3 overexpression. Our *in vitro* study found stimulating NOX4 expression via H_2O_2 or blocking NOX4 expression via setanaxib significantly influenced MMP-3 expression. Setanaxib, a selective NOX4 inhibitor, is a critical ROS inhibitor undergoing clinical trials for cancer therapies, while H_2O_2 was a strong ROS promoter in cancer cells [26, 27]. Through using setanaxib, the MMP-3 expression was similar in HG, MG, and LG. Reversely, interfering MMP-3 expression could not influence NOX4 expression. Single MMP-3 stimulation showed little influence on NOX4 expression from our experimental result and the bioinformatical analysis of GSE50931. As a result, ROS mediated by NOX4 is the upstream signal factor of MMP-3. We also found ROS mediates gemcitabine resistance and cancer invasion altered by a high glucose environment. Blocking NOX4 expression effectively inhibited PDA invasion and gemcitabine sensitivity. And the difference in cell viability between HG, MG, and LG was also reduced when treated with setanaxib. Because of this, ROS may be the intermediate factor in the mechanism of gemcitabine resistance caused by high glucose.

Interestingly, blocking MMP-3 had a better tumor-suppressive effect in gemcitabine-treated pancreatic cancer cells than blocking ROS. And we also found the gemcitabine resistance of the high glucose group was most elevated in 10 μmol/L H_2O_2 treated HG group, not the 50 μmol/L H_2O_2 treated group. This may be because

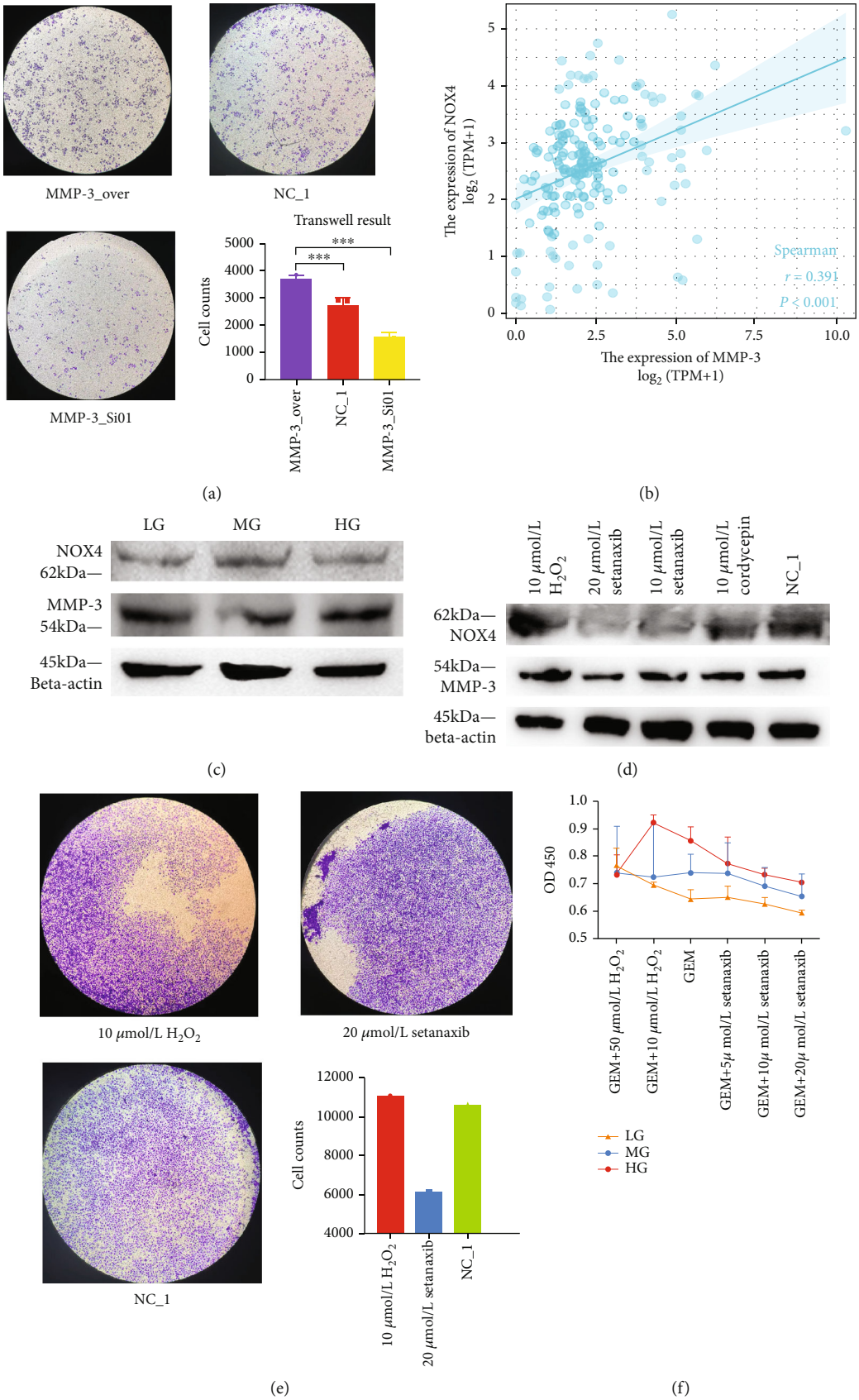

Figure 6: Continued.

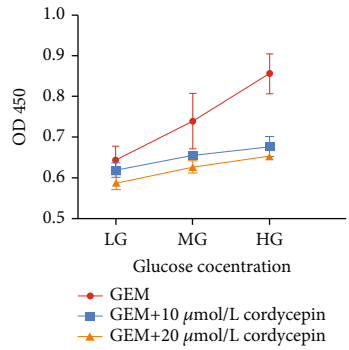

(g)

Figure 6: (a) Transwell analysis of MMP-3 overexpression group (MMP-3_OVER), normal control (NC_1), and MMP-3 silencing group (MMP-3_Si01) ($^{***}P < 0.001$) under 10 μmol/L gemcitabine environment. (b) Spearman analysis of the association between NOX4 and MMP-3 in TCGA database. (c) NOX4 and MMP-3 expression in 20 μmol/L setanaxib treated high glucose, medium glucose, and low glucose group. (d) MMP-3 and NOX4 expression in 10 μmol/L H_2O_2 group, 20 μmol/L NOX inhibitor (setanaxib), 10 μmol/L NOX inhibitor (setanaxib), 10 μmol/L cordycepin, and normal control (NC_1). (e) Transwell analysis of 10 μmol/L H_2O_2 group, normal control (NC_1), and 20 μmol/L NOX inhibitor (setanaxib). (f) The cell viability of BxPc-3 cells treated with 50 μmol/L H_2O_2+10 μmol/L gemcitabine (GEM) group, 10 μmol/L H_2O_2+10 μmol/L GEM group, single 10 μmol/L GEM group, 5 μmol/L setanaxib+10 μmol/L GEM group, 10 μmol/L setanaxib+10 μmol/L GEM group, and 20 μmol/L setanaxib+10 μmol/L GEM group under different glucose groups (HG, MG, and LG). (g) The cell viability of BxPc-3 cells treated with 10 μmol/L GEM group, 10 μmol/L GEM+10 μmol/L cordycepin group, and 10 μmol/L GEM+20 μmol/L cordycepin group under different glucose groups (HG, MG, and LG).

ROS is a double-edged sword in PDA development. ROS promotes cancer progression and induces chemoresistance to protect cancer cells from apoptosis within certain limits. However, exposure to an extremely high ROS level will directly cause DNA damage in cancer cells, thus leading to apoptosis. Based on this, ROS inhibition could lead to a dual inhibition in tumor apoptosis and antiapoptosis [28]. Moreover, ROS was reported to be generated by gemcitabine to impair DNA structure in pancreatic cancer. And this elevated ROS induced by gemcitabine may explain why MMP-3 was overexpressed in the naturally generated gemcitabine-resistant pancreatic cancer cells from another aspect.

5. Conclusion

In this project, we discovered that diabetic status or a high-glucose environment played as a vital role in PDA gemcitabine resistance and invasion, which significantly reduced the survival of pancreatic cancer patients. High glucose elevates gemcitabine resistance via upregulating ROS levels to stimulate MMP-3 overexpression in pancreatic cancer cells. *In vivo* and *in vitro* experiments revealed that targeting MMP-3 effectively relieved gemcitabine resistance and suppressing MMP-3 expression showed a batter effect than inhibiting ROS level. And RRM1 may be the potential downstream factor activated by MMP-3 in the high glucose-mediated gemcitabine resistant metabolism.

Data Availability

The RNA sequence data can be downloaded from https://portal.gdc.cancer.gov (The TCGA-PAAD cohort).

Conflicts of Interest

The authors declare that they have no competing interests in this section.

Authors' Contributions

Dr. Li and Dr. Deng designed the study direction and experimental scheme of this study. Dr. Deliang Fu revised and offered clinical information in this study. Dr. Tianlei Ying offered experiment assistance in this study. Dr. Yujie Guo, Dr. Baian Tao, Dr. Jichun Gu, and Dr. Jiali Du helped revise this study's manuscript and clinical follow-up. Junyuan Deng, Yujie Guo, and Xiaomu Hu contributed equally to this work and as the first author.

Acknowledgments

This project was supported and funded by the National Natural Science Foundation of China (No.81772566), the NSFC-DFG Cooperation Group (GZ1456), and The Future Star of Medical Doctor in Fudan University Training Program.

References

[1] L. Rahib, B. D. Smith, R. Aizenberg, A. B. Rosenzweig, J. M. Fleshman, and L. M. Matrisian, "Projecting cancer incidence and deaths to 2030: the unexpected burden of thyroid, liver, and pancreas cancers in the United States," *Cancer Research*, vol. 74, no. 11, pp. 2913–2921, 2014.

[2] S. Zeng, M. Pöttler, B. Lan, R. Grützmann, C. Pilarsky, and H. Yang, "Chemoresistance in pancreatic cancer," *International Journal of Molecular Sciences*, vol. 20, no. 18, p. 4504, 2019.

[3] Y. Binenbaum, S. Na'ara, and Z. Gil, "Gemcitabine resistance in pancreatic ductal adenocarcinoma," *Drug Resistance Updates*, vol. 23, pp. 55–68, 2015.

[4] C. Morizane, T. Okusaka, J. Mizusawa et al., "Combination gemcitabine plus S-1 versus gemcitabine plus cisplatin for advanced/recurrent biliary tract cancer: the FUGA-BT (JCOG1113) randomized phase III clinical trial," *Annals of Oncology*, vol. 30, no. 12, pp. 1950–1958, 2019.

[5] D. A. American, "2. Classification and diagnosis of diabetes:-standards of medical care in diabetes-2018," *Diabetes Care*, vol. 41, Supplement_1, pp. S13–S27, 2018.

[6] J. Ma, J. Wang, L. Ge, B. Long, and J. Zhang, "The impact of diabetes mellitus on clinical outcomes following chemotherapy for the patients with pancreatic cancer: a meta-analysis," *Acta Diabetologica*, vol. 56, no. 10, pp. 1103–1111, 2019.

[7] D. Li, Y. Mao, P. Chang et al., "Impacts of new-onset and long-term diabetes on clinical outcome of pancreatic cancer," *American Journal of Cancer Research*, vol. 5, no. 10, pp. 3260–3269, 2015.

[8] K. Zeiss, K. G. Parhofer, V. Heinemann et al., "Glucose and lipid metabolism in patients with advanced pancreatic cancer receiving palliative chemotherapy," *Anticancer Research*, vol. 33, no. 1, pp. 287–292, 2013.

[9] C. K. Chu, A. E. Mazo, J. M. Sarmiento et al., "Impact of diabetes mellitus on perioperative outcomes after resection for pancreatic adenocarcinoma," *Journal of the American College of Surgeons*, vol. 210, no. 4, pp. 463–473, 2010.

[10] C. M. Tseng, H. H. Wang, W. L. Wang et al., "Prognostic impact of diabetes mellitus on overall survival in a nationwide population-based cohort of patients with pancreatic cancer," *Endocrine Practice*, vol. 26, no. 7, pp. 707–713, 2020.

[11] S. Supabphol, W. Seubwai, S. Wongkham, and C. Saengboonmee, "High glucose: an emerging association between diabetes mellitus and cancer progression," *Journal of Molecular Medicine (Berlin, Germany)*, vol. 99, no. 9, pp. 1175–1193, 2021.

[12] C. Mehner, E. Miller, D. Khauv et al., "Tumor cell-derived MMP3 orchestrates Rac1b and tissue alterations that promote pancreatic adenocarcinoma," *Molecular Cancer Research*, vol. 12, no. 10, pp. 1430–1439, 2014.

[13] H. Kan, Y. Wang, D. Wang et al., "Cordycepin rescues lidocaine-induced neurotoxicity in dorsal root ganglion by interacting with inflammatory signaling pathway MMP3," *European Journal of Pharmacology*, vol. 827, pp. 88–93, 2018.

[14] Y. Li, K. Li, L. Mao et al., "Cordycepin inhibits LPS-induced inflammatory and matrix degradation in the intervertebral disc," *PeerJ*, vol. 4, article e1992, 2016.

[15] Y. R. Lee, E. M. Noh, E. Y. Jeong et al., "Cordycepin inhibits UVB-induced matrix metalloproteinase expression by suppressing the NF-κB pathway in human dermal fibroblasts," *Experimental & Molecular Medicine*, vol. 41, no. 8, pp. 548–554, 2009.

[16] E. M. Noh, J. S. Kim, H. Hur et al., "Cordycepin inhibits IL-1-induced MMP-1 and MMP-3 expression in rheumatoid arthritis synovial fibroblasts," *Rheumatology*, vol. 48, no. 1, pp. 45–48, 2008.

[17] Y. D. Bhutia, S. W. Hung, B. Patel, D. Lovin, and R. Govindarajan, "CNT1 expression influences proliferation and chemosensitivity in drug-resistant pancreatic cancer cells," *Cancer Research*, vol. 71, no. 5, pp. 1825–1835, 2011.

[18] J. García-Manteiga, M. Molina-Arcas, F. J. Casado, A. Mazo, and M. Pastor-Anglada, "Nucleoside transporter profiles in human pancreatic cancer cells: role of hCNT1 in 2′,2′-difluorodeoxycytidine- induced cytotoxicity," *Clinical Cancer Research*, vol. 9, no. 13, pp. 5000–5008, 2003.

[19] T. Kato, H. Ono, M. Fujii et al., "Cytoplasmic RRM1 activation as an acute response to gemcitabine treatment is involved in drug resistance of pancreatic cancer cells," *PLoS One*, vol. 16, no. 6, article e0252917, 2021.

[20] C. M. Zhu, X. Y. Lian, Y. H. Bi, C. C. Hu, Y. W. Liang, and Q. S. Li, "Prognostic value of ribonucleotide reductase subunit M1 (RRM1) in non-small cell lung cancer: a meta-analysis," *Clinica Chimica Acta*, vol. 485, pp. 67–73, 2018.

[21] F. Vena, E. Li Causi, M. Rodriguez-Justo et al., "The MEK1/2 inhibitor pimasertib enhances gemcitabine efficacy in pancreatic cancer models by altering ribonucleotide reductase subunit-1 (RRM1)," *Clinical Cancer Research*, vol. 21, no. 24, pp. 5563–5577, 2015.

[22] K. Kessenbrock, V. Plaks, and Z. Werb, "Matrix metalloproteinases: regulators of the tumor microenvironment," *Cell*, vol. 141, no. 1, pp. 52–67, 2010.

[23] J. N. Moloney and T. G. Cotter, "ROS signaling in the biology of cancer," *Seminars in Cell & Developmental Biology*, vol. 80, pp. 50–64, 2018.

[24] U. S. Srinivas, B. W. Q. Tan, B. A. Vellayappan, and A. D. Jeyasekharan, "ROS and the DNA damage response in cancer," *Redox Biology*, vol. 25, article 101084, 2019.

[25] K. Bedard and K.-H. Krause, "The NOX family of ROS-generating NADPH oxidases: physiology and pathophysiology," *Physiological Reviews*, vol. 87, no. 1, pp. 245–313, 2007.

[26] K. Ford, C. J. Hanley, M. Mellone et al., "NOX4 inhibition potentiates immunotherapy by overcoming cancer-associated fibroblast-mediated CD8 T-cell exclusion from tumors," *Cancer Research*, vol. 80, no. 9, pp. 1846–1860, 2020.

[27] L. Cao, X. Chen, X. Xiao, Q. Ma, and W. Li, "Resveratrol inhibits hyperglycemia-driven ROS-induced invasion and migration of pancreatic cancer cells via suppression of the ERK and p38 MAPK signaling pathways," *International Journal of Oncology*, vol. 49, no. 2, pp. 735–743, 2016.

[28] Z. He, Q. Xu, B. Newland et al., "Reactive oxygen species (ROS): utilizing injectable antioxidative hydrogels and ROS-producing therapies to manage the double-edged sword," *Journal of Materials Chemistry B*, vol. 9, no. 32, pp. 6326–6346, 2021.

Hindawi
Oxidative Medicine and Cellular Longevity
Volume 2022, Article ID 6439097, 11 pages
https://doi.org/10.1155/2022/6439097

Review Article

Epigenetic Alterations under Oxidative Stress in Stem Cells

Min Huang, Qiang Wu, and Zhi-Hong Jiang

State Key Laboratory of Quality Research in Chinese Medicine, Macau University of Science and Technology, Macau, SAR, China

Correspondence should be addressed to Qiang Wu; qwu@must.edu.mo and Zhi-Hong Jiang; zhjiang@must.edu.mo

Received 15 April 2022; Revised 16 July 2022; Accepted 27 July 2022; Published 29 August 2022

Academic Editor: Alin Ciobica

Epigenetic regulation of gene expression, including DNA methylation and histone modifications, provides finely tuned responses for cells that undergo cellular environment changes. Abundant evidences have demonstrated the detrimental role of oxidative stress in various human pathogenesis since oxidative stress results from the imbalance between reactive oxygen species (ROS) accumulation and antioxidant defense system. Stem cells can self-renew themselves and meanwhile have the potential to differentiate into many other cell types. As some studies have described the effects of oxidative stress on homeostasis and cell fate decision of stem cells, epigenetic alterations have emerged crucial for mediating the stem cell behaviours under oxidative stress. Here, we review recent findings on the oxidative effects on DNA and histone modifications in stem cells. We propose that epigenetic alterations and oxidative stress may influence each other in stem cells.

1. Introduction

Oxidative stress is due to pathologically accumulated excessive free radicals in the body associated with increased lipid peroxidation. Reactive oxygen species (ROS) are broadly considered as a deleterious reactive by-product of oxidative phosphorylation (OXPHOS) through aerobic mitochondrial respiration, although appropriate concentration of harmless ROS is essential to intracellular signaling transduction [1]. Physiological ROS is heavily regulated by antioxidant enzymes, while verbose ROS production is caused by certain lesions. Consequently, the antioxidant defense system fails to scavenge the ROS in time since excessive oxygen free radicals are strong and unstable molecules that represent in varying valences, including singlet oxygen ($^1O_2$), super anion (O_2^-), the hydroxyl radical (OH^-), and hydrogen peroxide (H_2O_2) [2]. These free radicals are reactive to display their inherent chemical properties, which confer reactivity to different biological processes. ROS are generally connected with oxidative stress, which comprehensively damages the cells from molecular to cellular level. Constant exposure to oxidative stress can not only irreversibly retrofit the functional structure of intracellular biomacromolecules but also ultimately result in permanent DNA lesions, leading to cellular damage, homeostasis impairment, and cell fate changes [3].

Chromatin represents the dynamic macromolecular complexes of DNA and histones that folds DNA sequences into eukaryotic nucleus. A nucleosome is a fundamental unit of chromatin that contains a 147 bp of DNA wrapped around the core histone octamers [4]. The N-terminal tails of histones are subjected to provide the reaction sites to undergo multiple posttranslational modifications (PTMs), including acetylation, methylation, phosphorylation and ubiquitylation, and SUMOylation [5]. These covalent modifications are mediated by a set of histone-modifying enzymes [6]. It is widely accepted that PTMs can alter the chromatin conformation into either opening state (euchromatin) or compaction state (heterochromatin) in order to activate/silence gene expression. Interestingly, histone PTMs can be altered by ROS-mediated oxidative stress [7] and plays a role in transcriptional regulation [8].

Human body is an endogenous system of regeneration mediated by tissue stem cells [9]. Stem cells are characterized by their unique properties: self-renewal and multipotency. The self-renewal allows stem cells to be sustained for prolonged periods while holding the potential to differentiate into other cell types [10]. Stem cells can also give rise to

one or more cell type(s) which functionally reconstitute of the tissue of origin [11]. According to their origins, stem cells can be classified into two groups: embryonic stem cells (ESCs) and adult stem cells. ESCs are derived from the inner cell mass of blast-stage embryos. ES cells are pluripotent since they can differentiate into almost all cell types except placental cells [12–14]. In contrast to ESCs, adult stem cells are widely presented in many adult tissues. Adult stem cells are generally restricted to differentiate into a certain cell type as their original organs. It is appeared all stem cells are devoted to regulate a balanced ROS and oxidative stress that maintain their uncommitted state and avoid progressive genetic damages. Hence, understanding the redox biology of stem cells is significant to stem cell therapy in high quality.

This review is aimed at (1) underscoring the redox regulation of stem cell fate decision and (2) reviewing epigenetic alterations and oxidative stress in stem cells.

2. Redox Biology in the Cells

Continuous chemical fuel supplement in the form of ATP is necessary to functionally support essential biomacromolecule synthesis and cellular activities. With the catalysis of ATP synthase, electron transport chain (ETC) is remodeled from the reduced enzymes, such as NADH, and transported to molecular oxygen to from a high-throughput proton current [15]. ATP is mainly produced in mitochondria via TCA/oxidative phosphorylation but also can be generated by other metabolic pathways, such as glycolysis, fatty acid oxidation, and fermentation [16]. Activation of mitochondrial ETC produces powerful proton beam. However, meanwhile, it promotes the formation of ROS on the inner mitochondrial membranes during oxidative phosphorylation [17]. NADH family proteins are the major molecules which response to transfer electrons to the molecular oxygens, while the strong proton current results in creation of mitochondrial membrane potentials by recruiting large amount of positively charged photons from the mitochondrial matrix and transporting them to the intermembrane space [18]. With the assistance of enzymatic complexes, the protons are reciprocally transported to the mitochondrial matrix and alighted to produce a strong force that forms ATP.

In some circumstance, such as exposure of environmental oxygen tension, the electrons from ETC are abruptly blocked, and the partial reduction of molecular oxygen generates electrophilic superoxide anion radicals in the mitochondrial matrix [19]. Such successive generation of free radicals is thought to be mitochondrial ROS molecules. ROS can behave as a key signal molecules freely tramping between inter- and intracellular communication though emitting signal transduction [20]. Another recent view shows that ROS acts as an essential signal transductor that contributes to adapt the environmental cues in the evaluation process [21]. Indeed, ROS in prokaryotes activates the transcription factors for adaptation to stress [22].

Abnormal accumulation of cellular oxygen concentrations may result in an aggravate pressure known as oxidative stress. It is widely accepted that the oxidative stress is primarily caused by the imbalance between generation and elimination of ROS [23]. Under physiological conditions, a certain concentration of acceptable ROS level is maintained with a safe threshold. However, when cells are exposed in unfavorite circumstances, the level of ROS can be dramatically increased and break through the safe threshold [24]. To defense the excessive ROS, the antioxidant systems will rapidly be activated to reduce the ROS level back to the safe threshold. This process is considered as acute oxidative stress [25]. Of note, acute oxidative stress is a temporary pathological process that induces the oxidative damage to the cells within a short period. Yet, in some cases, such as antioxidant system failure or inactivation of antioxidant enzymes, the ROS level is not permanently neutralized. The substantial deposit of ROS no longer returns to the stationary threshold, and the high level of ROS becomes a chronic oxidative stress [26]. Unlike acute oxidative stress, chronic oxidative stress is shown as an irreversible hierarchical damage which can be maintained at a relative higher level. Indeed, chronical oxidative stress is defined as quasi-stationary level [27]. As the continuous load of oxidative stress, many pathological processes result from the associated oxidative stress which can be defined as a pathological term.

Cells must maintain a genetically stable genome against hostile endogenous and exogenous DNA damage agents. Toxic oxidate agents may endanger the genetic materials and result in abrupt upregulation of DNA lesions. In order to protect the genetic materials form DNA damage, cells employ DNA damage response (DDR) pathways that purge, delete, and reset the DNA lesions [28]. In eukaryotes, DNA damage and its repair mechanism are occurred in the context of chromatin. Upon recognizing the DNA damage, several key mediators of DDR are activated immediately to prevent the cumulation of cascading damages. These mediators work cooperatively to delete the errors in different aspects. The DNA lesions are preliminarily recognized by the sensor protein though inspecting lesion sites or chromatin alterations. The transducers are responded to initiate the repair action and transit the damage signal to the downstream effectors [29]. Failure to fix DNA errors may multifacetedly result in genetic mutation and deviant chromosomal remodelling [30]. Remarkably, a robust DDR is critical to maintain a redox homeostasis in stem cells since replication errors in stem cells not only inherit a detrimental genetic material to the progeny but also destroy their differentiation potentials [31]. For example, in mouse ESCs, p53 suppresses Nanog transcription though binding to its promoter. The inhibition of Nanog by p53 facilitates the elimination of damaged cells from the replicating stem cells, followed by the establishment of an efficient p53-dependent cell cycle arrest or apoptotic program in differentiated progeny cells [32].

Notably, many studies have demonstrated that ROS, mitochondria, and oxidative stress play important roles in apoptosis [33]. Conversely, antioxidants and thiol reductants can inhibit apoptosis [33]. For instance, increase of ROS level resulted from environmental toxicants can be harmful

to oocyte mitochondria and may lead to mitochondria dysfunction and cellular apoptosis [34]. Bmi1 is important to regulate mitochondrial function and control ROS level in diverse cell types [35]. However, in T cells, depletion of Bcl-2 is not related to Bmi1 but can cause T cells be sensitized to apoptosis by ROS [36]. In addition, p62/SQSTM1 plays an important role in the antioxidant property of hepatocytes [37]. Interestingly, recent studies have shown that nanoparticles can be a useful mediator for ROS release specifically to cancer cells for cancer therapy. Stannic oxide nanoparticles (NPs) can induce oxidative stress, inhibit cell growth, and induce apoptosis of breast [38] and oral cancer cells [39]. However, a more in-depth study is needed to determine its roles. Bismuth oxide NPs can induce ROS generation and cytotoxicity, thus causing cancer cell apoptosis [40]. In contrary, oxidative stress and cytotoxicity induced by heavy metal Pb in human lung cells (A549) can be prevented by TiO_2 nanoparticles [41]. Hence, it will be worth further research on different nanoparticles which can mediate oxidative stress in cancer therapy.

2.1. Oxidative Stress in Stem Cells. The dose of oxidative stress loaded in stem cells is critical to maintain their stem cell identity and homeostasis. Low concentration of ROS is essential for maintaining ESCs in undifferentiated state, while ROS-mediated oxidative stress can modulate stem cell differentiation, senescence, apoptosis, and repopulation [42]. In addition, appropriate level of ROS can accelerate reprogramming process [43]. Therefore, ROS signaling is critical to the stem cell fate decision.

It is noteworthy that pluripotent stem cells and adult stem cells have complete different metabolic programs. Pluripotent stem cells (PSCs) including embryonic stem cells (ESCs) and induced pluripotent stem cells (iPSCs) heavily reply on glycolysis as main energy source to meet their energy demands. Similarly, suppression of mitochondrial respiration is beneficial to maintain the pluripotency. Indeed, either promotion of glycolysis or suppression of oxidative phosphorylation can accelerate the reprogramming process during which somatic cells are converted into induced pluripotent stem cells (iPSCs) [44]. Considering the hypoxic condition in the uterus, it is not surprising that ESCs—the *in vitro* counterpart of inner cell mass in the early embryo—prefer glycolysis. ESCs indeed have less mitochondria mass with immature morphology and maintain their stemness at lower oxygen level [45]. Interestingly, human ESCs showed stronger resistance to oxidative and genotoxic stress as compared with somatic cells [46]. Consistently, pluripotent stem cells in naïve state present a relatively higher oxidative phosphorylation level in primed state [47]. In addition, most iPSC clones produced from aged tissue donors do not suppress the oxidative phosphorylation; only young iPSCs produced from young tissue donor and ESCs are able to reset the oxidative phosphorylation into glycolysis [48]. Hence, the dynamic equilibrium between the generation and elimination of ROS must be tightly regulated in pluripotent stem cells.

Although ESCs favor glycolysis to generate energy, regulating balanced ROS level is important to preserving mtDNA integrity in ESCs [49]. Compared with nuclear DNA, mtDNA has a relatively higher risk of mutation because they are structurally naked and have higher chance of replication errors [50]. The expression of mtDNA remains at a low level in ESCs, and it only shows a transient increase during ESC differentiation. In addition, the mitochondrial genome is spatially close to the inner mitochondrial membrane and thereby susceptible to the ROS damage [51]. The pathogenic mtDNA molecules result in aberrant mitochondrial respiration. Therefore, an optimal ROS is important to functionally preserve the normal mtDNA integrity in ESCs.

In order to maintain the genomic stability, the stress control and DNA repair in ESCs are particularly more stringent, compared with differentiated cells [52], while DNA repair capability may gradually loss during development. The high proliferation of ESC is attributed to the distinct cell cycle where the G1 phase is much shorter than differentiated cells since ESCs do not suffer from replicative senescence [53]. Like many cells, ESCs are exquisitely sensitive to the oxidative toxicity which can directly alter their regular cell cycle. Under high oxygen tension, ESCs shortly enter the cell cycle arrest state at G2/M phase although they can establish an expeditious recovery machinery to restore the normal cell cycle [54]. In addition, increased mitochondrial ROS production retards the cell proliferation rate with longer S phase [55]. Taken together, these studies suggest that endogenous ROS regulates ES cell propagation through modulating their cell cycle progression.

Though ESCs are originally resistant to the oxidative stress due to their recovery machinery of cell cycle, high level of oxidative phosphorylation in ESCs not only gradually results in ESC differentiation but also induces apoptosis [56]. Several studies have demonstrated the benign effects of elevated ROS during cardiac differentiation. At pluripotent state, ROS degrades the SIRT1 deacetylase by recruiting the FOXO proteins [57], which is a key family that regulates the master pluripotent genes in human ESCs [56]. During differentiation, acute eruption of ROS promotes ESC development towards cardiomyocyte phenotype, while chronic treatment of H_2O_2 terminates the differentiation process [58]. Oxidative stress further activates the Notch1 pathway and hence enhances the cardiogenic lineage specification [59].

Adult stem cells, such as mesenchymal stem cells (MSCs), hematopoietic stem cells (HSCs), and neural stem cells (NSCs), are more sensitive to physiological oxygen tension than pluripotent stem cells. Indeed, MSCs cultured in an atmospheric oxygen show a low cell proliferation with accelerating senescence in comparison with the physiological oxygen [60]. Similarly, exposure of HSCs to an environmental oxygen tension may induce extra physiologic oxygen shock/stress [61]. Prolonged quiescent HSCs barely need cellular ROS, while active HSCs require endogenous ROS for proper differentiation [62]. Approximately 1% of low oxygen condition is advantageous to maintain the human c-Kit+ cardiac progenitor cell survival and expansion [63]. In addition, the concentration of intracellular ROS varies in different state of the adult stem cells. For instance, embryonic neural stem cells have slightly higher cellular ROS level

to support their stem cell survival and expansion and further increase when stem cells transit from proliferation to differentiation [64]. The ROS level in MSCs, another examples, is tightly regulated in an extremely low stage in undifferentiated state while relatively enhanced during their differentiation into adipocytes [65]. Analogous study also suggests that high level of ROS with addition of exogenous H_2O_2 promotes the redirectional differentiation of MSCs into adipocytes [66]. In fact, the suppression of mitochondrial metabolism decelerates the adipogenic differentiation process because reduction of mitochondrial respiration diminishes the production of ROS [67]. Furthermore, increased ROS level is essential to support the chondrogenesis in ATDC5 cells and primary chondrocytes derived from mouse embryos [68]. These evidences concordantly demonstrate that ROS and oxidative stress are necessary for stemness and differentiation of adult stem cells.

2.2. Oxidative Stress and DNA. DNA methylation and histone modifications are the most well-understood epigenetic mechanisms. DNA methylation occurs on CpG dinucleotide and mainly mediates gene silencing. The addition of methyl groups by DNA methyltransferases (DNMTs) alters the structure of the major groove of DNA where the proteins attach, leading to heritable changes in the chromatin structure [69, 70]. In early embryonic development, lineage-specific genomic methylation patterns are created by *de novo* transferases DNMT3A and DNMT3B. The established patterns are further copied by cell divisions by the preservation of DNMT1. Loss of DNMT3A in iPSCs affects the physiological cardiomyocyte homeostasis though activating PPARγ, where it accumulates with lipid vacuoles [71]. Mice with DNMT3B aberrant methylation are featured as neural disorder [72].

DNA constituents are especially susceptible to the damaging effects of ROS, such as 8-hydroxyguanine (8-oxo-dG), which is the most familiarly generated base lesion and a good measure of oxidative damage in DNA. Upon oxidative stress, the hydroxyl radical reacts with the guanine (G) sites of DNA sequence which is the most sensitive to oxidative stress out of the four bases in DNA. 8-oxo-dG further destroys other bases to cause oxidation where occurs G ➔ T mutations [73]. Such a transversion caused by ROS is believed as inherently mutant site on a nascent strand, and the presence of 8-oxo-dG may give an undesirable methylation to the adjacent sites, such as cytosine bases from the damaged guanine [74, 75]. A relatively high dose of 8-oxo-dG in the DNA seemly tends to change various stem cell activities. In mouse ESCs, a steady-level of 8-oxo-dG theoretically can arise a considerable amount of mutation sties after cell division [76]. A recent study reports that oxidative stress generated from immune cells can suppress the DNMT activity in proliferating cells [77]. Consistently, a genome-wide study showed that oxidative damage can induce an inheritable mutated DNA methylation pattern and sublethal dose of hydrogen peroxide is enough to damage DNA methylation patterns in proliferation cells [78]. Deletion of DGCR8 in MSCs is associated with a hypermethylation in the CpG island upstream of SOD2, leading to slow proliferation rate with increased ROS level [79].

During embryonic development, a key epigenetic factor known as ten-eleven translocation (TET) can reprogram DNA methylation pattern. In mouse ESCs, Tet1 is acquired for ES cell maintenance, and downregulation of Tet1 correlatively suppresses DNA methylation of *Nanog* promoter, indicating a causative role of Tet1 in DNA methylation [80]. Interestingly, the TET proteins can successively oxidize 5-methylcytosine (5-mc) to 5-hydroxymethylcytosine (5-hmC) [81] as a resultant of demethylation of CpG site modification [82] and subsequently into 5-formylcytosine and 5-carboxylcytosine [83]. All 5-mc oxidation products behave as the intermediates which response to the conversion of 5-mc to the unmodified cytosines. In advanced pronuclear-stage zygotes of mouse embryogenesis, the paternal pronucleus has a certain level of 5-hmC but low level of 5-mC. Importantly, deficiency of Tet3 may erase both 5-hmC and 5-mC pattern [84].

Like methylation of nuclear DNA, mtDNA can also methylated into 5-mC in presence of mtDNMT1. Cells with the ample energy demand are expected to increase mitochondria mass with a relatively high copied number of mtDNA, which is used to monitor the mtDNA methylation state. Deletion of mtDNA may change nuclear genome which is caused by damaging the potential of oxidative damage recovery [85]. In addition, a proportion of global DNA methylation is potentially mtDNA methylation [86]. In mammals, redox stress contributes to activate a set of nuclear-encoded transcription factors, such as PCG1alpha and NRF1 [87]. The PCG1alpha/NRF1 complex positively regulates the TFAM transcription and ordinates the core ETC complexes, which imply that mitochondria proper may also regulate the cytosine methylation level [88]. Therefore, it appears that there is a delicate interrelationship between nuclear and mitochondria. For instance, 5-hmc can be detected in mtDNA and TET proteins can be also identified in the mitochondrial protein fractions [89]. TET proteins can interact with several intermediates of Krebs cycle, such as JmjC and alpha-ketoglutarate, that serve as a potent substrate of mitochondrial ROS production. Therefore, mitochondrial integration can influence DNA methylation by multifaced aspects, either by modulating the ROS level or regulating the intermediates of Krebs cycle, and thereby regulate the DNMTs and TET proteins [90].

mtDNA methylation is a critical epigenetic regulation in mitochondrial activity in stem cells. The mitochondrial methylation level is downregulated in aged human cardiac mesenchymal stem cells [91]. By profiling the CpG methylation status across the mitochondrial genome, researchers showed that aged MSCs treated with chronic oxidated stress appear to show a global mtDNA hypomethylation [92]. In turn, the nuclear *de novo* methyltransferase level can disturb the mitochondrial biogenesis. In human ESCs, loss of DNMT3B destroys the mitochondrial fission and fusion balance, leading to decreased mtDNA level and transition from the glycolytic metabolism to oxidative phosphorylation [93]. Indeed, ESCs that have different DNA haplotypes display multiple gene activities associated with stemness, DNA methyltransferases, and energy metabolism [94]. Overall, these results show that mitochondrial DNA methylation

significantly contributes to global methylation pattern in stem cells.

In all, mitochondrial DNA methylation has been recognized as an emerging DNA methylation pattern that is sensitive to oxidative stress. Mitochondrial ROS production modulates the epigenetic prolife in both nuclear DNA and mitochondrial DNA. Thus, it is of great interest to further study the correlations among mitochondrial DNA methylation, genomic DNA methylation, and oxidative stress.

2.3. Oxidative Stress and Histone (De)acetylation in Stem Cells. Histone acetylation is mediated by histone acetyltransferases (HATs). It is generally associated with open chromatin and gene activation. On the contrary, histone deacetylation is mediated by histone deacetylases (HDACs) that condenses the chromatin and inhibits transcriptional activities [95]. Hyperacetylation on the N-terminal tail of histones H3 and histone H4 has a strong propensity to activate the gene expression through unfastening the chromatin condensation and thereby increasing the accessibility of DNA to transcription factors. There are three HAT families: p300/CBP, GNAT, and MYST [96]. To date, a total of 18 mammalian HDACs have been identified and categorized into four classes in accordance with their homology to yeast HDACs. Class I HDACs are mainly to regulate the cell growth and death, and class II HDACs are predominantly in lineage specification during embryonic development. NAD+-dependent class III HDACs are responsible for sirtuin-associated metabolism. Class IV HDAC (only one member HDAC11) is restricted in several organs, such as kidneys, testis, and brain [97].

The redox state of cells contributes to regulate chromatin remodelling and mediate gene expression. It is widely accepted that increased oxidative stress is implicated to enhance histone acetylation, particularly in acetylation of histone H3 and H4. High oxidative stress level has been reported to alter the hyperacetylation of histone proteins by activation of nuclear factor kappa B in human alveolar epithelial cells [98]. ROS production has been shown to control the histone acetylation differentially in various cell types [99]. A recent study shows that an increased mitochondrial ROS caused by Sod2 downregulation in stromal precursor cells inhibits differentiation potentials of osteogenesis and adipogenesis and induces chromatin condensation with a reduction of histone H3K27 acetylation [100]. Indeed, high level of SOD2 causes increased ROS level and facilitates histone H3 acetylation though promoting the recruitment of p300/CBP [101]. On the other hand, p300/CBP can also acetylate histone H3K9 to increase the ROS production [90]. Therefore, HAT p300/CBP complex appears to dynamically regulate the balance of ROS in cells.

Acetylation state in mitochondrial proteins is determinant to the mitochondrial function. Differentiation of MSCs into osteoblast differentiation is accompanied with increasing KLF2 level which activates histone H3K27ac and H3K4me3, during which mitochondrial ROS is suppressed [102]. The acetylation level modulated by oxidative stress was recently shown to determine the HSC quiescence by regulating SRC expression [103]. SRC3 is not only essential to maintain the quiescence status of HSCs by the prevention of ROS accumulation but also retains the acetylation level though direct recruitment of GCN5 to its promoter region. In mice model, high level of GCN5 can prevent the overactivated mitochondrial metabolism which may give excessive production of ROS induced by SRC3 deficiency, thereby rescuing the cell from oxidative damage [104]. During mammalian development, Hat1 is responsible for catalysing histone H4 on lys 5 and 12 in chromatin remodelling. Partially knocking down MEFs is shown to induce redox damage with increased the sensitivity to ROS level, leading to mitochondria developmental failure [105].

ROS can also change the regular molecular mechanisms of HDACs, particularly in class I and II HDACs. The condensed chromatin structure mediated by HDACs can be relaxed by ROS-mediated alterations, thus activating the aberrant gene expression [106]. More seriously, the oxidative damage mediated by other redox stress, such as lipid peroxides, may further result in carbonylation of class I HDACs [107]. Under pathophysiological oxidative stress, covalently modified cysteine residues of the HDAC1 can cause the decrease of histone deacetylase activity. In addition, the activity of HDAC2 can be downregulated by undergoing hypophosphorylation in high oxygen tension [108]. In mouse model, Sirt3 belonged to class III HDACs and can reduce ROS level though deacetylating Foxo3 [109]. Sirt3 can also stimulate antioxidant enzymes by activating the NF-κB pathway [110]. Collectively, these evidences suggest that oxidative stress related to HDACs may attenuate their activity and expression and initiate the gene expression.

Proper regulation of HDACs decisively contributes to maintain a steady homeostasis in stem cells. SIRT1, the most conserved NAD+-dependent protein deacetylase, is involved in various stem cell activities. Sirt1 regulates mouse ESC differentiation through regulating the deacetylation of CRABPII [111]. In human MSCs, SIRT1 is supposed to regulate RUNX2 transcription which was induced by deacetylation of FOXO3 [112]. Suppression of SIRT1 leads to impairment of adipogenic/osteoblastic lineage commitment. Interestingly, the oxygen tension may change the stem cell characteristics, and subtle change in redox stress change found in different brain pathologies controls the cell fate of NPCs through histone deacetylase (HDAC) SIRT1 [113]. SIRT3 is also correlated to antioxidant enzyme activities. Upregulation of SIRT3 supports the human MSC to against the high oxidative stress. Conversely, loss of SIRT3 in human MSCs stimulates the cellular susceptibility to oxidative stress [114].

Overall, oxidative stress largely affects HDAC-mediated proliferation and differentiation in stem cells.

2.4. Oxidative Stress and Histone (De)methylation in Stem Cells. Unlike histone acetylation, methylation of histone proteins can be associated with either activation or silence of gene transcription. Histone methylation is catalysed by histone methyltransferases (HMTs) on specific histone lysine/arginine residues, particularly in histone H3 and H4, contributing to the high order of the chromatin structures. Histone H3K4me3 marks active promoters, while histone H3K9me3 and H3K27me3 silenced genes. Histone

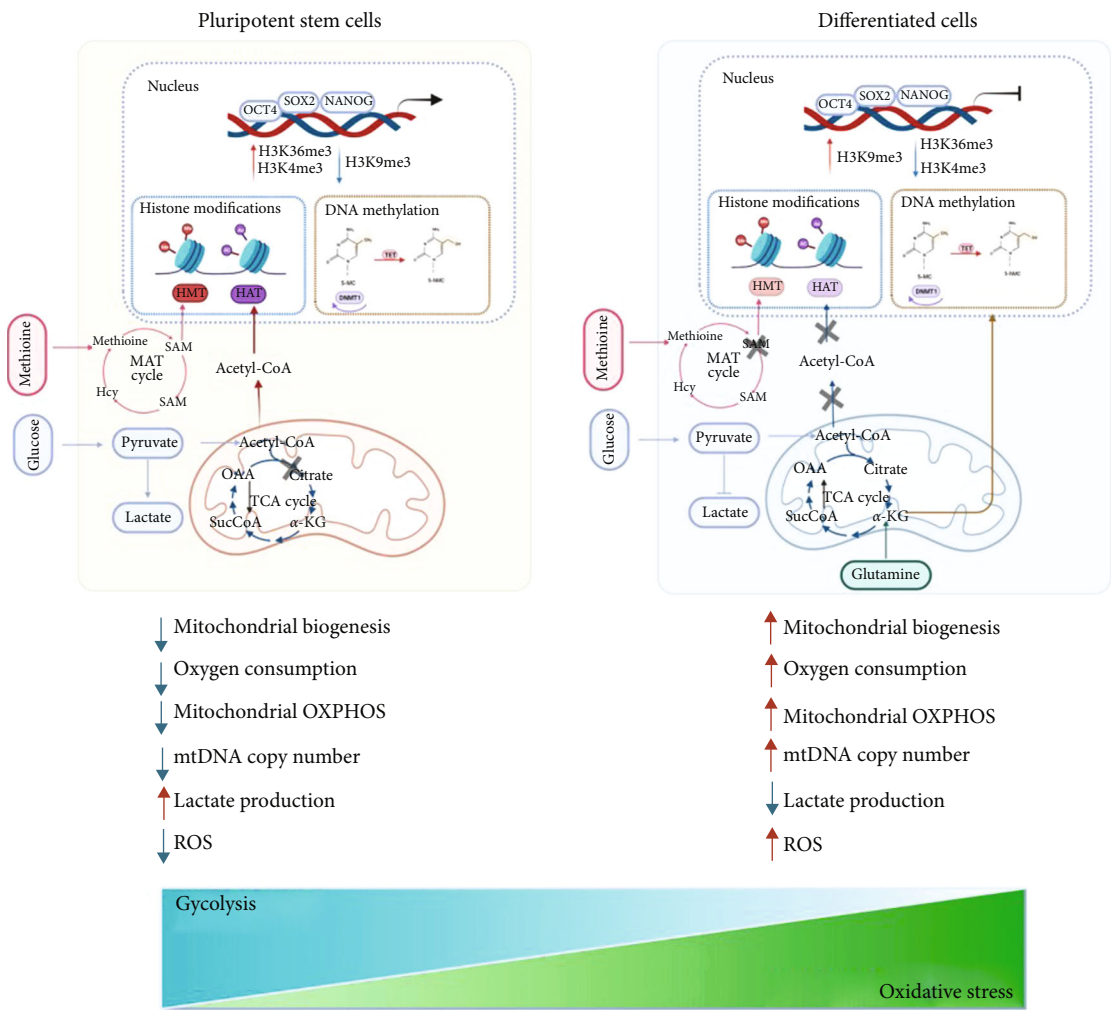

Figure 1: Epigenetic landscape modulated by oxidative stress in pluripotent stem cells and differentiated cells. OCT4, SOX2, and NANOG are core regulators to control cell identity in pluripotent stem cells. Histone marks H3K4me3 and H3K36me3 are located at pluripotent genes and H3K9me3 marks silenced genes. Histone proteins undergo a series of histone modifications, while DNA located at the CpG island is prone to occur DNA methylation. MAT cycle produces SAM which provides a methyl donor molecule utilized in histone methylation. Pluripotent stem cells (PSCs) heavily rely on glycolysis as the main the energy resource. In PSCs, most acetyl-CoA produced from TCA cycle are used for histone acetylation. The mitochondrial biogenesis is suppressed in PSCs. Subsequently, low level of αKG suppresses DNA methylation. In differentiated cells, OCT4, SOX2, and NANOG were suppressed. Loss of SAM inactivates histone methylation. Differentiated cells exhibit active aerobic respiration. Most acetyl-CoA enters the TCA cycle. Meanwhile, glutamine metabolism promotes high level of αKG that subsequently facilitates DNA methylation. HMT: histone methyltransferase; HAT: histone acetyltransferase; TET: ten-eleven translocation; DMT1: DNA methyltransferases 1; MAT: methionine adenosyltransferase; SAT: S-adenosyl methionine.

H3K27me3 is important in stem cells as it marks many silenced lineage genes [115–118]. Gene silence mark H3K9me3 is thought to positively correlate to the degree of adjacent lysine residues on H3 [119]. The reversible removal of histone methylation marks is mediated by histone demethylases [120]. Interestingly, a histone demethylase, JHDM1, can oxidatively catalyse H3K36me2 by configurating its evolutionarily conserved JmjC domain, which can induce radical-based oxidative reactions and catalyse methylation of trimethylated substrates [121]. Therefore, oxidative stress level can change histone methylation status through modulating the level of HMTs. Notably, both JmjC and LSD1 require the cofactors to mediate de methylation. LSD1-mediated demethylation via a FAD-dependent oxidative reaction suggests that methylation of histone lysine can be removed by oxidative histone demethylases [120]. JmjC domain proteins require iron (II), molecular oxygen, and ą-ketoglutarate and are relatively highly sensitive to oxidative stress [122]. The free radicals oxidize the iron (II) to (III) in the catalytical centre of histone demethylases and suppress their activity, hence inducing histone hypermethylation.

Several studies have demonstrated that aberrant methylation on histone can regulate the lineage differentiation of bone marrow-derived MSCs [123]. EZH2 also known as KMT6A catalyses the addition of methyl groups to H3K27, and it selectively promotes the adipogenesis with suppression of osteogenic lineages during MSC differentiation [124]. EZH2 is recently reported that it behaves as a

suppressor of the antioxidant defense system in MSCs. EZH2 can enhance the level of H3K27me3 on the promoter of *Foxo1* and suppress its function to activate the downstream genes in antioxidant defense, leading to oxidative damage [125].

2.5. Epigenetic Control of Oxidative Stress in Embryogenesis. Genes are inherited from parental genomes and subsequently remodelled their specific sequence during meiosis. The recombined sequence remains unaltered through cell divisions, only when there is a replication error or harmful external exogenous source. Any epigenetic alteration presented in the genetic materials is correlated with the states of the gene activity during embryogenesis. The ovary is thought to a metabolically activated organ where the embryo faces oxygen paradox. A carefully balanced redox condition is a necessary prerequisite for early embryo development. Oxidative level in maternal reproductive system is associated with tissue remodelling, steady hormone maintenance, and cyclic endometrial regulation during menstruation. Undoubtedly, considerable production of ROS certainly facilitates the ovulation and germ cell identity [126]. During folliculogenesis, the involvement of acceptable oxidative tension promotes dominant follicle selection and ovulation induction [127]. However, involvement of superfluous ROS has been acknowledged as a decisive factor in early embryonic development. Evidence from human studies has shown that elevated oxidative DNA damage in sperm may reduce pregnancy rates [128]. High tension of seminal oxygen has also been correlated with sperm morphological defects [129] and rewrites the global methylation pattern in sperm, which in turn results in an increased preimplantation embryonic loss [130]. These evidences strongly suggest oxidative stress, and resulted epigenetic alterations play negative role in proper early embryogenesis. Nonetheless, given that epigenetic modifications are crucial to establish the correct epigenetic marks that regulate the physiological gene pattern at early stage of mammalian development, it is of great interest to further investigate histone modifications and DNA methylation/demethylation alterations in embryogenesis under oxidative stress.

3. Concluding Remarks

Recent studies have provided persuasive evidences that have highlighted the linkage of oxidative stress and epigenetic regulation in stem cells. Here, we illustrate the roles of oxidative stress in the evens of DNA methylation and histone PTMs (Figure 1). However, the epigenetic alterations under oxidative stress in stem cells have been poorly studied. More efforts are required to comprehensively understand the role of oxidative stress in stem cell epigenetics. For instance, epigenetics appears to delegate a complicated mechanism that involves various factors with ordination of multiple signal transduction. However, we lack ideal stem cell model system that simulates the nature of epigenetics in presence of ROS. High-throughput sequencing may help us to speculate the global changes in epigenetics caused by ROS. Apart from these issues, identifying novel epigenetic regulators can not only deepen our knowledge about oxidative stress in stem cells but also can provide new insights into stem cell therapy. Therefore, elucidating the molecular mechanism of epigenetic alterations mediated by oxidative stress in stem cells not only achieves the regenerative goals but also provides a novel and selective therapeutic approach to treat various diseases.

Data Availability

Data used to support the findings of this study are included within the article.

Conflicts of Interest

The authors declare that they have no conflicts of interest.

Acknowledgments

This work was supported by the Macau Science and Technology Development Fund (FDCT) (file number 0072/2019/A2 and file number SKL-QRCM (MUST)-2020-2022).

References

[1] D. D. Gutterman, "Mitochondria and reactive oxygen species: an evolution in function," *Circulation Research*, vol. 97, no. 4, pp. 302–304, 2005.

[2] J. N. Peoples, A. Saraf, N. Ghazal, T. T. Pham, and J. Q. Kwong, "Mitochondrial dysfunction and oxidative stress in heart disease," *Experimental & Molecular Medicine*, vol. 51, no. 12, pp. 1–13, 2019.

[3] L. Hecker, J. Cheng, and V. J. Thannickal, "Targeting NOX enzymes in pulmonary fibrosis," *Cellular and Molecular Life Sciences*, vol. 69, no. 14, pp. 2365–2371, 2012.

[4] R. D. Kornberg and J. O. Thomas, "Chromatin structure; oligomers of the histones," *Science*, vol. 184, no. 4139, pp. 865–868, 1974.

[5] T. Kouzarides, "Chromatin modifications and their function," *Cell*, vol. 128, no. 4, pp. 693–705, 2007.

[6] F. Gong and K. M. Miller, "Histone methylation and the DNA damage response," *Mutation Research, Reviews in Mutation Research*, vol. 780, pp. 37–47, 2019.

[7] J. L. García-Giménez, C. Garcés, C. Romá-Mateo, and F. V. Pallardó, "Oxidative stress-mediated alterations in histone post-translational modifications," *Free Radical Biology & Medicine*, vol. 170, pp. 6–18, 2021.

[8] D. Ziech, R. Franco, A. Pappa, and M. I. Panayiotidis, "Reactive oxygen species (ROS)–induced genetic and epigenetic alterations in human carcinogenesis," *Mutation Research*, vol. 711, no. 1-2, pp. 167–173, 2011.

[9] S. Bajada, I. Mazakova, B. A. Ashton, J. B. Richardson, and N. Ashammakhi, "Stem cells in regenerative medicine," *Topics in tissue engineering*, vol. 4, pp. 1–28, 2008.

[10] M. Amit, M. K. Carpenter, M. S. Inokuma et al., "Clonally derived human embryonic stem cell lines maintain pluripotency and proliferative potential for prolonged periods of culture," *Developmental Biology*, vol. 227, no. 2, pp. 271–278, 2000.

[11] T. Reya, S. J. Morrison, M. F. Clarke, and I. L. Weissman, "Stem cells, cancer, and cancer stem cells," *Nature*, vol. 414, no. 6859, pp. 105–111, 2001.

[12] M. J. Evans and M. H. Kaufman, "Establishment in culture of pluripotential cells from mouse embryos," *Nature*, vol. 292, no. 5819, pp. 154–156, 1981.

[13] G. R. Martin, "Isolation of a pluripotent cell line from early mouse embryos cultured in medium conditioned by teratocarcinoma stem cells," *Proceedings of the National Academy of Sciences of the United States of America*, vol. 78, no. 12, pp. 7634–7638, 1981.

[14] J. A. Thomson, J. Itskovitz-Eldor, S. S. Shapiro et al., "Embryonic stem cell lines derived from human blastocysts," *Science*, vol. 282, no. 5391, pp. 1145–1147, 1998.

[15] A. M. Morelli, S. Ravera, and I. Panfoli, "The aerobic mitochondrial ATP synthesis from a comprehensive point of view," *Open Biology*, vol. 10, no. 10, article 200224, 2020.

[16] P. Neupane, S. Bhuju, N. Thapa, and H. K. Bhattarai, "ATP synthase: structure, function and inhibition," *Biomolecular concepts*, vol. 10, no. 1, pp. 1–10, 2019.

[17] R. Chianese and R. Pierantoni, "Mitochondrial reactive oxygen species (ROS) production alters sperm quality," *Antioxidants (Basel)*, vol. 10, no. 1, p. 92, 2021.

[18] X. Li, P. Fang, J. Mai, E. T. Choi, H. Wang, and X. F. Yang, "Targeting mitochondrial reactive oxygen species as novel therapy for inflammatory diseases and cancers," *Journal of Hematology & Oncology*, vol. 6, no. 1, p. 19, 2013.

[19] W. Peng, G. Cai, Y. Xia et al., "Mitochondrial dysfunction in atherosclerosis," *DNA and Cell Biology*, vol. 38, no. 7, pp. 597–606, 2019.

[20] B. S. Khakh and G. Burnstock, "The double life of ATP," *Scientific American*, vol. 301, no. 6, pp. 84–92, 2009.

[21] Z. A. Wood, L. B. Poole, and P. A. Karplus, "Peroxiredoxin evolution and the regulation of hydrogen peroxide signaling," *Science*, vol. 300, no. 5619, pp. 650–653, 2003.

[22] P. J. Kiley and G. Storz, "Exploiting thiol modifications," *PLoS Biology*, vol. 2, no. 11, 2004.

[23] V. Bhatia and S. Sharma, "Role of mitochondrial dysfunction, oxidative stress and autophagy in progression of Alzheimer's disease," *Journal of the Neurological Sciences*, vol. 421, article 117253, 2021.

[24] V. I. Lushchak, "Free radicals, reactive oxygen species, oxidative stress and its classification," *Chemico-Biological Interactions*, vol. 224, pp. 164–175, 2014.

[25] H. Sies, "Oxidative stress: oxidants and antioxidants," *Experimental Physiology*, vol. 82, no. 2, pp. 291–295, 1997.

[26] V. I. Lushchak, "Environmentally induced oxidative stress in aquatic animals," *Aquatic Toxicology*, vol. 101, no. 1, pp. 13–30, 2011.

[27] V. I. Lushchak, "Glutathione homeostasis and functions: potential targets for medical interventions," *Journal of Amino Acids*, vol. 2012, Article ID 736837, 26 pages, 2012.

[28] J. W. Harper and S. J. Elledge, "The DNA damage response: ten years after," *Molecular Cell*, vol. 28, no. 5, pp. 739–745, 2007.

[29] A. Barzilai and K. Yamamoto, "DNA damage responses to oxidative stress," *DNA Repair*, vol. 3, no. 8-9, pp. 1109–1115, 2004.

[30] E. P. Rogakou, D. R. Pilch, A. H. Orr, V. S. Ivanova, and W. M. Bonner, "DNA double-stranded breaks induce histone H2AX phosphorylation on serine 139," *The Journal of Biological Chemistry*, vol. 273, no. 10, pp. 5858–5868, 1998.

[31] R. Hakem, "DNA-damage repair; the good, the bad, and the ugly," *The EMBO Journal*, vol. 27, no. 4, pp. 589–605, 2008.

[32] T. Lin, C. Chao, S.'. Saito et al., "p53 induces differentiation of mouse embryonic stem cells by suppressing Nanog expression," *Nature Cell Biology*, vol. 7, no. 2, pp. 165–171, 2005.

[33] K. Kannan and S. K. Jain, "Oxidative stress and apoptosis," *Pathophysiology*, vol. 7, no. 3, pp. 153–163, 2000.

[34] K. F. Malott and U. Luderer, "Toxicant effects on mammalian oocyte mitochondria†," *Biology of Reproduction*, vol. 104, no. 4, pp. 784–793, 2021.

[35] Y. Chen, L. Li, W. Ni et al., "Bmi1 regulates auditory hair cell survival by maintaining redox balance," *Cell Death & Disease*, vol. 6, no. 1, article e1605, 2015.

[36] D. A. Hildeman, T. Mitchell, B. Aronow, S. Wojciechowski, J. Kappler, and P. Marrack, "Control of Bcl-2 expression by reactive oxygen species," *Proceedings of the National Academy of Sciences of the United States of America*, vol. 100, no. 25, pp. 15035–15040, 2003.

[37] S. Haga, T. Ozawa, Y. Yamada et al., "p62/SQSTM1 plays a protective role in oxidative injury of steatotic liver in a mouse hepatectomy model," *Antioxidants & Redox Signaling*, vol. 21, no. 18, pp. 2515–2530, 2014.

[38] M. Ahamed, M. J. Akhtar, M. A. M. Khan, and H. A. Alhadlaq, "SnO2-doped ZnO/reduced graphene oxide nanocomposites: synthesis, characterization, and improved anticancer activity via oxidative stress pathway," *International Journal of Nanomedicine*, vol. Volume 16, pp. 89–104, 2021.

[39] H. Li, Q. Li, Y. Li, X. Sang, H. Yuan, and B. Zheng, "Stannic oxide nanoparticle regulates proliferation, invasion, apoptosis, and oxidative stress of oral cancer cells," *Frontiers in Bioengineering and Biotechnology*, vol. 8, p. 768, 2020.

[40] M. Ahamed, M. J. Akhtar, M. A. M. Khan, S. A. Alrokayan, and H. A. Alhadlaq, "Oxidative stress mediated cytotoxicity and apoptosis response of bismuth oxide (Bi_2O_3) nanoparticles in human breast cancer (MCF-7) cells," *Chemosphere*, vol. 216, pp. 823–831, 2019.

[41] M. Ahamed, M. J. Akhtar, and H. A. Alhadlaq, "Preventive effect of TiO_2 nanoparticles on heavy metal Pb-induced toxicity in human lung epithelial (A549) cells," *Toxicology in Vitro*, vol. 57, pp. 18–27, 2019.

[42] W. Droge, "Free radicals in the physiological control of cell function," *Physiological Reviews*, vol. 82, no. 1, pp. 47–95, 2002.

[43] G. Zhou, S. Meng, Y. Li, Y. T. Ghebre, and J. P. Cooke, "Optimal ROS signaling is critical for nuclear reprogramming," *Cell Reports*, vol. 15, no. 5, pp. 919–925, 2016.

[44] X. Liu, M. Wang, T. Jiang, J. He, X. Fu, and Y. Xu, "IDO1 maintains pluripotency of primed human embryonic stem cells by promoting glycolysis," *Stem Cells*, vol. 37, no. 9, pp. 1158–1165, 2019.

[45] S. Mandal, A. G. Lindgren, A. S. Srivastava, A. T. Clark, and U. Banerjee, "Mitochondrial function controls proliferation and early differentiation potential of embryonic stem cells," *Stem Cells*, vol. 29, no. 3, pp. 486–495, 2011.

[46] K. J. Vinoth, J. Manikandan, S. Sethu et al., "Differential resistance of human embryonic stem cells and somatic cell types to hydrogen peroxide-induced genotoxicity may be dependent on innate basal intracellular ROS levels," *Folia Histochemica et Cytobiologica*, vol. 53, no. 2, pp. 169–174, 2015.

[47] K. Huang, T. Maruyama, and G. Fan, "The naive state of human pluripotent stem cells: a synthesis of stem cell and preimplantation embryo transcriptome analyses," *Cell Stem Cell*, vol. 15, no. 4, pp. 410–415, 2014.

[48] C. Zhang, M. Skamagki, Z. Liu et al., "Biological significance of the suppression of oxidative phosphorylation in induced pluripotent stem cells," *Cell Reports*, vol. 21, no. 8, pp. 2058–2065, 2017.

[49] M. Schieber and N. S. Chandel, "ROS function in redox signaling and oxidative stress," *Current Biology*, vol. 24, no. 10, pp. R453–R462, 2014.

[50] A. L. Radzvilavicius, Z. Hadjivasiliou, A. Pomiankowski, and N. Lane, "Selection for mitochondrial quality drives evolution of the germline," *PLoS Biology*, vol. 14, no. 12, article e2000410, 2016.

[51] C. Haag-Liautard, N. Coffey, D. Houle, M. Lynch, B. Charlesworth, and P. D. Keightley, "Direct estimation of the mitochondrial DNA mutation rate in Drosophila melanogaster," *PLoS Biology*, vol. 6, no. 8, article e204, 2008.

[52] S. Maynard, A. M. Swistowska, J. W. Lee et al., "Human embryonic stem cells have enhanced repair of multiple forms of DNA damage," *Stem Cells*, vol. 26, no. 9, pp. 2266–2274, 2008.

[53] K. A. Becker, P. N. Ghule, J. A. Therrien et al., "Self-renewal of human embryonic stem cells is supported by a shortened G1 cell cycle phase," *Journal of Cellular Physiology*, vol. 209, no. 3, pp. 883–893, 2006.

[54] Y. L. Guo, S. Chakraborty, S. S. Rajan, R. Wang, and F. Huang, "Effects of oxidative stress on mouse embryonic stem cell proliferation, apoptosis, senescence, and self-renewal," *Stem Cells and Development*, vol. 19, no. 9, pp. 1321–1331, 2010.

[55] N. Pashkovskaia, U. Gey, and G. Rodel, "Mitochondrial ROS direct the differentiation of murine pluripotent P19 cells," *Stem Cell Research*, vol. 30, pp. 180–191, 2018.

[56] X. Zhang, S. Yalcin, D. F. Lee et al., "FOXO1 is an essential regulator of pluripotency in human embryonic stem cells," *Nature Cell Biology*, vol. 13, no. 9, pp. 1092–1099, 2011.

[57] A. Brunet, L. B. Sweeney, J. F. Sturgill et al., "Stress-dependent regulation of FOXO transcription factors by the SIRT1 deacetylase," *Science*, vol. 303, no. 5666, pp. 2011–2015, 2004.

[58] H. Sauer, G. Rahimi, J. Hescheler, and M. Wartenberg, "Effects of electrical fields on cardiomyocyte differentiation of embryonic stem cells," *Journal of Cellular Biochemistry*, vol. 75, no. 4, pp. 710–723, 1999.

[59] A. V. Boopathy, K. D. Pendergrass, P. L. Che, Y. S. Yoon, and M. E. Davis, "Oxidative stress-induced Notch1 signaling promotes cardiogenic gene expression in mesenchymal stem cells," *Stem Cell Research & Therapy*, vol. 4, no. 2, p. 43, 2013.

[60] I. Höfig, Y. Ingawale, M. J. Atkinson, H. Hertlein, P. J. Nelson, and M. Rosemann, "p53-Dependent Senescence in Mesenchymal Stem Cells under Chronic Normoxia Is Potentiated by Low-Dose γ-Irradiation," *Stem Cells International*, vol. 2016, Article ID 6429853, 11 pages, 2016.

[61] C. R. Mantel, H. A. O'Leary, B. R. Chitteti et al., "Enhancing hematopoietic stem cell transplantation efficacy by mitigating oxygen shock," *Cell*, vol. 161, no. 7, pp. 1553–1565, 2015.

[62] T. Simsek, F. Kocabas, J. Zheng et al., "The distinct metabolic profile of hematopoietic stem cells reflects their location in a hypoxic niche," *Cell Stem Cell*, vol. 7, no. 3, pp. 380–390, 2010.

[63] K. I. Korski, D. A. Kubli, B. J. Wang et al., "Hypoxia prevents mitochondrial dysfunction and senescence in human c-kit(+) cardiac progenitor cells," *Stem Cells*, vol. 37, no. 4, pp. 555–567, 2019.

[64] A. Chui, Q. Zhang, and S. H. Shi, "Oxidative stress regulates progenitor behavior and cortical neurogenesis," *Development*, vol. 147, no. 5, 2020.

[65] M. Higuchi, G. J. Dusting, H. Peshavariya et al., "Differentiation of human adipose-derived stem cells into fat involves reactive oxygen species and Forkhead box O1 mediated upregulation of antioxidant enzymes," *Stem Cells and Development*, vol. 22, no. 6, pp. 878–888, 2013.

[66] S. Reykdal, C. Abboud, and J. Liesveld, "Effect of nitric oxide production and oxygen tension on progenitor preservation in ex vivo culture," *Experimental Hematology*, vol. 27, no. 3, pp. 441–450, 1999.

[67] Y. Zhang, G. Marsboom, P. T. Toth, and J. Rehman, "Mitochondrial respiration regulates adipogenic differentiation of human mesenchymal stem cells," *PLoS One*, vol. 8, no. 10, article e77077, 2013.

[68] K. S. Kim, H. W. Choi, H. E. Yoon, and I. Y. Kim, "Reactive oxygen species generated by NADPH oxidase 2 and 4 are required for chondrogenic differentiation," *The Journal of Biological Chemistry*, vol. 285, no. 51, pp. 40294–40302, 2010.

[69] P. A. Jones and D. Takai, "The role of DNA methylation in mammalian epigenetics," *Science*, vol. 293, no. 5532, pp. 1068–1070, 2001.

[70] E. Li, T. H. Bestor, and R. Jaenisch, "Targeted mutation of the DNA methyltransferase gene results in embryonic lethality," *Cell*, vol. 69, no. 6, pp. 915–926, 1992.

[71] A. Madsen, G. Höppner, J. Krause et al., "An important role for DNMT3A-mediated DNA methylation in cardiomyocyte metabolism and contractility," *Circulation*, vol. 142, no. 16, pp. 1562–1578, 2020.

[72] G. L. Xu, T. H. Bestor, D. Bourc'his et al., "Chromosome instability and immunodeficiency syndrome caused by mutations in a DNA methyltransferase gene," *Nature*, vol. 402, no. 6758, pp. 187–191, 1999.

[73] A. M. Barciszewska, M. Giel-Pietraszuk, P. M. Perrigue, and M. Naskręt-Barciszewska, "Total DNA methylation changes reflect random oxidative DNA damage in gliomas," *Cell*, vol. 8, no. 9, p. 1065, 2019.

[74] S. A. Weitzman, P. W. Turk, D. H. Milkowski, and K. Kozlowski, "Free radical adducts induce alterations in DNA cytosine methylation," *Proceedings of the National Academy of Sciences of the United States of America*, vol. 91, no. 4, pp. 1261–1264, 1994.

[75] P. W. Turk, A. Laayoun, S. S. Smith, and S. A. Weitzman, "DNA adduct 8-hydroxyl-2'-deoxyguanosine (8-hydroxyguanine) affects function of human DNA methyltransferase," *Carcinogenesis*, vol. 16, no. 5, pp. 1253–1255, 1995.

[76] T. Pfaffeneder, F. Spada, M. Wagner et al., "Tet oxidizes thymine to 5-hydroxymethyluracil in mouse embryonic stem cell DNA," *Nature Chemical Biology*, vol. 10, no. 7, pp. 574–581, 2014.

[77] K. M. O'Connor, A. B. das, C. C. Winterbourn, and M. B. Hampton, "Inhibition of DNA methylation in proliferating human lymphoma cells by immune cell oxidants," *The Journal of Biological Chemistry*, vol. 295, no. 23, pp. 7839–7848, 2020.

[78] A. R. Seddon, Y. Liau, P. E. Pace et al., "Genome-wide impact of hydrogen peroxide on maintenance DNA methylation in replicating cells," *Epigenetics & Chromatin*, vol. 14, no. 1, p. 17, 2021.

[79] Y. D. Jung, S. K. Park, D. Kang et al., "Epigenetic regulation of miR-29a/miR-30c/DNMT3A axis controls SOD2 and mitochondrial oxidative stress in human mesenchymal stem cells," *Redox Biology*, vol. 37, article 101716, 2020.

[80] S. Ito, A. C. D'Alessio, O. V. Taranova, K. Hong, L. C. Sowers, and Y. Zhang, "Role of Tet proteins in 5mC to 5hmC conversion, ES-cell self-renewal and inner cell mass specification," *Nature*, vol. 466, no. 7310, pp. 1129–1133, 2010.

[81] K. D. Rasmussen and K. Helin, "Role of TET enzymes in DNA methylation, development, and cancer," *Genes & Development*, vol. 30, no. 7, pp. 733–750, 2016.

[82] M. R. Branco, G. Ficz, and W. Reik, "Uncovering the role of 5-hydroxymethylcytosine in the epigenome," *Nature Reviews. Genetics*, vol. 13, no. 1, pp. 7–13, 2011.

[83] Y. Niu, T. L. DesMarais, Z. Tong, Y. Yao, and M. Costa, "Oxidative stress alters global histone modification and DNA methylation," *Free Radical Biology & Medicine*, vol. 82, pp. 22–28, 2015.

[84] K. Iqbal, S. G. Jin, G. P. Pfeifer, and P. E. Szabó, "Reprogramming of the paternal genome upon fertilization involves genome-wide oxidation of 5-methylcytosine," *Proceedings of the National Academy of Sciences of the United States of America*, vol. 108, no. 9, pp. 3642–3647, 2011.

[85] K. K. Singh, M. Kulawiec, I. Still, M. M. Desouki, J. Geradts, and S. I. Matsui, "Inter-genomic cross talk between mitochondria and the nucleus plays an important role in tumorigenesis," *Gene*, vol. 354, pp. 140–146, 2005.

[86] S. Celik Uzuner, "Mitochondrial DNA methylation misleads global DNA methylation detected by antibody-based methods," *Analytical Biochemistry*, vol. 601, article 113789, 2020.

[87] R. C. Scarpulla, "Transcriptional paradigms in mammalian mitochondrial biogenesis and function," *Physiological Reviews*, vol. 88, no. 2, pp. 611–638, 2008.

[88] L. S. Shock, P. V. Thakkar, E. J. Peterson, R. G. Moran, and S. M. Taylor, "DNA methyltransferase 1, cytosine methylation, and cytosine hydroxymethylation in mammalian mitochondria," *Proceedings of the National Academy of Sciences of the United States of America*, vol. 108, no. 9, pp. 3630–3635, 2011.

[89] D. Bellizzi, P. D'Aquila, M. Giordano, A. Montesanto, and G. Passarino, "Global DNA methylation levels are modulated by mitochondrial DNA variants," *Epigenomics*, vol. 4, no. 1, pp. 17–27, 2012.

[90] T. Kietzmann, A. Petry, A. Shvetsova, J. M. Gerhold, and A. Görlach, "The epigenetic landscape related to reactive oxygen species formation in the cardiovascular system," *British Journal of Pharmacology*, vol. 174, no. 12, pp. 1533–1554, 2017.

[91] D. Yu, Z. Du, L. Pian et al., "Mitochondrial DNA hypomethylation is a biomarker associated with induced senescence in human fetal heart mesenchymal stem cells," *Stem Cells International*, vol. 2017, Article ID 1764549, 12 pages, 2017.

[92] X. Sun, Z. Wang, X. Cong et al., "Mitochondrial gene COX2 methylation and downregulation is a biomarker of aging in heart mesenchymal stem cells," *International Journal of Molecular Medicine*, vol. 47, no. 1, pp. 161–170, 2021.

[93] A. Cieslar-Pobuda, T. D. Ahrens, S. Caglayan, S. Behringer, L. Hannibal, and J. Staerk, "DNMT3B deficiency alters mitochondrial biogenesis and α-ketoglutarate levels in human embryonic stem cells," *Stem Cells*, vol. 38, no. 11, pp. 1409–1422, 2020.

[94] R. D. Kelly, A. E. Rodda, A. Dickinson et al., "Mitochondrial DNA haplotypes define gene expression patterns in pluripotent and differentiating embryonic stem cells," *Stem Cells*, vol. 31, no. 4, pp. 703–716, 2013.

[95] Z. Wang, C. Zang, K. Cui et al., "Genome-wide mapping of HATs and HDACs reveals distinct functions in active and inactive genes," *Cell*, vol. 138, no. 5, pp. 1019–1031, 2009.

[96] G. J. Narlikar, H.-Y. Fan, and R. E. Kingston, "Cooperation between complexes that regulate chromatin structure and transcription," *Cell*, vol. 108, no. 4, pp. 475–487, 2002.

[97] S. Shukla and B. L. Tekwani, "Histone deacetylases inhibitors in neurodegenerative diseases, neuroprotection and neuronal differentiation," *Frontiers in pharmacology*, vol. 11, p. 537, 2020.

[98] P. S. Gilmour, I. Rahman, K. Donaldson, and W. MacNee, "Histone acetylation regulates epithelial IL-8 release mediated by oxidative stress from environmental particles," *American Journal of Physiology. Lung Cellular and Molecular Physiology*, vol. 284, no. 3, pp. L533–L540, 2003.

[99] K. Ito, S. Lim, G. Caramori, K. F. Chung, P. J. Barnes, and I. M. Adcock, "Cigarette smoking reduces histone deacetylase 2 expression, enhances cytokine expression, and inhibits glucocorticoid actions in alveolar macrophages," *The FASEB Journal*, vol. 15, no. 6, pp. 1110–1112, 2001.

[100] K. Singh, L. Krug, A. Basu et al., "Alpha-ketoglutarate curbs differentiation and induces cell death in mesenchymal stromal precursors with mitochondrial dysfunction," *Stem Cells*, vol. 35, no. 7, pp. 1704–1718, 2017.

[101] T. R. Bartling, S. Subbaram, R. R. Clark, A. Chandrasekaran, S. Kar, and J. Andres Melendez, "Redox-sensitive gene-regulatory events controlling aberrant matrix metalloproteinase-1 expression," *Free Radical Biology & Medicine*, vol. 74, pp. 99–107, 2014.

[102] J. Maity, M. Deb, C. Greene, and H. das, "KLF2 regulates dental pulp-derived stem cell differentiation through the induction of mitophagy and altering mitochondrial metabolism," *Redox Biology*, vol. 36, article 101622, 2020.

[103] M. Hu, H. Zeng, S. Chen et al., "SRC-3 is involved in maintaining hematopoietic stem cell quiescence by regulation of mitochondrial metabolism in mice," *Blood*, vol. 132, no. 9, pp. 911–923, 2018.

[104] C. Lerin, J. T. Rodgers, D. E. Kalume, S. H. Kim, A. Pandey, and P. Puigserver, "GCN5 acetyltransferase complex controls glucose metabolism through transcriptional repression of PGC-1α," *Cell Metabolism*, vol. 3, no. 6, pp. 429–438, 2006.

[105] P. Nagarajan, P. A. Agudelo Garcia, C. C. Iyer, L. V. Popova, W. D. Arnold, and M. R. Parthun, "Early-onset aging and mitochondrial defects associated with loss of histone acetyltransferase 1 (Hat1)," *Aging Cell*, vol. 18, no. 5, article e12992, 2019.

[106] A. R. Cyr and F. E. Domann, "The redox basis of epigenetic modifications: from mechanisms to functional consequences," *Antioxidants & Redox Signaling*, vol. 15, no. 2, pp. 551–589, 2011.

[107] K. Doyle and F. A. Fitzpatrick, "Redox signaling, alkylation (carbonylation) of conserved cysteines inactivates class I

histone deacetylases 1, 2, and 3 and antagonizes their transcriptional repressor function," *The Journal of Biological Chemistry*, vol. 285, no. 23, pp. 17417–17424, 2010.

[108] S. Rajendrasozhan, S. R. Yang, I. Edirisinghe, H. Yao, D. Adenuga, and I. Rahman, "Deacetylases and NF-kappaB in redox regulation of cigarette smoke-induced lung inflammation: epigenetics in pathogenesis of COPD," *Antioxidants & Redox Signaling*, vol. 10, no. 4, pp. 799–812, 2008.

[109] N. R. Sundaresan, M. Gupta, G. Kim, S. B. Rajamohan, A. Isbatan, and M. P. Gupta, "Sirt3 blocks the cardiac hypertrophic response by augmenting Foxo3a-dependent antioxidant defense mechanisms in mice," *The Journal of Clinical Investigation*, vol. 119, no. 9, pp. 2758–2771, 2009.

[110] J. Checa and J. M. Aran, "Reactive oxygen species: drivers of physiological and pathological processes," *Journal of Inflammation Research*, vol. Volume 13, pp. 1057–1073, 2020.

[111] S. Tang, G. Huang, W. Fan et al., "SIRT1-mediated deacetylation of CRABPII regulates cellular retinoic acid signaling and modulates embryonic stem cell differentiation," *Molecular Cell*, vol. 55, no. 6, pp. 843–855, 2014.

[112] C. H. Lin, N. T. Li, H. S. Cheng, and M. L. Yen, "Oxidative stress induces imbalance of adipogenic/osteoblastic lineage commitment in mesenchymal stem cells through decreasing SIRT1 functions," *Journal of Cellular and Molecular Medicine*, vol. 22, no. 2, pp. 786–796, 2018.

[113] T. Prozorovski, U. Schulze-Topphoff, R. Glumm et al., "Sirt1 contributes critically to the redox-dependent fate of neural progenitors," *Nature Cell Biology*, vol. 10, no. 4, pp. 385–394, 2008.

[114] X. Q. Wang, Y. Shao, C. Y. Ma et al., "Decreased SIRT3 in aged human mesenchymal stromal/stem cells increases cellular susceptibility to oxidative stress," *Journal of Cellular and Molecular Medicine*, vol. 18, no. 11, pp. 2298–2310, 2014.

[115] K. Agger, P. A. C. Cloos, J. Christensen et al., "UTX and JMJD3 are histone H3K27 demethylases involved in _HOX_ gene regulation and development," *Nature*, vol. 449, no. 7163, pp. 731–734, 2007.

[116] Y. B. Schwartz and V. Pirrotta, "Polycomb silencing mechanisms and the management of genomic programmes," *Nature Reviews. Genetics*, vol. 8, no. 1, pp. 9–22, 2007.

[117] F. Lan, P. E. Bayliss, J. L. Rinn et al., "A histone H3 lysine 27 demethylase regulates animal posterior development," *Nature*, vol. 449, no. 7163, pp. 689–694, 2007.

[118] X. Shen, Y. Liu, Y. J. Hsu et al., "EZH1 mediates methylation on histone H3 lysine 27 and complements EZH2 in maintaining stem cell identity and executing pluripotency," *Molecular Cell*, vol. 32, no. 4, pp. 491–502, 2008.

[119] J. C. Black and J. R. Whetstine, "Chromatin landscape: methylation beyond transcription," *Epigenetics*, vol. 6, no. 1, pp. 9–15, 2011.

[120] J. R. Whetstine, A. Nottke, F. Lan et al., "Reversal of histone lysine trimethylation by the JMJD2 family of histone demethylases," *Cell*, vol. 125, no. 3, pp. 467–481, 2006.

[121] Y. Tsukada, J. Fang, H. Erdjument-Bromage et al., "Histone demethylation by a family of JmjC domain-containing proteins," *Nature*, vol. 439, no. 7078, pp. 811–816, 2006.

[122] C. Polytarchou, R. Pfau, M. Hatziapostolou, and P. N. Tsichlis, "The JmjC domain histone demethylase Ndy1 regulates redox homeostasis and protects cells from oxidative stress," *Molecular and Cellular Biology*, vol. 28, no. 24, pp. 7451–7464, 2008.

[123] L. Ye, Z. Fan, B. Yu et al., "Histone demethylases KDM4B and KDM6B promote osteogenic differentiation of human MSCs," *Cell Stem Cell*, vol. 23, no. 6, pp. 898-899, 2018.

[124] Y. Wei, Y. H. Chen, L. Y. Li et al., "CDK1-dependent phosphorylation of EZH2 suppresses methylation of H3K27 and promotes osteogenic differentiation of human mesenchymal stem cells," *Nature Cell Biology*, vol. 13, no. 1, pp. 87–94, 2011.

[125] X. Su, H. Zhang, F. Lei, R. Wang, T. Lin, and L. Liao, "Epigenetic therapy attenuates oxidative stress in BMSCs during ageing," *Journal of Cellular and Molecular Medicine*, vol. 26, no. 2, pp. 375–384, 2022.

[126] N. Sugino, "Roles of reactive oxygen species in the corpus luteum," *Animal Science Journal*, vol. 77, no. 6, pp. 556–565, 2006.

[127] K. Shkolnik, A. Tadmor, S. Ben-Dor, N. Nevo, D. Galiani, and N. Dekel, "Reactive oxygen species are indispensable in ovulation," *Proceedings of the National Academy of Sciences of the United States of America*, vol. 108, no. 4, pp. 1462–1467, 2011.

[128] B. Zorn, G. Vidmar, and H. Meden-Vrtovec, "Seminal reactive oxygen species as predictors of fertilization, embryo quality and pregnancy rates after conventional In Vitro fertilization and intracytoplasmic sperm injection," *International Journal of Andrology*, vol. 26, no. 5, pp. 279–285, 2003.

[129] E. Gomez, D. W. Buckingham, J. Brindle, F. Lanzafame, D. S. Irvine, and R. J. Aitken, "Development of an image analysis system to monitor the retention of residual cytoplasm by human spermatozoa: correlation with biochemical markers of the cytoplasmic space, oxidative stress, and sperm function," *Journal of Andrology*, vol. 17, no. 3, pp. 276–287, 1996.

[130] O. Tunc and K. Tremellen, "Oxidative DNA damage impairs global sperm DNA methylation in infertile men," *Journal of Assisted Reproduction and Genetics*, vol. 26, no. 9-10, pp. 537–544, 2009.

Hindawi
Oxidative Medicine and Cellular Longevity
Volume 2022, Article ID 5216786, 20 pages
https://doi.org/10.1155/2022/5216786

Research Article

Deletion of ACLY Disrupts Histone Acetylation and IL-10 Secretion in Trophoblasts, Which Inhibits M2 Polarization of Macrophages: A Possible Role in Recurrent Spontaneous Abortion

Xin Chen,[1] Qian Lin Song,[2] Ze Hong Li,[1] Rui Ji,[1] Jia Yu Wang,[1] Chang Ge,[1] Zhuo Ni Xiao,[1] Duan Ying Guo,[3] and Jing Yang[1]

[1]*Reproductive Medical Center, Renmin Hospital of Wuhan University and Hubei Clinic Research Center for Assisted Reproductive Technology and Embryonic Development, Wuhan, Hubei, China*
[2]*Department of Urology, Renmin Hospital of Wuhan University, Wuhan, Hubei, China*
[3]*Longgang District People's Hospital of Shenzhen, Shenzhen, China*

Correspondence should be addressed to Zhuo Ni Xiao; rm0011111@whu.edu.can, Duan Ying Guo; guo.duanying@163.com, and Jing Yang; dryangjing@whu.edu.cn

Received 22 January 2022; Revised 10 April 2022; Accepted 20 April 2022; Published 11 May 2022

Academic Editor: Ying Li

Changes to macrophage polarization affect the local microenvironment of the placenta, resulting in pathological pregnancy diseases such as recurrent spontaneous abortion (RSA). Macrophages are in close contact with trophoblasts during placental development, and trophoblast-derived cytokines are important regulators of macrophage polarization and function. Histone acetylation can affect the expression and secretion of cytokines, and ATP citrate lyase (ACLY) is an important factor that regulates histone acetylation. The aim of this study was to investigate the effect of ACLY expression differences in trophoblast on macrophage polarization and its mechanism. Our data demonstrate that ACLY level in placental villi of patients with RSA is decreased, which may lead to the inhibition of histone acetylation in trophoblasts, thereby reducing the secretion of IL-10. Reduced IL-10 secretion activates endoplasmic reticulum stress in macrophages, thus inhibiting their M2 polarization.

1. Introduction

Throughout pregnancy, the polarity and function of macrophages play an important role in intrauterine immune homeostasis and can also affect the process of pregnancy by promoting spiral artery remodeling and regulating trophoblast invasion and apoptosis [1–3]. Therefore, the polarity and function of macrophages are very important for the maintenance of a normal pregnancy.

According to the different inducing factors, phenotypes, and functions, M φ macrophages can be divided into M1 and M2 macrophages, similar to Th1 and Th2 T helper cells. M1 cells usually have proinflammatory activity, while M2 cells have an anti-inflammatory role [4–6]. In the placenta of an early pregnancy, macrophages are mainly the M2 type, which is very important for normal pregnancy [7]. A decrease in the proportion of M2 macrophages or an increase in the proportion of M1 macrophages can lead to recurrent abortion [8]. Trophoblast-derived cytokines are very important to induce the balance and immune tolerance of local M1 and M2 cells in the uterus, thus maintaining a normal pregnancy [9]. The functional diversity of macrophages reflects the high plasticity of the microenvironment at the maternal-fetal interface [10]. Appropriate and timely regulation of M1 to M2 polarization is considered the key factor to establish and maintain pregnancy at different stages. However, an imbalance of this polarization will lead to disruption of the microenvironment at the maternal-fetal interface, leading to pathological pregnancy and diseases, such as recurrent spontaneous abortion (RSA) [11].

ATP citrate lyase (ACLY) is one of the main enzymes that catalyze the formation of cytoplasmic acetyl CoA. In addition to providing the classical function of acetyl CoA for new fat production, ACLY also participates in epigenetic regulation through histone acetylation [12]. There is evidence that epigenetic modifications are involved in early embryogenesis, and defects in epigenetic patterns contribute to the occurrence and development of RSA [13, 14]. Histone modification is one of the main epigenetic mechanisms [15]. In recent years, studies have found that histone acetylation plays an important role in the expression of cytokines [16]. For example, the application of histone deacetylase (HDAC) inhibitors, such as trichostatin A (TSA), leads to extensive acetylation of histones, thus reducing the expression of genes encoding inflammatory cytokines, such as interleukin- (IL-) 2, IL-6, and interferon- (IFN-) γ, as well as reducing the symptoms of lupus prone mice [17]. However, despite being a powerful epigenetic regulator, it is still unknown whether ACLY plays an important role in the maintenance of the maternal fetal-interface immune system, and whether ACLY participates in macrophage polarization and their functional regulation, thus affecting the pathogenesis of recurrent abortion.

In this study, we aimed to evaluate the localization and expression of ACLY in placental tissues of patients with a normal pregnancy and patients with RSA and to determine the role, if any, of ACLY in RSA. Through *in vitro* cell experiments, it was confirmed that knockdown of *ACLY* in trophoblasts led to the inhibition of histone acetylation, which reduced the secretion of IL-10 from trophoblasts. This reduction of IL-10 activated endoplasmic reticulum stress in macrophages, thus inhibiting their M2 polarization. Therefore, the results of the present study provide new insights and ideas for the pathogenesis of RSA.

2. Materials and Methods

2.1. Patient and Tissue Samples. A total of 25 patients with induced abortion due to accidental pregnancy (the healthy control, HC group) and 25 patients with RSA were included in this study. Patients with the following characteristics were excluded: (1) pelvic examination and ultrasound showing genital malformations, (2) chromosomal abnormality of the parent or embryo, (3) infectious diseases, and (4) symptoms of endocrine or metabolic diseases. Samples were collected immediately after curettage and washed with PBS. One part of the collected placental tissue was fixed in 4% paraformaldehyde and embedded in paraffin. The other part of the tissue was frozen and stored in liquid nitrogen. All samples were collected with the informed consent of the patients, and all relevant procedures were approved by the internal review and ethics committee of the Renmin Hospital of Wuhan University. The baseline characteristics of the patients are summarized in Table 1.

2.2. Immunofluorescence. Tissue sections were dewaxed, washed, subjected to antigen repair, and blocked. Primary antibodies recognizing cytokeratin 7 (CK7) (66483-1-Ig, 1 : 1,000 dilution, Proteintech, Wuhan, China), human leukocyte antigen-G (HLA-G) (66447-1-Ig, 1 : 200 dilution, Proteintech), and ACLY (15421-1-ap, 1 : 100 dilution, Proteintech) were added and incubated overnight at 4°C. After washing with PBST, horseradish peroxidase- (HRP-) labeled Goat anti rabbit (5220-0336, 1 : 1,000 dilution, SeraCare, Millford, MA, USA) or HRP-labeled Goat anti mouse (5220-0341, 1 : 1,000 dilution, SeraCare) secondary antibodies were added and incubated in the dark at room temperature for 50 min. Tyramine salt-CY3 or Tyramine salt-488 was added and incubated in the dark at room temperature for 20 min. The nuclei were stained using 4′,6-diamidino-2-phenylindole (DAPI) and then observed using an orthographic microscope system (Olympus BX51, Tokyo, Japan).

Table 1: Demographic and clinical characteristics of the study population.

Characteristics	HC	RSA	p value
Age (years)	30.04 ± 3.03	30.36 ± 2.41	0.681
BMI (kg/m^2)	21.81 ± 1.49	22.09 ± 1.72	0.536
Gestation age (weeks)	7.32 ± 0.80	7.44 ± 1.08	0.658
Number of miscarriages	0.12 ± 0.33	2.76 ± 0.72	< 0.001

HC: healthy control; RSA: recurrent spontaneous abortion; BMI: body mass index.

2.3. Immunohistochemistry. The tissue sections were dewaxed, washed, subjected to antigen repair, and blocked. Primary antibodies recognizing cytokeratin 7 (CK7) (66483-1-Ig, 1 : 2,000 dilution, Proteintech), human leukocyte antigen-G (HLA-G) (66447-1-Ig, 1 : 400 dilution, Proteintech), ACLY (15421-1-ap, 1 : 100 dilution, Proteintech), acetyl-Histone H3 (af4365, 1 : 100 dilution, Affinity Biosciences, Jiangsu, China), activating transcription factor 6 (ATF6) (24169-1-ap, 1 : 200 dilution, Proteintech), glucose-regulated protein, 78 kDa (GRP78) (11587-1-ap, 1 : 400 dilution, Proteintech), phosphorylated- (p-) PRKR-like endoplasmic reticulum kinase (PERK) (df7576, 1 : 200 dilution, Affinity Biosciences), p-inositol-requiring enzyme 1 (IRE1) (af7150, 1 : 200 dilution, Affinity Biosciences), and XBP1s (24868-1-AP, 1 : 400 dilution, Proteintech) were added and incubated overnight at 4°C. The sections were washed with PBST, and HRP-labeled Goat anti-rabbit (5220-0336, 1 : 1,000 dilution, SeraCare) or HRP-labeled Goat anti-mouse (5220-0341, 1 : 1,000 dilution, SeraCare) secondary antibodies were added to cover the tissue, followed by incubation at room temperature in the dark for 50 min. Diaminobenzidine (DAB) chromogenic solution was added, and the sections were observed under an upright microscope system (Olympus BX51).

2.4. Cell Culture. HTR-8 and JEG-3 cells were cultured in Dulbecco's modified Eagle's medium (DMEM)/F12 medium, JAR cells were cultured in DMEM medium, BeWo cells were cultured in minimal essential (MEM) medium, and THP-1 cells were cultured in Roswell Park Memorial Institute- (RPMI-) 1640 medium. All cells were cultured in a cell incubator containing 5% CO_2 and sufficient humidity at 37°C.

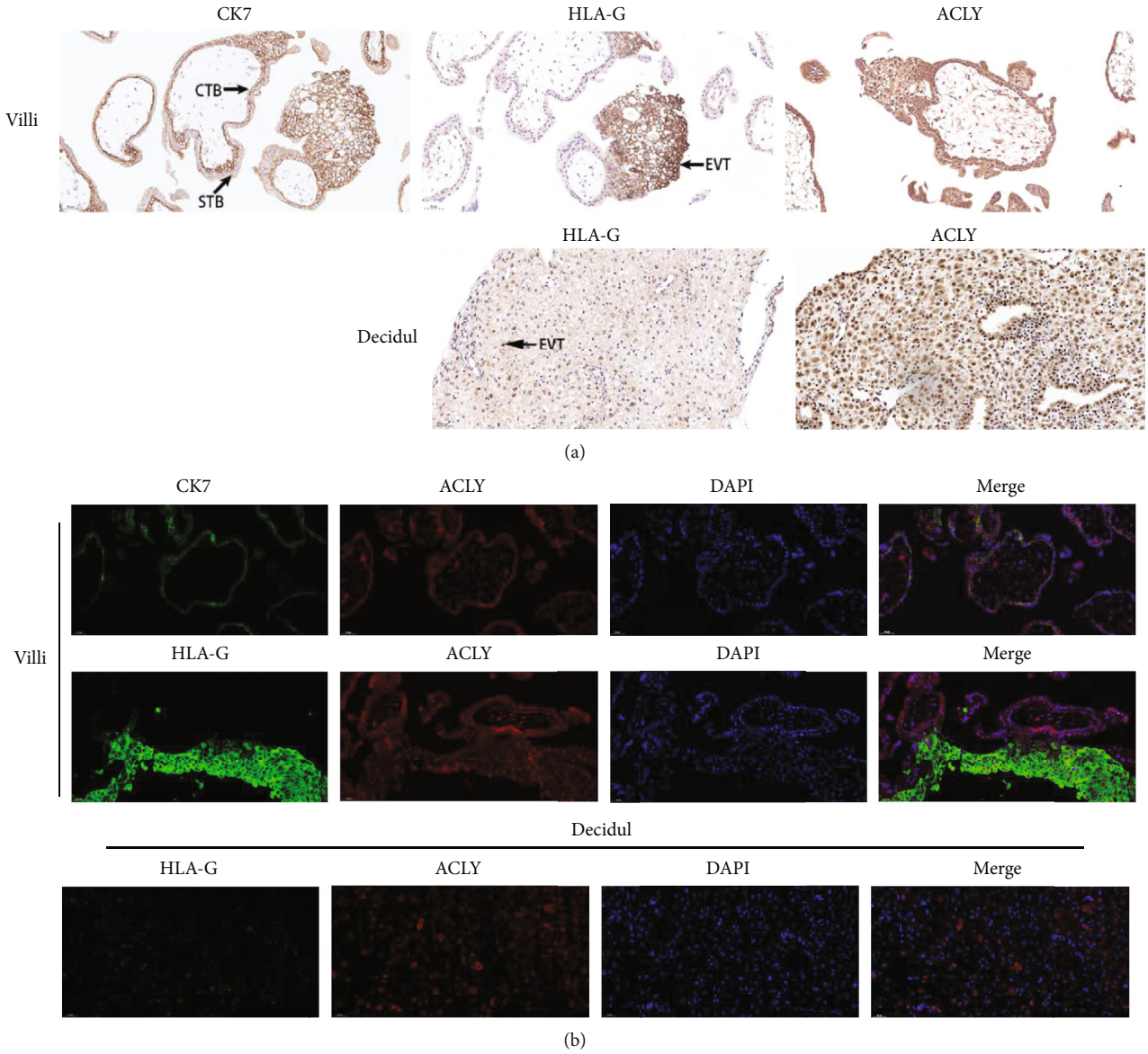

Figure 1: Location of ACLY in human placental tissue during early pregnancy. ACLY expression in cytotrophoblasts (CTBs), syncytiotrophoblasts (STBs), and extravillous trophoblasts (EVTs), as detected using immunohistochemistry (a) and immunofluorescence (b). Cytokeratin 7 (CK7) and human leukocyte antigen-G (HLA-G) were used as markers of CTBs and EVTs, respectively. Specific fluorescence staining of ACLY is stained red, CK7 or HLA-G is stained green, and the nucleus is stained blue (DAPI staining). All images are of a 200x visual field under the microscope. Scale bar = 50 μm.

2.5. Cell Transfection. Lentiviruses expressing a short hairpin RNA (shRNA) targeting *ACLY* or a control shRNA were synthesized by Shanghai GeneChem (Shanghai, China). The RNA interference (RNAi) target sequence was as follows: ACLY-RNAi-1 (CTAAGTACTCTTGCCAGTT), ACLY-RNAi-2 (TGAGAGCAATTCGAGATTA), and ACLY-RNAi-3 (AGGACTTGTACTTCACCTA). According to the manufacturer's instructions, the ACLY shRNA and control shRNA lentiviruses were transfected into cells, and the stably expressing cell lines were screened using puromycin.

2.6. THP-1 Differentiation and Coculture System. For macrophage polarization, THP-1 cells were incubated in 100 ng/ml phorbol 12 myristate 13 acetate (PMA, Sigma, St. Louis, MO, USA) for 24 hours to differentiate into M0 macrophages. To establish a coculture system, we cultured the M0 macrophages with culture supernatants of stably transfected and control HTR-8, JEG-3, and JAR cells as conditioned medium. After 72 hours of culture, the macrophages were collected for analysis.

2.7. RNA Isolation and Quantitative Real-Time Reverse Transcription PCR (qRT-PCR). Total RNA was extracted using the TRIzol reagent (Invitrogen, Waltham, MA, USA) according to the manufacturer's instructions. After the RNA concentration and purity were detected, the PrimeScript ™ RT Master Mix (perfect real-time) (Takara, Shiga,

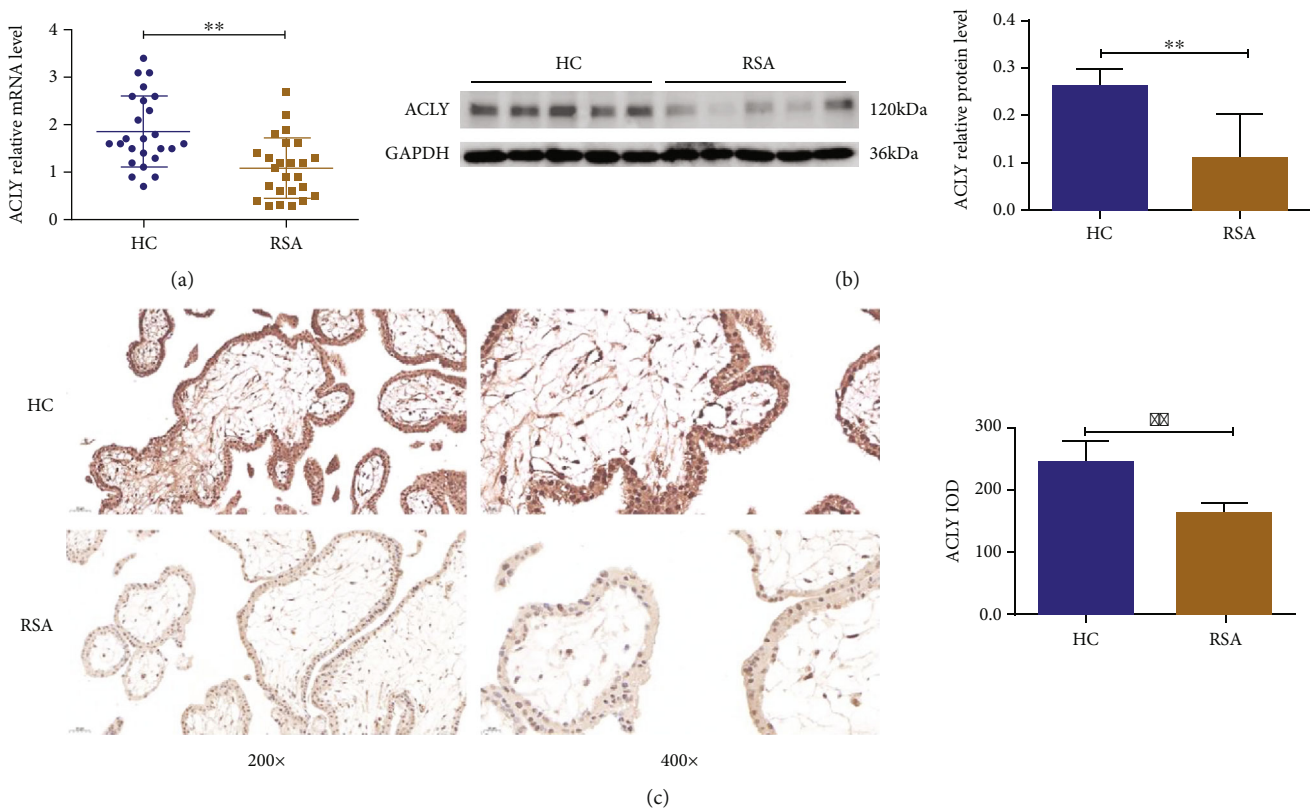

Figure 2: Decreased ACLY expression in chorionic tissue of patients with recurrent spontaneous abortion (RSA). (a) *ACLY* mRNA expression levels in the villi of patients with RSA and the healthy control (HC) group, as determined using qRT-PCR ($n = 25$). (b) The protein levels of ACLY in the villi of patients with RSA and the HC group, as analyzed using Western blot ($n = 5$). (c) The protein levels of ACLY in villi of patients with RSA and the HC group, as measured using immunohistochemistry ($n = 5$). $^{**}p < 0.01$, compared with the HC group. IOD: Integrated Optical Density. Scale bar: 200x = 50 μm, 400x = 20 μm.

Japan) was used to reverse transcribe the total RNA into cDNA. The cDNA was used as a template in a TB green ® Premix Ex Taq™ reaction to quantify the mRNA expression. *GAPDH* (encoding glyceraldehyde-3-phosphate dehydrogenase) was used as the internal reference. The primer sequences were as follows: *ACLY*, forward: 5′-GCTCTGCCTATGACAGCACCAT-3′, reverse: 5′-GTCCGATGATGGTCACTCCCTT-3′; *CD206*, forward: 5′-AGCCAACACCAGCTCCTCAAGA-3′, reverse: 5′-CAAAACGCTCGCGCATTGTCCA-3′; *CD163*, forward: 5′-CCAGAAGGAACTTGTAGCCACAG-3′, reverse: 5′-CAGGCACCAAGCGTTTTGAGCT-3′; *CCL18* (encoding C-C motif chemokine ligand 18), forward: 5′-GTTGACTATTC TGAAACCAGCCC-3′, reverse: 5′-GTCGCTGATGTATTTC TGGACCC-3′; CXCL16 (encoding C-X-C motif chemokine ligand 16), forward: 5′-CCTATGTGCTGTGCAAGAGGAG-3′, reverse: 5′-CTGGGCAACATAGAGTCCGTCT-3′; *IL10*, forward: 5′-TCTCCGAGATGCCTTCAGCAGA-3′, reverse: 5′-TCAGACAAGGCTTGGCAACCCA-3′; *IL6*, forward: 5′-AGACAGCCACTCACCTCTTCAG-3′, reverse: 5′-TTCTGC CAGTGCCTCTTTGCTG-3′; *IL-34*, forward: 5′-CCAAGG TGGAATCCGTGTTGTC-3′, reverse: 5′-CACCTCACAGT CCTGCCAGTTT-3′; *MCSF* (encoding macrophage colony stimulating factor), forward: 5′-TGAGACACCTCTCCAG TTGCTG-3′, reverse: 5′-GCAATCAGGCTTGGTCACC ACA-3′; *GAPDH*, forward: 5′-GTCTCCTCTGACTTCAACA GCG-3′, reverse: 5′-ACCACCCTGTTGCTGTAGCCAA-3′.

2.8. Flow Cytometry. After sample treatment, a single cell suspension was collected and incubated with Human TruStain FcX™ (BioLegend, San Diego, CA, USA) at room temperature for 10 minutes; then, a phycoerythrin- (PE-) coupled anti-CD206 antibody (BioLegend) was added, incubated at 4°C for 20 minutes, and washed twice with cell staining buffer (BioLegend). 7-Aminoactinomycin D (7-AAD) Viability Staining Solution (BioLegend) was added and incubated in the dark for 5 minutes. The cells were immediately analyzed using flow cytometry (BD FASC Calibur, USA).

2.9. Enzyme-Linked Immunosorbent Assay (ELISA). After sample collection, the level of IL-10 was determined using a human IL-10 ELISA kit (Cusabio, Wuhan, China) according to the manufacturer's instructions.

2.10. Western Blotting. Radio Immunoprecipitation Assay Lysis Buffer (P0013B, Beyotime, Shanghai, China) or Epi-Quik Total Histone Extraction Kit (OP-0006-100, Amyjet

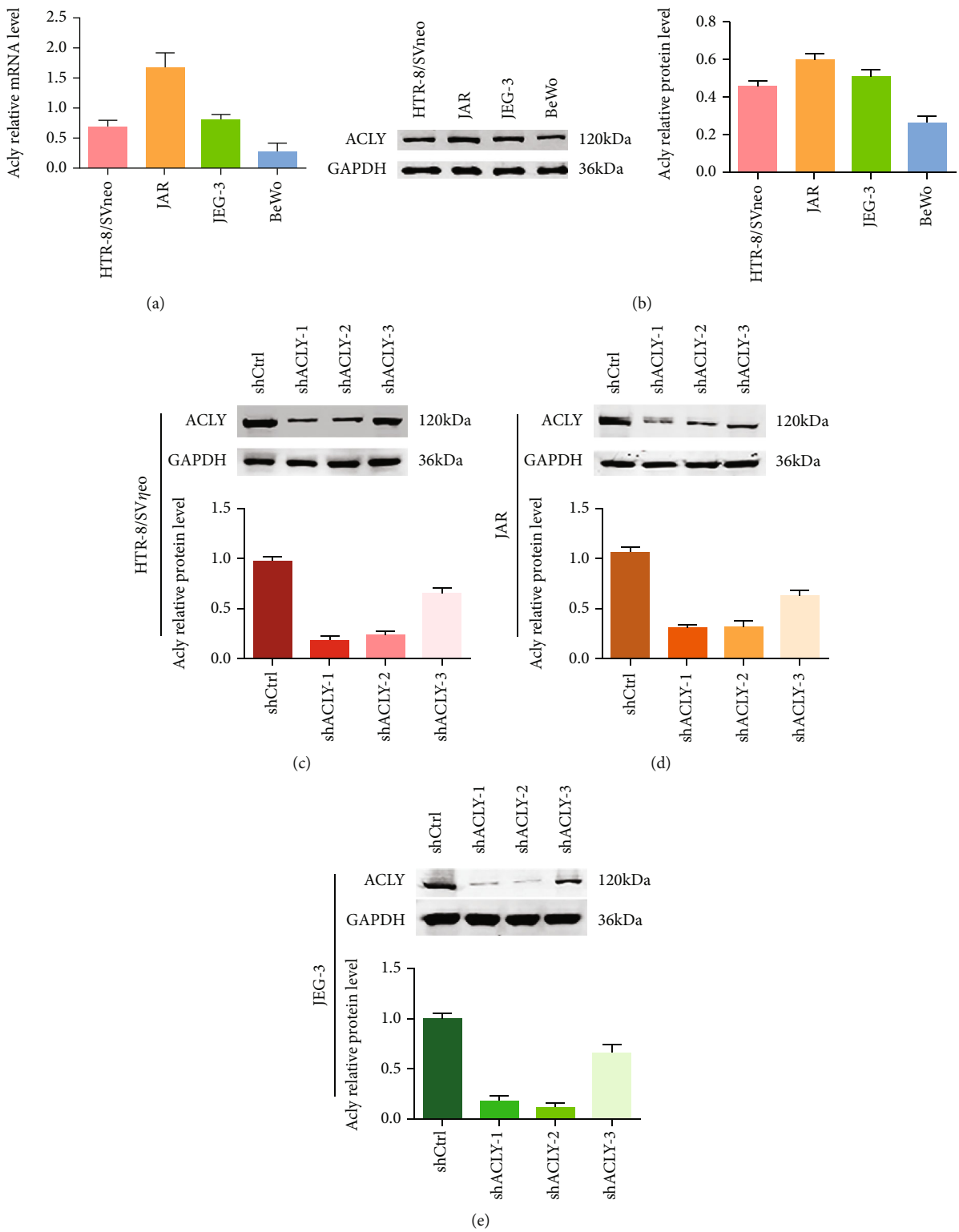

Figure 3: Construction of the *ACLY* knockdown trophoblast line. (a) The expression of *ACLY* in four trophoblastic cell lines, as detected using qRT-PCR. (b) The protein level of ACLY in four trophoblastic cell lines, as detected using Western blotting. (c–e) The protein level of ACLY in HTR-8, JEG-3, and JAR cells, as detected using Western blotting.

Scientific, Wuhan, China) was used to extract total protein or total histone, respectively. The protein sampled was subjected to protein gel electrophoresis and then transferred onto a PVDF membrane. The membrane was then incubated with primary antibodies recognizing Histone-H3 (17168-1-AP, 1 : 5,000 dilution, Proteintech), acetyl-Histone H3 (af4365, 1 : 1,000 dilution, Affinity Biosciences, Jiangsu, China), ACLY (15421-1-ap, 1 : 2,000 dilution, Proteintech),

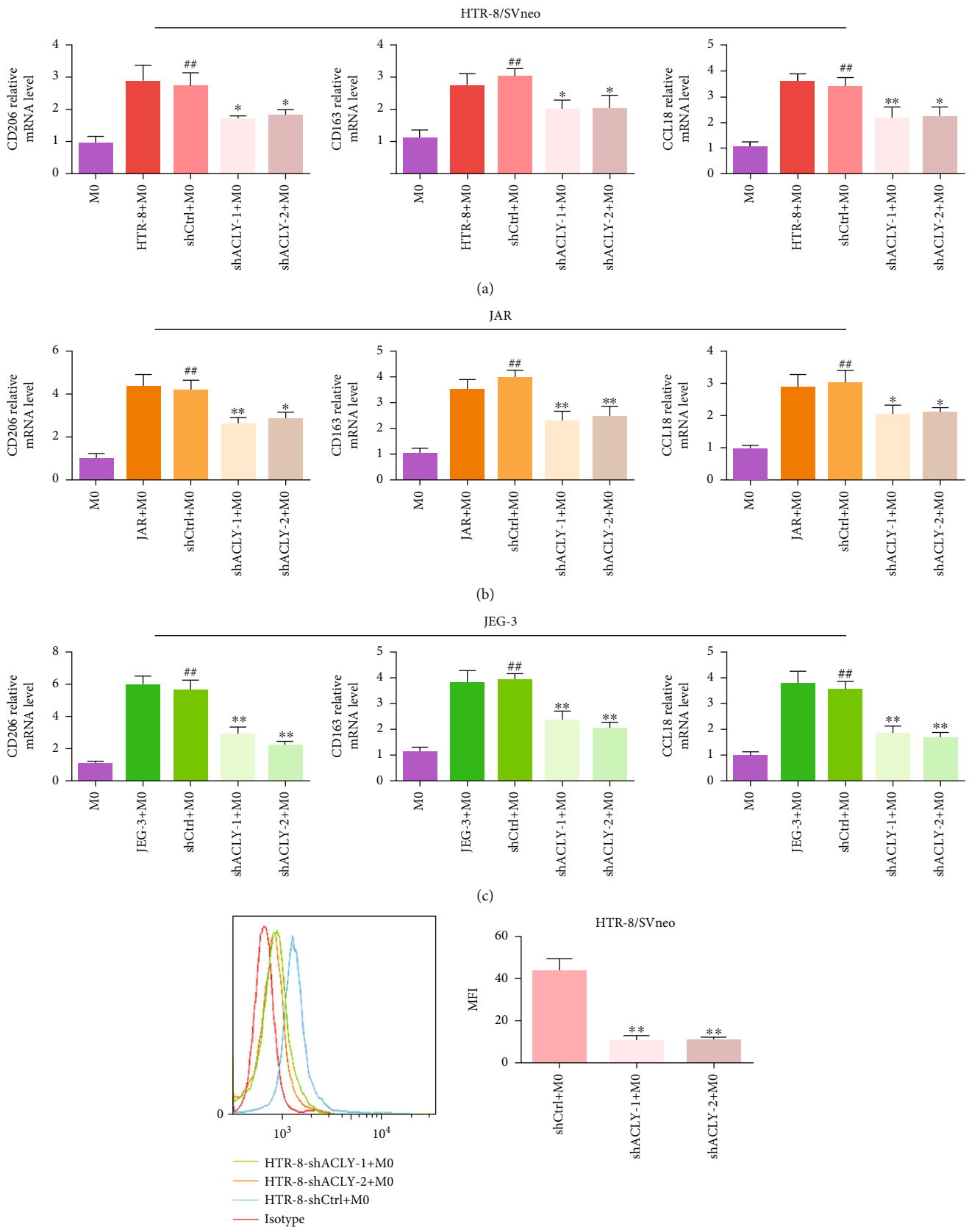

Figure 4: Continued.

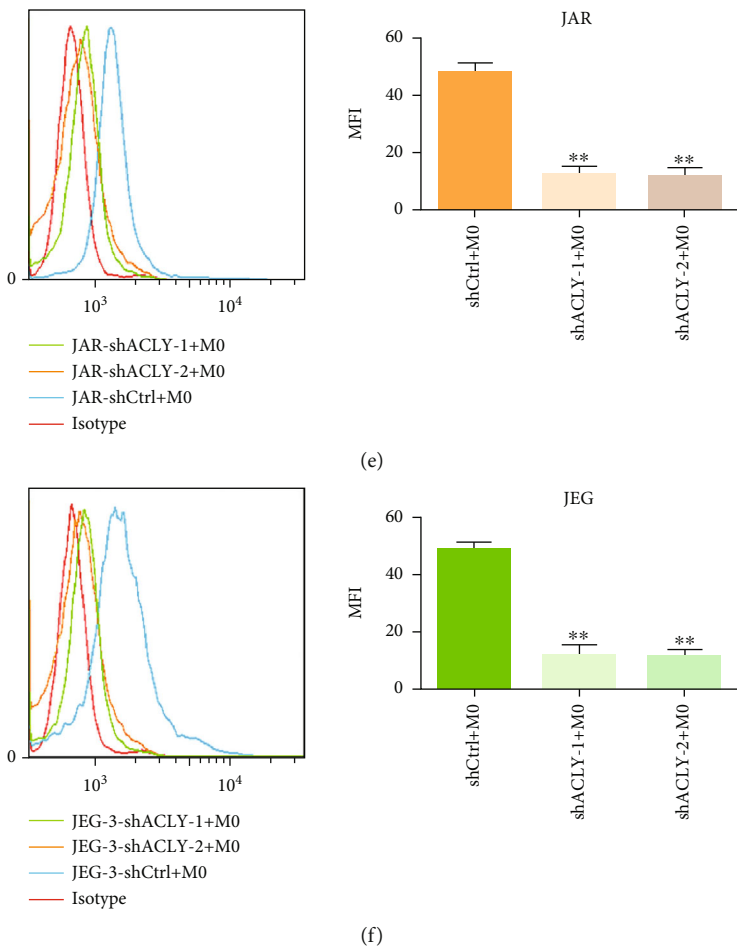

Figure 4: Knockdown of *ACLY* in HTR-8, JAR, and JEG-3 cells inhibited M2 polarization. (a–c) The expression of genes encoding M2 macrophage markers (CD163, CD206, and CCL18) in M0 macrophages and cocultured macrophages, as detected using qRT-PCR. (d–f) Mean fluorescence intensity (MFI) of CD206, as analyzed using flow cytometry in the three cell lines. $^{*}p < 0.05$, $^{**}p < 0.01$, compared with shCtrl+M0; $^{\#\#}p < 0.01$, compared with M0.

GAPDH (60004-1-Ig, 1 : 50,000 dilution, Proteintech), activating transcription factor 6 (ATF6) (24169-1-ap, 1 : 1,000 dilution, Proteintech), glucose-regulated protein, 78 kDa (GRP78) (11587-1-ap, 1 : 2,000 dilution, Proteintech), phosphorylated- (p-) PRKR-like endoplasmic reticulum kinase (PERK) (df7576, 1 : 2,000 dilution, Affinity Biosciences), p-inositol-requiring enzyme 1 (IRE1) (af7150, 1 : 1,000 dilution, Affinity Biosciences), and XBP1s (24868-1-AP, 1 : 1,000 dilution, Proteintech). After washing with Tris-buffered saline-Tween 20 (TBST), the membrane was incubated in anti-rabbit secondary antibody (5151, 1 : 30,000 dilution, CST) or anti-mouse secondary antibody (5257, 1 : 15,000 dilution, CST) at room temperature for 1 hour and then washed with TBST. The immunoreactive proteins on the membrane were visualized using the Odyssey infrared imaging system (LI-COR, Lincoln, NE, USA), and then, the gray value of the protein bands was analyzed using the ImageJ software (NIH, Manassas, MD, USA).

2.11. Statistical Analysis. Data from at least three independent experiments were analyzed, and all data are expressed as the mean ± standard error (SD) of mean. All statistical analyses were performed using GraphPad Prism 6.01 (GraphPad Inc., La Jolla, CA, USA). Student's *t*-test was used to evaluate difference between two groups, and one-way ANOVA was used to compare difference between multiple groups. $p < 0.05$ was considered statistically significant.

3. Results

3.1. Localization of ACLY in Human Placental Tissue. We first detected ACLY location in human placental tissue during early pregnancy using immunohistochemistry and immunofluorescence techniques, and all images were of a 200x visual field under the microscope (Figure 1). The results showed that ACLY was expressed in cytotrophoblasts (CTBs), syncytiotrophoblasts (STBs), and extravillous trophoblasts (EVTs) (Figures 1(a) and 1(b)).

3.2. ACLY Expression Is Decreased in Chorionic Tissue of Patients with RSA. To determine the difference in ACLY expression between normal pregnancy and patients with

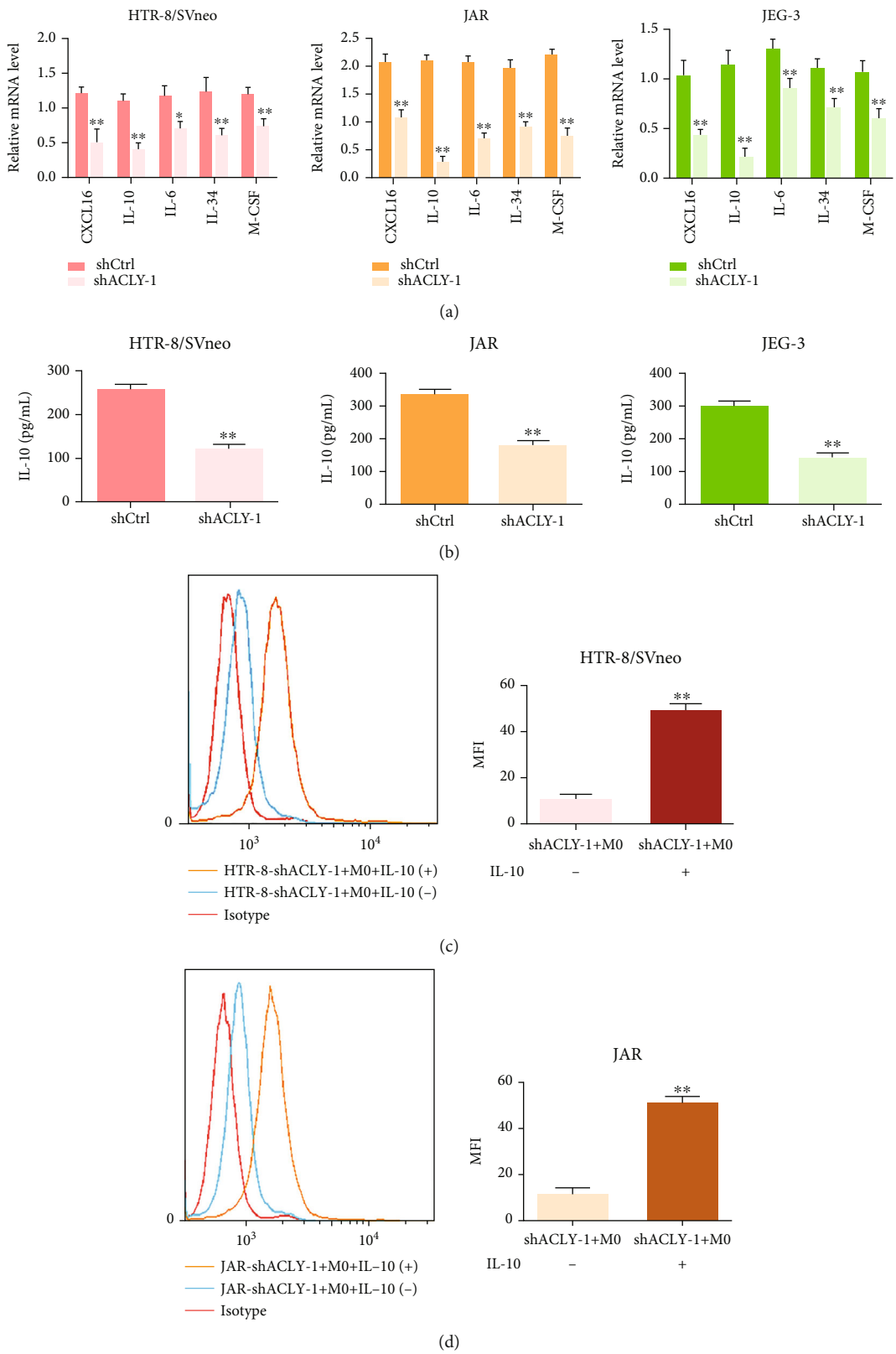

Figure 5: Continued.

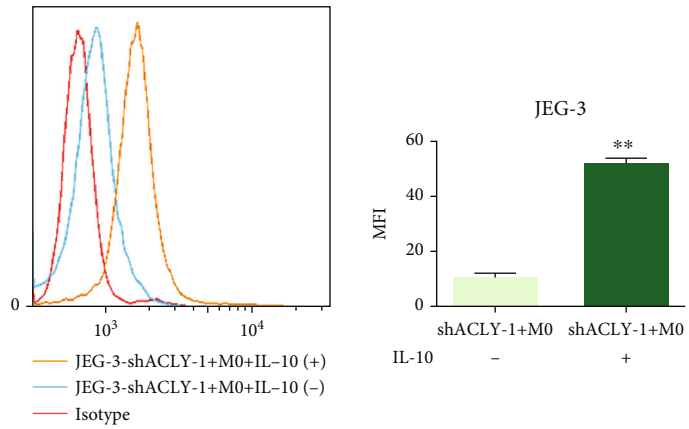

(e)

Figure 5: The trophoblast-derived cytokine IL-10 promotes M2 polarization. (a) The expression of genes encoding trophoblast-derived cytokines (IL-6, IL-10, CXCL16, M-CSF, and IL-34) that regulate macrophage M2 polarization, as detected using qRT-PCR. (b) The protein level of IL-10, as detected using ELISA. (c–e) The mean fluorescence intensity (MFI) of CD206, as analyzed using flow cytometry. $^{*}p < 0.05$, $^{**}p < 0.01$, compared with shCtrl or shACLY+M0 + IL-10(-). After M0 macrophages were treated with HTR-8, JAR, or JEG-3-shACLY supernatant, with or without IL-10 (50 ng/ml), the MFI of CD206 was analyzed using flow cytometry.

RSA, qRT-PCR and Western blotting were performed using villus tissues. The results showed that ACLY expression in the villi of patients in the RSA group was significantly lower than that in the HC group at the mRNA and protein levels (Figures 2(a) and 2(b)). In addition, we performed immunohistochemical staining on villi to further verify the expression of ACLY, and the images were of a 200x or 400x visual field under the microscope. The results showed that ACLY levels in villi of patients in the RSA group were significantly lower than those in the HC group (Figure 2(c)). These results suggest that ACLY expression is downregulated in villi of patients with RSA.

3.3. Construction of ACLY Knockdown Trophoblast Cell Line. The biological dysfunction of trophoblasts is closely related to the pathogenesis of RSA; therefore, we first observed the expression of ACLY in HTR-8, JEG-3, JAR, and BeWo trophoblast lines using qRT-PCR and Western blotting. The results showed that among the four cell lines, the expression of ACLY in BeWo cells was the lowest and was expressed at higher levels in HTR-8, JEG-3, and JAR cells (Figures 3(a) and 3(b)). Subsequently, we used three different sequences to knock down the *ACLY* genes in HTR-8, JEG-3, and JAR cells and then detected the knockdown efficiency using Western blotting. The results showed that the ACLY protein level in the shACLY-1 and shACLY-2 group was significantly reduced (Figures 3(c)–3(e)).

3.4. Knockdown of ACLY in Trophoblasts Inhibited M2 Polarization of THP-1 Macrophages. The functional distortion of decidual macrophages is closely related to the occurrence of RSA. In addition, there is crosstalk and interaction between trophoblast cells and decidual macrophages. To explore whether *ACLY* knockdown in trophoblasts affected the polarization of THP-1 macrophages, we selected shACLY-1 and shACLY-2 to knockdown the ACLY genes in HTR-8, JEG-3, and JAR cells. We transfected HTR-8, JAR, and JEG-3 cells with shRNA *ACLY* or empty vector virus. Then, THP-1 macrophages were cultured in the conditioned medium of the transfected cells for 72 hours. qRT-PCR was then used to detect the expression of M2 macrophage markers *CD206*, *CD163*, and *CCL18*. The results showed that compared with the M0 group, the mRNA levels of M2 macrophage markers *CD206*, *CD163*, and *CCL18* were upregulated after treatment with HTR-8/JAR/JEG-3-shctrl supernatant, while their mRNA levels were downregulated significantly after treatment with HTR-8, JAR, or JEG-3-shACLY-1/-2 supernatant (Figures 4(a)–4(c)). Moreover, flow cytometry analysis showed that the mean fluorescence intensity (MFI) of CD206 in the shACLY-1/-2 group was decreased compared with that in the shCtrl group in the three cell lines (Figures 4(d)–4(f)). These results suggested that a lack of ACLY in trophoblasts inhibited macrophage polarization to M2.

3.5. Trophoblast-Derived IL-10 Promotes M2 Polarization. Studies have shown that trophoblasts can transmit signals to decidual macrophages through secreted factors. To explore the potential mechanism, we first analyzed the mRNA expression of cytokines related to trophoblast-derived regulation of macrophage M2 polarization (IL-6, IL-10, CXCL16, M-CSF, and IL-34) using qRT-PCR. The results showed that compared with the control group (shCtrl), *IL6*, *IL10*, *CXCL16*, *MCSF*, and *IL34* in HTR-8, JAR, and JEG-3 cells transfected with shRNA ACLY virus decreased by varying degrees (Figure 5(a)). Studies have shown that IL-10 was closely related to epigenetic modifications [18]; therefore, we further detected the level of IL-10 using ELISA. The results showed that IL-10 levels were significantly reduced in HTR-8, JAR, and JEG-3 cells

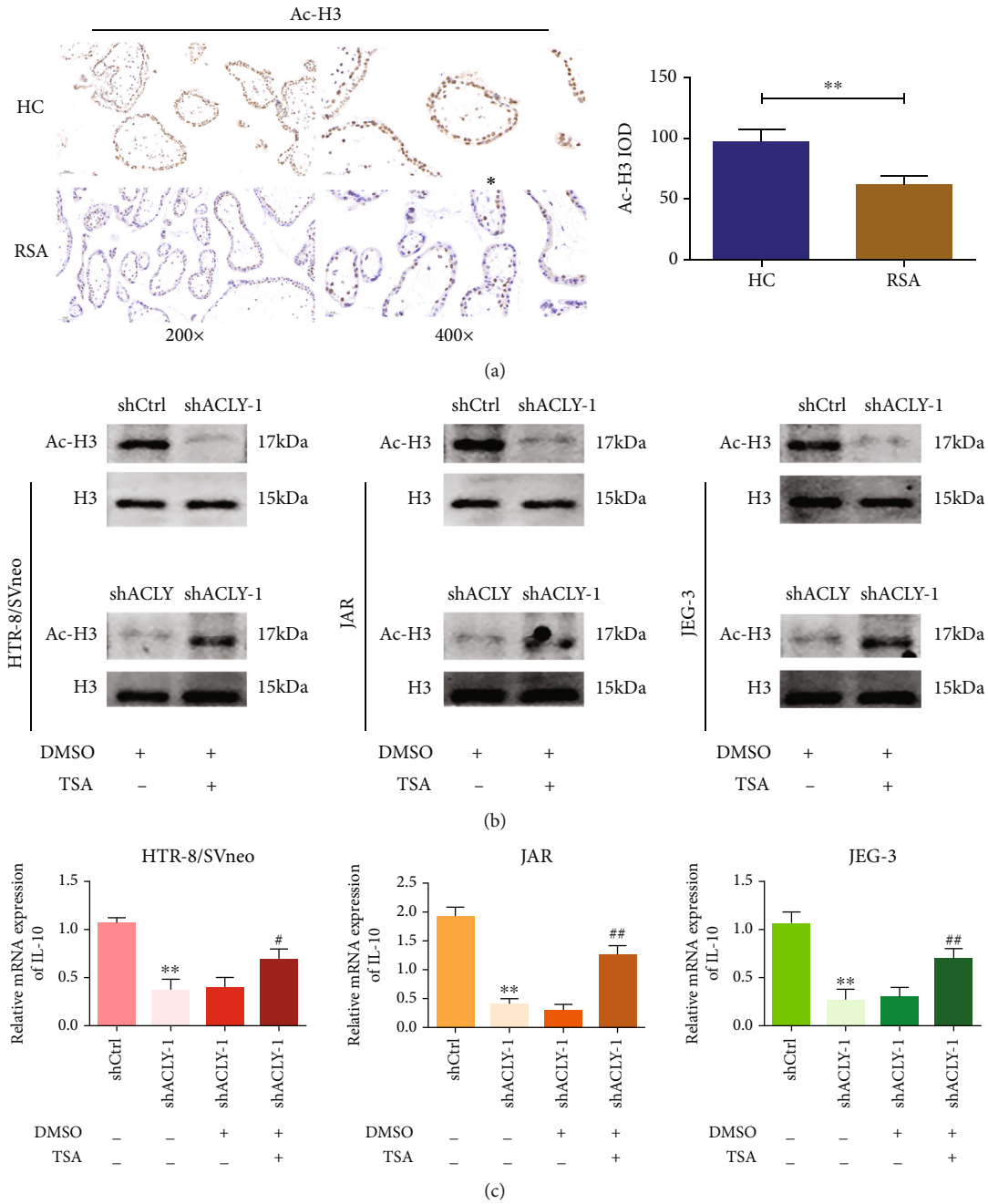

Figure 6: Continued.

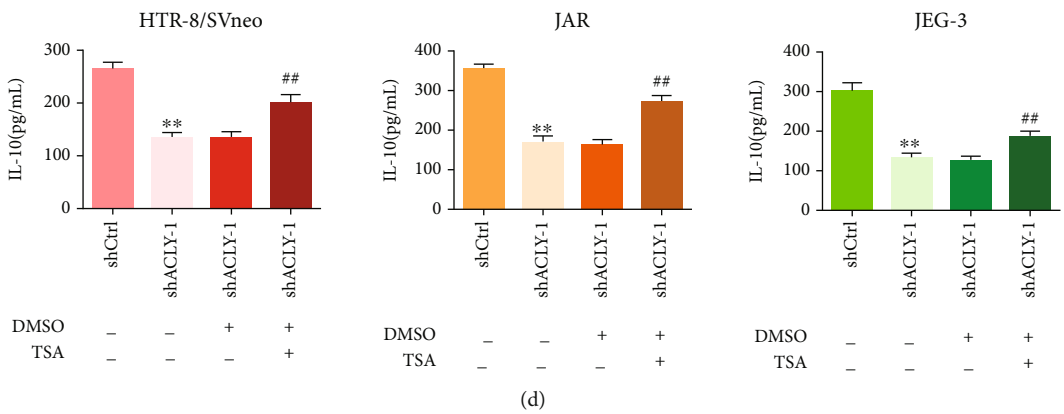

Figure 6: Downregulation of *ACLY* leads to change in IL-10 expression through histone acetylation. (a) The protein levels of acetylated histone H3 in villi of patients with the RSA and the HC groups, as measured using immunohistochemistry ($n = 5$). (b) The levels of total acetylated histone H3 and histone H3, as detected using Western blotting. (c) The expression of *IL10*, as detected using qRT-PCR. (d) The protein level of IL-10, as detected using ELISA. $^{**}p < 0.01$, compared with the HC group; $^{**}p < 0.01$, compared with shCtrl; $^{\#}p < 0.05$, $^{\#\#}p < 0.01$, compared with shACLY. IOD: Integrated Optical Density. Scale bar: 200x = 50 μm, 400x = 20 μm.

transfected with shRNA *ACLY* virus (Figure 5(b)), which was consistent with the results of qRT-PCR. Therefore, we focused on the role of IL-10. After M0 macrophages were treated with HTR-8, JAR, or JEG-3-shACLY-1 supernatant, with or without IL-10 (50 ng/ml), the average fluorescence intensity of CD206 was analyzed using flow cytometry. The results showed that the MFI of CD206 increased after adding IL-10, which promoted M2 polarization (Figures 5(c)–5(e)). These results suggest that trophoblast-derived cytokine IL-10 is involved in M2 polarization.

3.6. ACLY Knockdown Leads to Changes in IL-10 Expression through Histone Acetylation. ACLY is very important for the epigenetic regulation of histone acetylation. First, we performed immunohistochemical staining on villi to verify the expression of H3 acetylation, and the images were of a 200x or 400x visual field under the microscope. It showed that histone H3 acetylation in villi of patients in the RSA group was significantly lower than those in the HC group (Figure 6(a)) These results suggest that H3 acetylation is downregulated in villi of patients with RSA. To further clarify the potential mechanism of ACLY, we detected histone H3 acetylation in trophoblasts. The results showed that compared with that in the shCtrl group, histone H3 acetylation in HTR-8, JAR, and JEG-3 cells transfected with shRNA *ACLY* virus decreased by varying degrees but did not affect the total level of H3. Subsequently, treatment with the histone deacetylase inhibitor trichostatin A (TSA) rescued the histone H3 acetylation level (Figure 6(b)). Considering the effect of ACLY on the expression of trophoblast-derived IL-10, we further studied whether ACLY regulates the expression of cytokine IL-10 by regulating histone acetylation. The results of qRT-PCR and ELISA consistently showed that IL-10 level decreased significantly in HTR-8, JAR, and JEG-3 cells transfected with shRNA *ACLY* virus, and downregulation of IL-10 could be restored after TSA treatment (Figures 6(c) and 6(d)). It suggests that a lack of ACLY in trophoblasts may inhibit IL-10 expression by inhibiting histone acetylation.

3.7. Endoplasmic Reticulum Stress Is Involved in IL-10-Mediated Macrophage Polarization. Studies have shown that endoplasmic reticulum stress is involved in the process of M2 polarization of macrophages. To explore the internal mechanism, we treated M0 macrophages with HTR-8, JAR, or JEG-3 supernatant, with or without IL-10 (50 ng/ml) and detected the levels of endoplasmic reticulum stress-related proteins in macrophages using Western blotting. The results showed that compared with the HTR-8, JAR, and JEG-3-shCtrl groups, the level of endoplasmic reticulum stress-related proteins XBP1, p-PERK, p-IRE1, ATF6, and GRP78 in macrophages increased significantly after HTR-8, JAR, or JEG-3-shACLY-1 supernatant treatment; however, the levels of endoplasmic reticulum stress-related proteins in macrophages were decreased after IL-10 addition (Figures 7(a)–7(c)). Then, we performed immunohistochemical staining to detected the levels of endoplasmic reticulum stress-related proteins XBP1, p-PERK, p-IRE1, ATF6, and GRP78 in decidua from normal pregnancy and patients with RSA (Figures 8(a)–8(e)), and the results were consistent with those of Western blotting. The above results suggested that inhibition of endoplasmic reticulum stress mediated by trophoblast-derived IL-10 might be involved in macrophage polarization.

4. Discussion

The present study demonstrated that ACLY was highly expressed in placental villi and extravillous trophoblasts of normal pregnancy but was downregulated in the placental villi of RSA. Knockdown of *ACLY* in trophoblasts reduced the secretion of IL-10 by inhibiting histone acetylation. The reduced secretion of IL-10 by trophoblasts activated

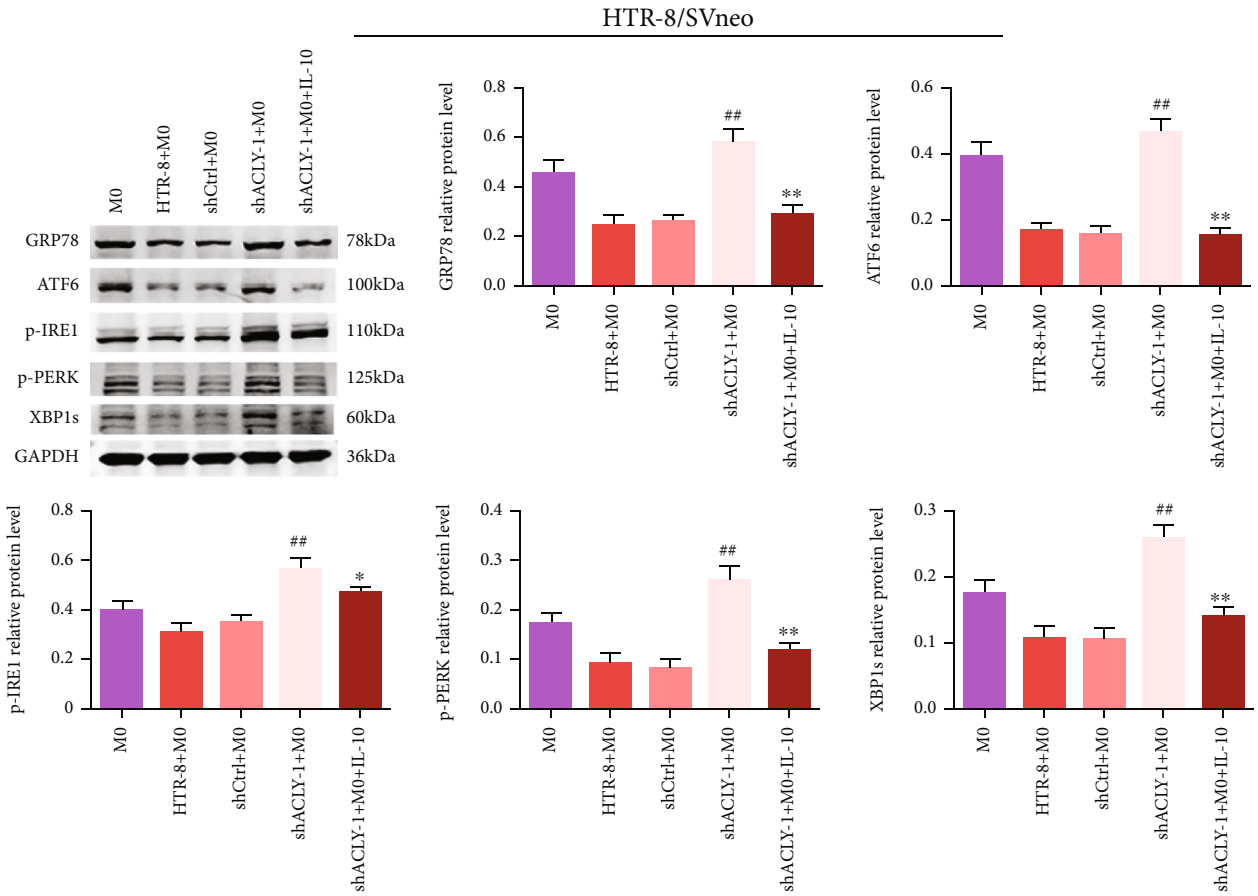

(a)

Figure 7: Continued.

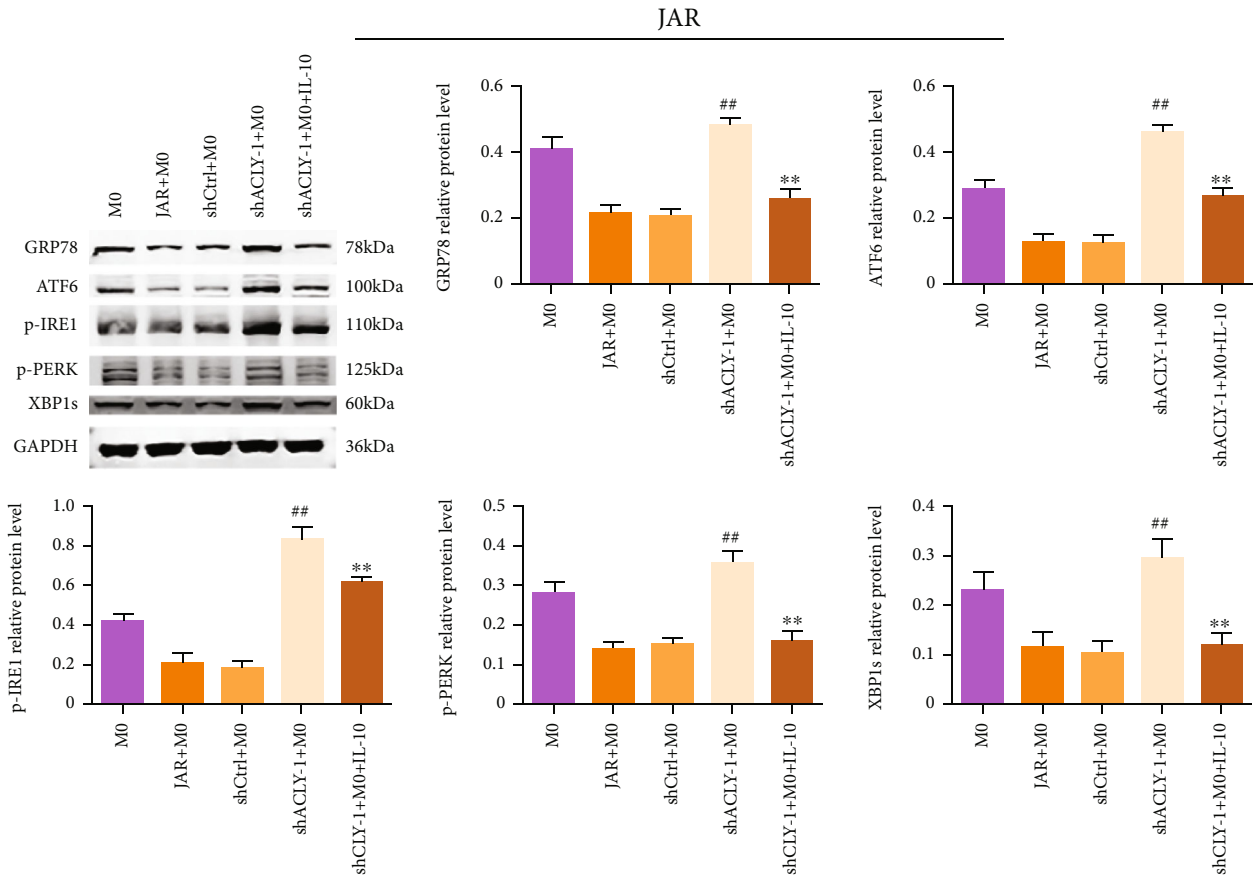

(b)

Figure 7: Continued.

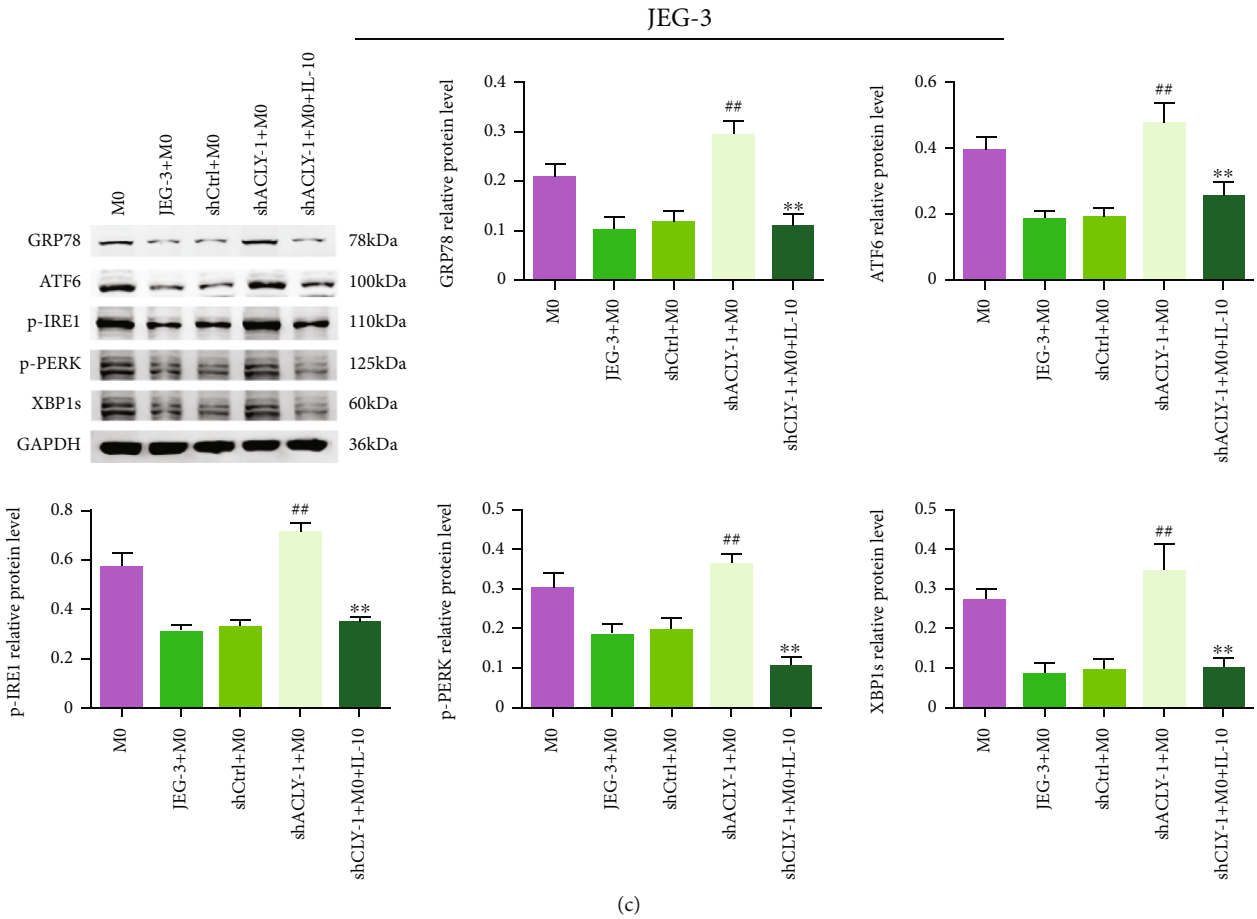

Figure 7: Endoplasmic reticulum stress is involved in IL-10-mediated macrophage polarization. (a–c) The levels of endoplasmic reticulum stress-related proteins, as detected using Western blotting (final concentration of IL-10 was 50 ng/ml). $^{\#\#}p < 0.01$, compared with shCtrl +M0; $^{*}p < 0.05$, $^{**}p < 0.01$, compared with shACLY+M0.

endoplasmic reticulum stress in macrophages, inhibiting their polarization to the M2 phenotype (Figure 9).

RSA, defined as two or more consecutive abortions, affects 5% of women of childbearing age [19]. The causes of RSA are complex, including genetic factors, abnormal female anatomy, hormones, infection, and mental health [20]. The fetus can be regarded as a semiallogeneic graft implanted into the mother. In a successful pregnancy, the mother will not reject the fetus because of the immune tolerance mechanism at the maternal-fetal interface [21]. The generation of maternal-fetal immune tolerance is very important for the successful establishment of mammalian pregnancies. Failure of maternal-fetal immune tolerance might lead to abnormal pregnancy diseases, including RSA [22–24]. The maternal-fetal interface comprises of a series of immune cells, such as decidual natural killer (dNK) cells, macrophages, T cells, dendritic cells, and B cells [25, 26]. In addition to these immune cells, fetal-derived trophoblast cells invade the maternal myometrium, which is also essential for maintaining immune tolerance [27, 28]. Decidual macrophages are in close contact with trophoblast cells during placental development, and the relationship between them is very important to establish and maintain a healthy pregnancy [1].

ATP citrate lyase (ACLY), an enzyme that generates acetyl CoA from citric acid, is the first rate control enzyme responsible for lipid synthesis and connects cell metabolism with histone acetylation [29]. Acetyl CoA is a key metabolic intermediate connecting metabolism, signal transduction, and epigenetics. It is an acetyl donor for protein acetylation reactions and plays an important role in chromatin dynamics and gene regulation [30, 31]. Many studies have established a close relationship between epigenetic regulation and placental trophoblast function by proving the key role of epigenetic regulatory factors in maintaining a healthy pregnancy [32, 33]. Disorder of ACLY is related to various diseases, including cancer [34]. Recent studies have shown that ACLY-mediated metabolic recombination is essential for epigenetic regulation of macrophage activation through histone acetylation [35, 36]; however, the role of ACLY in the maternal-fetal interface is unclear. Our results showed that ACLY was expressed positively in cytotrophoblasts (CTBs), syncytiotrophoblasts (STBs), and extravillous trophoblasts (EVTs). Interestingly, we found that ACLY was

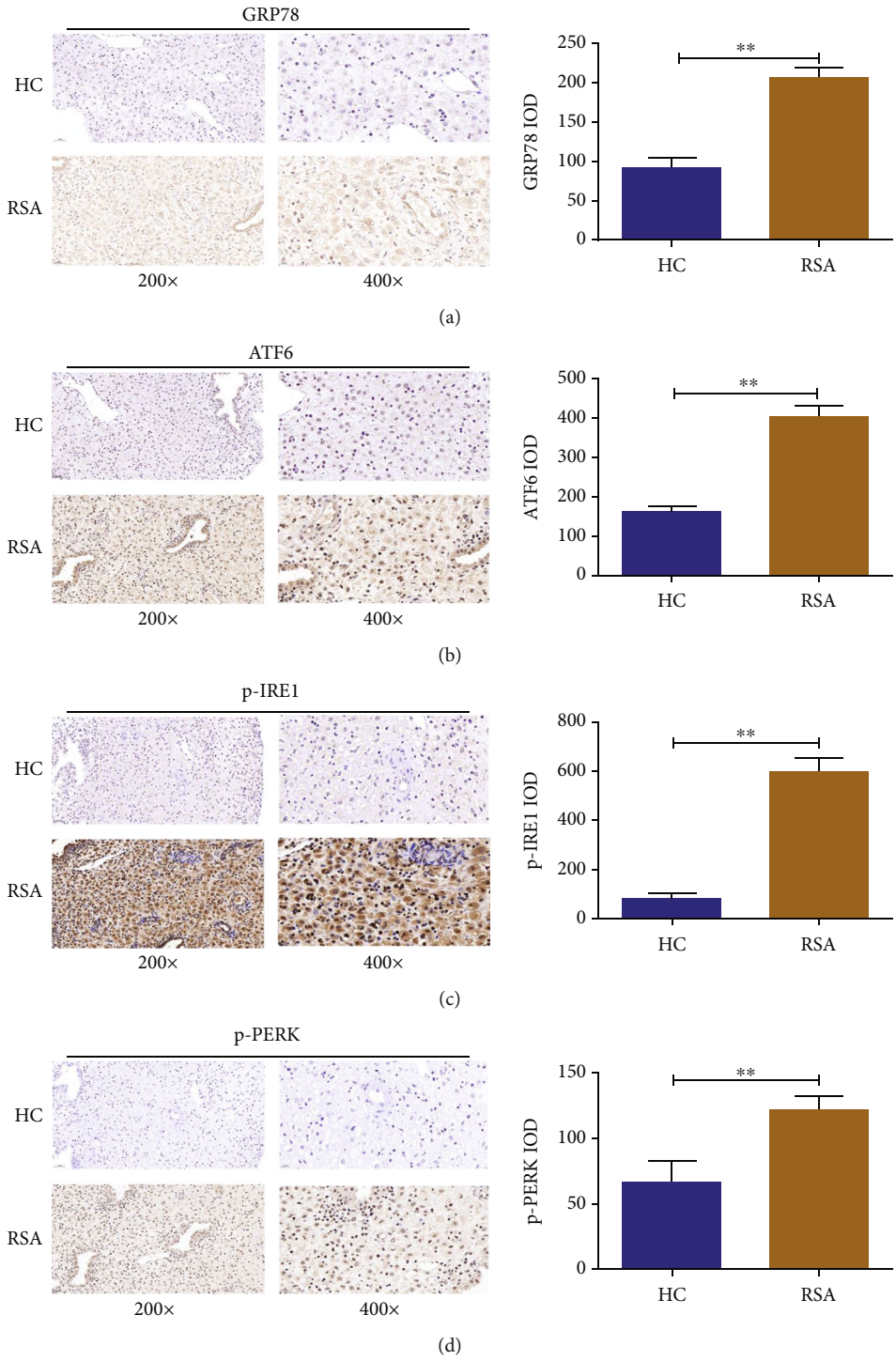

Figure 8: Continued.

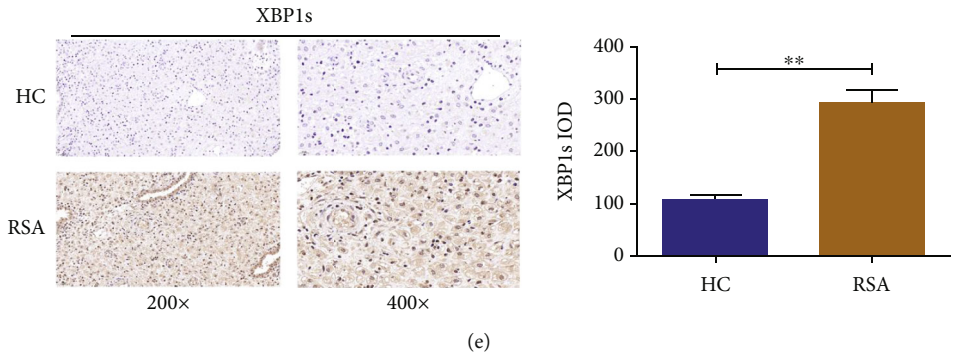

Figure 8: (a–e) The protein levels of endoplasmic reticulum stress-related proteins in decidua of patients with the RSA and the HC groups, as measured using immunohistochemistry ($n = 5$). $^{**}p < 0.01$, compared with the HC group. IOD: Integrated Optical Density. Scale bar: 200x = 50 μm, 400x = 20 μm.

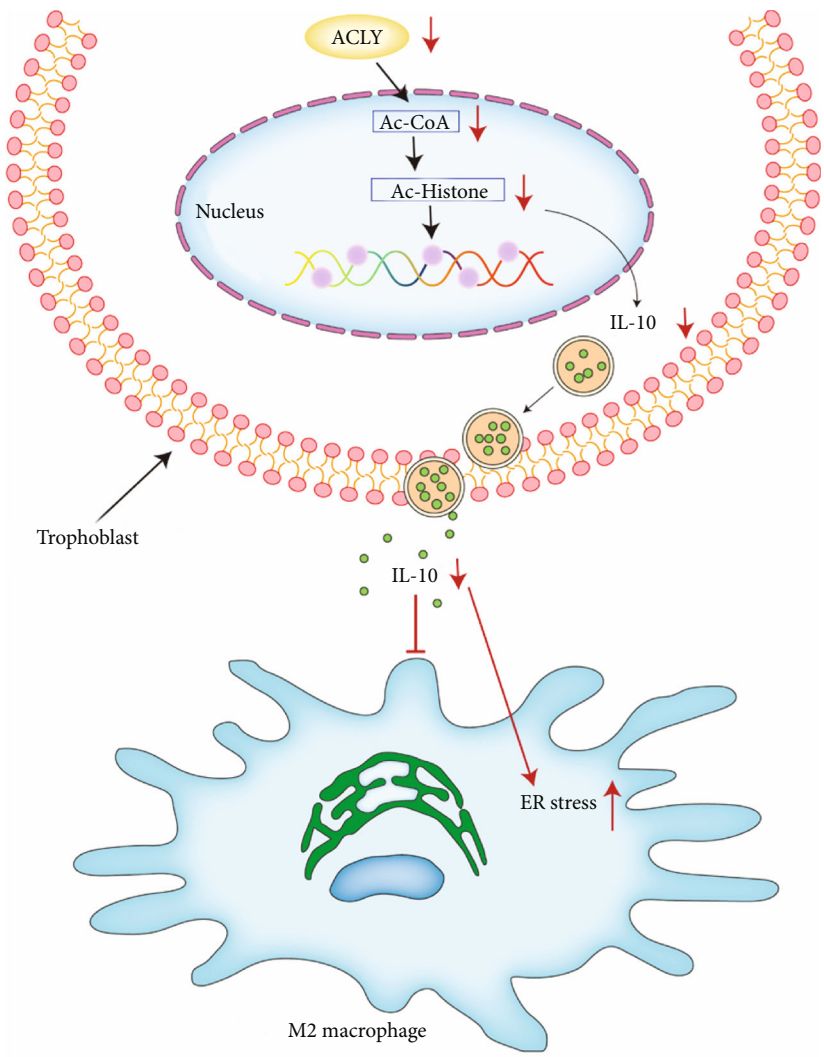

Figure 9: ACLY is decreased in placental villi from RSA, which may lead to the inhibition of histone acetylation in trophoblasts, thereby reducing the secretion of IL-10. Reduced IL-10 secretion activates endoplasmic reticulum stress in macrophages, thus inhibiting their M2 polarization.

also expressed in other cells in decidua, and their existence may have a certain pathophysiological effect, but we think it has nothing to do with the theme of this study. Moreover, we found that ACLY was significantly reduced in the villous tissue in the RSA group. These results suggested that the decrease in the ACLY level in villous trophoblasts is associated with RSA. Therefore, we detected the expression level of ACLY in four trophoblast cell lines (HTR-8, JEG-3, JAR, and BeWo), which showed that ACLY was highly expressed in HTR-8, JAR, and JEG-3 cell lines relative to that in BeWo cells. To clarify the function of ACLY, we knocked down the *ACLY* gene in HTR-8, JEG-3, and JAR cells for further experiments.

Macrophages are the second most abundant immune cell group in the pregnant uterus, accounting for about 20% of the total number of decidual leukocytes [37]. Macrophages can be divided into two polarization types according to their phenotype and secreted cytokines, namely, classically activated M1 macrophages and selectively activated M2 macrophages [38]. Macrophage polarization plays an important role in immune tolerance at the maternal-fetal interface. A change in macrophage polarization can lead to adverse pregnancy outcomes, such as infertility, RSA, and preterm birth [39]. Macrophages in the maternal-fetal interface are mainly M2 type, secreting high level of inhibitory cytokine IL-10 and low level of proinflammatory cytokine IL-1β, which is conducive to maintaining immune tolerance and normal pregnancy [40]. In maternal-fetal crosstalk, fetal trophoblast cells can secrete a variety of molecules to regulate immune tolerance, such as cytokines and chemokines [41, 42]. In addition, trophoblast cells can regulate the behavior of decidual macrophages by secreting cytokines or chemokines and participate in the induction of decidual macrophages into the M2 phenotype [43]. To investigate whether ACLY knockdown in trophoblasts is involved in the polarization of THP-1 macrophages, HTR-8, JAR, and JEG-3 cells were transfected with shRNA ACLY or empty vector virus. M0 macrophages were then incubated in conditioned media from HTR-8, JAR, or JEG cells transfected with shCtrl and HTR-8, JAR, or JEG cells transfected with shACLY for 72 hours. Untreated M0 macrophages were used as the control group. Our results showed that impaired ACLY expression in trophoblasts inhibited the M2 polarization of macrophages.

Trophoblasts can transmit signals to decidual macrophages through trophoblast secretory factors [44]. Interesting findings reported by Wang et al. [45] that trophoblast-derived CXCL16 induces M2 macrophage polarization that in turn inactivates NK cells at the maternal-fetal interface. Svensson-Arvelund et al. [46] found that that the human fetal placenta itself, particularly through trophoblast cells, was able to create a homeostatic and tolerant environment by producing soluble factors (M-CSF, IL-10, TGF-β, and TRAIL) that induced the polarization of homeostatic macrophages and the expansion of Tregs, as well as limited excessive Th cell activation. Recently, Ding et al. [47] found that trophoblast-derived IL-6 served as an important factor for normal pregnancy by activating Stat3-mediated M2 macrophage polarization. Besides, IL-34, a newly discovered cytokine, was present at the fetal-maternal interface and induced immunoregulatory macrophages of a decidual phenotype in vitro [48]. Therefore, to explore the potential mechanism, we first analyzed the expression of trophoblast-derived cytokines (IL-6, IL-10, CXCL16, M-CSF, and IL-34) in trophoblast cell lines. We found that compared with the control group (shCtrl), IL6, IL10, CXCL16, MCSF, and IL34 in HTR-8, JAR, and JEG-3 cells transfected with shRNA ACLY virus decreased by varying degrees.

ACLY produces acetyl CoA, which provides a donor substrate for histone acetylation [49]. In addition, histone acetylation is important for the expression of cytokines [50, 51]. Studies have shown that IL-10 was closely related to epigenetic modifications [18]. In addition, changes in histone modifications, especially histone acetylation, can lead to abnormal expression of IL-10 mRNA [52, 53]. Therefore, we focused on the role of IL-10. It showed that trophoblast-derived cytokine IL-10 was involved in M2 polarization. And we further explored whether the changes in IL-10 secretion caused by ACLY deletion were related to histone acetylation. The results showed that a lack of ACLY in trophoblasts might reduce the expression of IL-10 by inhibiting histone acetylation. A previous study showed that changes in histone modification, especially histone acetylation, can lead to abnormal expression of *IL10* mRNA [18], which is consistent with our results.

The endoplasmic reticulum (ER) is an important intracellular organelle responsible for protein synthesis, folding, and modification; lipid synthesis; and calcium storage [54]. The unfolded protein response (UPR) is an adaptive intracellular signaling pathway that responds to ER stress by weakening overall protein translation and degrading unfolded proteins [55]. Hypersecretory cell types, such as immune cells, might be highly sensitive to ER stress because of their required increased protein synthesis and folding [56]. For example, a study found IRE1α ablation enhanced M2 polarization of macrophages in a cellular autonomous manner [57]. Other studies have shown that the activation of ER stress plays a role in inhibiting the M2 polarization of macrophages [58]. These results suggest that the polarization of M2 macrophages is closely related to their ER stress state. Therefore, after using the coculture system, we detected the expression of ER stress marker proteins such as p-PERK, p-IRE1, ATF6, and GRP78 in macrophages. The results showed that compared with the HTR-8, JAR, and JEG-3-shCtrl groups, the ER stress marker proteins of macrophages increased significantly after culture with the supernatants of HTR-8, JAR, or JEG-3-shACLY. Adding IL-10 could reverse the increase in ER stress marker proteins in macrophages caused by *ACLY* knockdown in trophoblasts. This is consistent with previous research results [58].

In conclusion, our data demonstrated the important role of ACLY in the pathogenesis of RSA. ACLY was strongly expressed in the placental villi and extravillous trophoblasts of normal pregnancy but was downregulated in the placental villi of RSA. The knockdown of *ACLY* in trophoblasts reduced the secretion of IL-10 by inhibiting histone acetylation. The reduced secretion of IL-10 by trophoblasts caused activation of ER stress of macrophages, which inhibited the polarization of macrophages to M2 macrophages. Therefore, ACLY targeting acetyl CoA production might be a potential

therapeutic intervention for RSA. The epigenetic effect of ACLY on RSA is very important and cannot be ignored. However, there are still some limitations in this study, as further in vivo investigations is warranted in the future. In-depth studies relating to the regulation of the ACLY on trophoblasts will help us to elucidate the pathogenesis of a class of primary trophoblastic diseases such as RSA and provide new therapeutic targets for the treatment of RSA.

Data Availability

The original data is available upon reasonable request.

Conflicts of Interest

The authors declare that the research was conducted in the absence of any commercial or financial relationships that could be construed as a potential conflict of interest.

Authors' Contributions

Xin Chen, Qian Lin Song, and Ze Hong Li contributed equally to this work. Xin Chen and Qian Lin Song prepared the preliminary draft. Xin Chen designed the study. Zhuo Ni Xiao, Duan Ying Guo, and Jing Yang supervised the study. Xin Chen, Qian Lin Song, Ze Hong Li, Rui Ji, Jia Yu Wang, and Chang Ge performed the experiments. All authors have read and agreed to the published version of the manuscript. Xin Chen, Qian Lin Song, and Ze Hong Li contributed equally to this work.

Acknowledgments

This work was supported by the National Key Research and Development Program of China (Nos. 501100012166) and the National Natural Science Foundation of China (Nos. 81771662, 81771618, and 81971356).

References

[1] G. Mor and V. M. Abrahams, "Potential role of macrophages as immunoregulators of pregnancy," *Reproductive Biology and Endocrinology*, vol. 1, no. 1, p. 119, 2003.

[2] J. N. Bulmer, P. J. Williams, and G. E. Lash, "Immune cells in the placental bed," *The International Journal of Developmental Biology*, vol. 54, no. 2-3, pp. 281–294, 2010.

[3] S. J. Renaud, L. M. Postovit, S. K. Macdonald-Goodfellow, G. T. McDonald, J. D. Caldwell, and C. H. Graham, "Activated macrophages inhibit human cytotrophoblast invasiveness in vitro," *Biology of Reproduction*, vol. 73, no. 2, pp. 237–243, 2005.

[4] C. D. Mills, K. Kincaid, J. M. Alt, M. J. Heilman, and A. M. Hill, "M-1/M-2 macrophages and the Th1/Th2 paradigm," *Journal of Immunology*, vol. 164, no. 12, pp. 6166–6173, 2000.

[5] D. L. Laskin, V. R. Sunil, C. R. Gardner, and J. D. Laskin, "Macrophages and tissue injury: agents of defense or destruction?," *Annual Review of Pharmacology and Toxicology*, vol. 51, no. 1, pp. 267–288, 2011.

[6] S. Gordon and F. O. Martinez, "Alternative activation of macrophages: mechanism and functions," *Immunity*, vol. 32, no. 5, pp. 593–604, 2010.

[7] A. B. Amara, L. Gorvel, K. Baulan et al., "Placental macrophages are impaired in chorioamnionitis, an infectious pathology of the placenta," *Journal of Immunology*, vol. 191, no. 11, pp. 5501–5514, 2013.

[8] F. Y. Tsao, M. Y. Wu, Y. L. Chang, C. T. Wu, and H. N. Ho, "M1 macrophages decrease in the deciduae from normal pregnancies but not from spontaneous abortions or unexplained recurrent spontaneous abortions," *Journal of the Formosan Medical Association*, vol. 117, no. 3, pp. 204–211, 2018.

[9] L. Xu, Y. Li, Y. Sang, D. J. Li, and M. Du, "Crosstalk between trophoblasts and decidual immune cells: the cornerstone of maternal-fetal immunotolerance," *Frontiers in Immunology*, vol. 12, article 642392, 2021.

[10] A. Sica and A. Mantovani, "Macrophage plasticity and polarization: in vivo veritas," *The Journal of Clinical Investigation*, vol. 122, no. 3, pp. 787–795, 2012.

[11] S. Guenther, T. Vrekoussis, S. Heublein et al., "Decidual macrophages are significantly increased in spontaneous miscarriages and over-express FasL: a potential role for macrophages in trophoblast apoptosis," *International Journal of Molecular Sciences*, vol. 13, no. 7, pp. 9069–9080, 2012.

[12] M. Dominguez, B. Brune, and D. Namgaladze, "Exploring the role of ATP-citrate lyase in the immune system," *Frontiers in Immunology*, vol. 12, article 632526, 2021.

[13] L. A. Arias-Sosa, I. D. Acosta, E. Lucena-Quevedo, H. Moreno-Ortiz, C. Esteban-Perez, and M. Forero-Castro, "Genetic and epigenetic variations associated with idiopathic recurrent pregnancy loss," *Journal of Assisted Reproduction and Genetics*, vol. 35, no. 3, pp. 355–366, 2018.

[14] K. Rull, L. Nagirnaja, and M. Laan, "Genetics of recurrent miscarriage: challenges, current knowledge, future directions," *Frontiers in Genetics*, vol. 3, p. 34, 2012.

[15] V. Pietropaolo, C. Prezioso, and U. Moens, "Role of virus-induced host cell epigenetic changes in cancer," *International Journal of Molecular Sciences*, vol. 22, no. 15, p. 8346, 2021.

[16] S. K. Munro, B. Balakrishnan, A. C. Lissaman, P. Gujral, and A. P. Ponnampalam, "Cytokines and pregnancy: potential regulation by histone deacetylases," *Molecular Reproduction and Development*, vol. 88, no. 5, pp. 321–337, 2021.

[17] N. Mishra, C. M. Reilly, D. R. Brown, P. Ruiz, and G. S. Gilkeson, "Histone deacetylase inhibitors modulate renal disease in the MRL-lpr/lpr mouse," *The Journal of Clinical Investigation*, vol. 111, no. 4, pp. 539–552, 2003.

[18] Z. Zheng, G. Huang, T. Gao et al., "Epigenetic changes associated with interleukin-10," *Frontiers in Immunology*, vol. 11, p. 1105, 2020.

[19] Z. Williams, "Inducing tolerance to pregnancy," *The New England Journal of Medicine*, vol. 367, no. 12, pp. 1159–1161, 2012.

[20] T. C. Li, M. Makris, M. Tomsu, E. Tuckerman, and S. Laird, "Recurrent miscarriage: aetiology, management and prognosis," *Human Reproduction Update*, vol. 8, no. 5, pp. 463–481, 2002.

[21] W. X. Li, X. H. Xu, and L. P. Jin, "Regulation of the innate immune cells during pregnancy: an immune checkpoint perspective," *Journal of Cellular and Molecular Medicine*, vol. 25, no. 22, pp. 10362–10375, 2021.

[22] J. Trowsdale and A. G. Betz, "Mother's little helpers: mechanisms of maternal-fetal tolerance," *Nature Immunology*, vol. 7, no. 3, pp. 241–246, 2006.

[23] A. Leber, M. L. Zenclussen, A. Teles et al., "Pregnancy: tolerance and suppression of immune responses," *Methods in Molecular Biology*, vol. 677, pp. 397–417, 2011.

[24] Y. Tao, Y. H. Li, D. Zhang et al., "Decidual CXCR4+ CD56brightNK cells as a novel NK subset in maternal–foetal immune tolerance to alleviate early pregnancy failure," *Clinical and Translational Medicine*, vol. 11, no. 10, article e540, 2021.

[25] F. Yang, Q. Zheng, and L. Jin, "Dynamic function and composition changes of immune cells during normal and pathological pregnancy at the maternal-fetal interface," *Frontiers in Immunology*, vol. 10, p. 2317, 2019.

[26] M. M. Faas and P. de Vos, "Uterine NK cells and macrophages in pregnancy," *Placenta*, vol. 56, pp. 44–52, 2017.

[27] P. C. Arck and K. Hecher, "Fetomaternal immune cross-talk and its consequences for maternal and offspring's health," *Nature Medicine*, vol. 19, no. 5, pp. 548–556, 2013.

[28] X. Wu, L. P. Jin, M. M. Yuan, Y. Zhu, M. Y. Wang, and D. J. Li, "Human first-trimester trophoblast cells recruit CD56brightCD16- NK cells into decidua by way of expressing and secreting of CXCL12/stromal cell-derived factor 1," *Journal of Immunology*, vol. 175, no. 1, pp. 61–68, 2005.

[29] J. Wen, X. Min, M. Shen et al., "ACLY facilitates colon cancer cell metastasis by CTNNB1," *Journal of Experimental & Clinical Cancer Research*, vol. 38, no. 1, p. 401, 2019.

[30] F. Pietrocola, L. Galluzzi, J. M. Bravo-San Pedro, F. Madeo, and G. Kroemer, "Acetyl coenzyme A: a central metabolite and second messenger," *Cell Metabolism*, vol. 21, no. 6, pp. 805–821, 2015.

[31] W. Zheng, L. Tasselli, T. M. Li, and K. F. Chua, "Mammalian SIRT6 represses invasive cancer cell phenotypes through ATP citrate lyase (ACLY)-dependent histone acetylation," *Genes (Basel)*, vol. 12, no. 9, p. 1460, 2021.

[32] H. R. Kohan-Ghadr, L. Kadam, C. Jain, D. R. Armant, and S. Drewlo, "Potential role of epigenetic mechanisms in regulation of trophoblast differentiation, migration, and invasion in the human placenta," *Cell Adhesion & Migration*, vol. 10, no. 1-2, pp. 126–135, 2016.

[33] M. Hemberger, "Epigenetic landscape required for placental development," *Cellular and Molecular Life Sciences*, vol. 64, no. 18, pp. 2422–2436, 2007.

[34] P. Icard, Z. Wu, L. Fournel, A. Coquerel, H. Lincet, and M. Alifano, "ATP citrate lyase: a central metabolic enzyme in cancer," *Cancer Letters*, vol. 471, pp. 125–134, 2020.

[35] M. A. Lauterbach, J. E. Hanke, M. Serefidou et al., "Toll-like receptor signaling rewires macrophage metabolism and promotes histone acetylation via ATP-citrate lyase," *Immunity*, vol. 51, no. 6, 2019.

[36] A. J. Covarrubias, H. I. Aksoylar, J. Yu et al., "Akt-mTORC1 signaling regulates Acly to integrate metabolic input to control of macrophage activation," *eLife*, vol. 5, 2016.

[37] A. Erlebacher, "Immunology of the maternal-fetal interface," *Annual Review of Immunology*, vol. 31, no. 1, pp. 387–411, 2013.

[38] S. K. Biswas, M. Chittezhath, I. N. Shalova, and J. Y. Lim, "Macrophage polarization and plasticity in health and disease," *Immunologic Research*, vol. 53, no. 1-3, pp. 11–24, 2012.

[39] M. B. Brown, M. von Chamier, A. B. Allam, and L. Reyes, "M1/M2 macrophage polarity in normal and complicated pregnancy," *Frontiers in Immunology*, vol. 5, p. 606, 2014.

[40] T. Nagamatsu and D. J. Schust, "The immunomodulatory roles of macrophages at the maternal-fetal interface," *Reproductive Sciences*, vol. 17, no. 3, pp. 209–218, 2010.

[41] L. Ren, Y. Q. Liu, W. H. Zhou, and Y. Z. Zhang, "Trophoblast-derived chemokine CXCL12 promotes CXCR4 expression and invasion of human first-trimester decidual stromal cells," *Human Reproduction*, vol. 27, no. 2, pp. 366–374, 2012.

[42] Y. Sun, S. Wu, Q. Zhou, and X. Li, "Trophoblast-derived interleukin 9 mediates immune cell conversion and contributes to maternal-fetal tolerance," *Journal of Reproductive Immunology*, vol. 148, article 103379, 2021.

[43] F. Sun, S. Wang, and M. Du, "Functional regulation of decidual macrophages during pregnancy," *Journal of Reproductive Immunology*, vol. 143, article 103264, 2021.

[44] P. B. Aldo, K. Racicot, V. Craviero, S. Guller, R. Romero, and G. Mor, "Trophoblast induces monocyte differentiation into CD14+/CD16+ macrophages," *American Journal of Reproductive Immunology*, vol. 72, no. 3, pp. 270–284, 2014.

[45] X. Q. Wang, W. J. Zhou, X. X. Hou, Q. Fu, and D. J. Li, "Trophoblast-derived CXCL16 induces M2 macrophage polarization that in turn inactivates NK cells at the maternal-fetal interface," *Cellular & Molecular Immunology*, vol. 15, no. 12, pp. 1038–1046, 2018.

[46] J. Svensson-Arvelund, R. B. Mehta, R. Lindau et al., "The human fetal placenta promotes tolerance against the semiallogeneic fetus by inducing regulatory T cells and homeostatic M2 macrophages," *Journal of Immunology*, vol. 194, no. 4, pp. 1534–1544, 2015.

[47] J. Ding, C. Yang, Y. Cheng et al., "Trophoblast-derived IL-6 serves as an important factor for normal pregnancy by activating Stat3-mediated M2 macrophages polarization," *International Immunopharmacology*, vol. 90, article 106788, 2021.

[48] R. Lindau, R. B. Mehta, G. E. Lash et al., "Interleukin-34 is present at the fetal-maternal interface and induces immunoregulatory macrophages of a decidual phenotype in vitro," *Human Reproduction*, vol. 33, no. 4, pp. 588–599, 2018.

[49] Q. Guo, H. Kang, J. Wang et al., "Inhibition of ACLY leads to suppression of osteoclast differentiation and function via regulation of histone acetylation," *Journal of Bone and Mineral Research*, vol. 36, no. 10, pp. 2065–2080, 2021.

[50] T. Rauen, C. M. Hedrich, K. Tenbrock, and G. C. Tsokos, "cAMP responsive element modulator: a critical regulator of cytokine production," *Trends in Molecular Medicine*, vol. 19, no. 4, pp. 262–269, 2013.

[51] N. Kiguchi, Y. Kobayashi, F. Saika, and S. Kishioka, "Epigenetic upregulation of CCL2 and CCL3 via histone modifications in infiltrating macrophages after peripheral nerve injury," *Cytokine*, vol. 64, no. 3, pp. 666–672, 2013.

[52] L. Duan, M. Yi, J. Chen, S. Li, and W. Chen, "Mycobacterium tuberculosis EIS gene inhibits macrophage autophagy through up-regulation of IL-10 by increasing the acetylation of histone H3," *Biochemical and Biophysical Research Communications*, vol. 473, no. 4, pp. 1229–1234, 2016.

[53] S. Mukherjee, B. Mukherjee, R. Mukhopadhyay et al., "Imipramine exploits histone deacetylase 11 to increase the IL-12/IL-10 ratio in macrophages infected with antimony-resistant Leishmania donovani and clears organ parasites in experimental infection," *Journal of Immunology*, vol. 193, no. 8, pp. 4083–4094, 2014.

[54] D. S. Schwarz and M. D. Blower, "The endoplasmic reticulum: structure, function and response to cellular signaling," *Cellular and Molecular Life Sciences*, vol. 73, no. 1, pp. 79–94, 2016.

[55] D. Ron and P. Walter, "Signal integration in the endoplasmic reticulum unfolded protein response," *Nature Reviews. Molecular Cell Biology*, vol. 8, no. 7, pp. 519–529, 2007.

[56] D. R. Soto-Pantoja, A. S. Wilson, K. Y. Clear, B. Westwood, P. L. Triozzi, and K. L. Cook, "Unfolded protein response signaling impacts macrophage polarity to modulate breast cancer cell clearance and melanoma immune checkpoint therapy responsiveness," *Oncotarget*, vol. 8, no. 46, pp. 80545–80559, 2017.

[57] B. Shan, X. Wang, Y. Wu et al., "The metabolic ER stress sensor IRE1α suppresses alternative activation of macrophages and impairs energy expenditure in obesity," *Nature Immunology*, vol. 18, no. 5, pp. 519–529, 2017.

[58] K. Minton, "Immunometabolism: Stress-induced macrophage polarization," *Nature Reviews Immunology*, vol. 17, no. 5, p. 277, 2017.

Hindawi
Oxidative Medicine and Cellular Longevity
Volume 2022, Article ID 1681623, 20 pages
https://doi.org/10.1155/2022/1681623

Research Article

Aberrant Expression of Mitochondrial SAM Transporter SLC25A26 Impairs Oocyte Maturation and Early Development in Mice

Gui-ping Cheng,[1] Shi-meng Guo,[1] Ying Yin,[2] Yuan-yuan Li,[1] Ximiao He,[2] and Li-quan Zhou[1]

[1]*Institute of Reproductive Health, Tongji Medical College, Huazhong University of Science and Technology, Wuhan, China*
[2]*School of Basic Medicine, Tongji Medical College, Huazhong University of Science and Technology, Wuhan, Hubei, China*

Correspondence should be addressed to Li-quan Zhou; zhouliquan@hust.edu.cn

Received 16 November 2021; Revised 27 February 2022; Accepted 9 March 2022; Published 13 April 2022

Academic Editor: Xing Xing Fan

The immature germinal vesicle (GV) oocytes proceed through metaphase I (MI) division, extrude the first polar body, and become mature metaphase II (MII) oocytes for fertilization which is followed by preimplantation and postimplantation development until birth. *Slc25a26* is the gene encoding S-adenosylmethionine carrier (SAMC), a member of the mitochondrial carrier family. Its major function is to catalyze the uptake of S-adenosylmethionine (SAM) from cytosol into mitochondria, which is the only known mitochondrial SAM transporter. In the present study, we demonstrated that excessive SLC25A26 accumulation in mouse oocytes mimicked naturally aged oocytes and resulted in lower oocyte quality with decreased maturation rate and increased reactive oxygen species (ROS) by impairing mitochondrial function. Increased level of *Slc25a26* gene impacted gene expression in mouse oocytes such as *mt-Cytb* which regulates mitochondrial respiratory chain. Furthermore, increased level of *Slc25a26* gene in fertilized oocytes slightly compromised blastocyst formation, and *Slc25a26* knockout mice displayed embryonic lethality around 10.5 dpc. Taken together, our results showed that *Slc25a26* gene plays a critical role in oocyte maturation and early mouse development.

1. Introduction

In female mice, primordial germ cells (PGCs) initiate entry into prophase of meiosis I on embryonic day 13.5. Around the time of birth, oocytes are arrested at the diplotene stage in prophase I of meiosis for an extended period of time (up to months in mice and decades in humans) which is also called germinal vesicle (GV) stage [1, 2]. Upon hormonal surge, a limited number of immature oocytes resume meiosis which is indicated by GV breakdown. Accompanying with the chromatin condensation and microtubule organization, the oocytes proceed through the meiosis I (MI) division and extrude the first polar body (Pb1), and then, meiosis becomes arrested again at metaphase II (MII) until fertilization activates it to complete the second meiotic division [3–5]. Any errors during this process will affect meiotic progression and fertilization, producing low-quality oocytes [6]. In most mammals, oocyte quality declines with increase in maternal age [7]. Successful fertilization and subsequent embryonic development depend on oocyte quality which can be assessed by oocyte maturation, spindle formation, energy supply, syngamy, and early embryonic development and epigenetic modifications [8]. During oocyte maturation, mitochondria are the major source of energy supply of the oocytes, and changes of function and distribution of mitochondria may affect energy supply and oocyte maturation [8]. In addition, mitochondrial dysfunction also impairs early embryo development and can cause postimplantation failure [9].

SAM (S-adenosylmethionine) is the universal methyl donor involved in a broad range of biological methylation reactions [10, 11]. In the cytosol, SAM is synthesized from

methionine and adenosine under the action of methionine adenosine transferase [12–14]. *Slc25a26* is the gene encoding S-adenosylmethionine carrier (SAMC), a member of the mitochondrial carrier family, which is the only known mitochondrial SAM transporter catalyzing the uptake of SAM from the cytosol into mitochondria [15]. In mitochondria, SAM is required for methylation of DNA, RNA, and proteins and as an intermediate in the biosynthesis of lipoic acid, ubiquinone [16]. Aberrant expression of SLC25A26 may induce various mitochondrial dysfunctions, leading to impairment of oxidative phosphorylation, increased oxidative stress, decrease in glutathione (GSH) defense and apoptosis, and impaired cellular functions by regulating methyl metabolism [15, 17]. In addition, impairment of SAMC function, as consequence of mutations in *Slc25a26*, causes various mitochondrial defects, including those affecting RNA stability, protein modification, mitochondrial translation, and the biosynthesis of CoQ10 and lipoic acid [18].

Thus, we asked whether *Slc25a26* plays an important role in determining oocyte quality by controlling mitochondrial functions. In present study, we used *Slc25a26*-overexpressed oocytes/embryos and knockout embryos to demonstrate that proper level of *Slc25a26* is important for oocyte maturation and early embryo development.

2. Materials and Methods

2.1. Animals. Young (4-5 weeks) and naturally aged ICR mice (10-12 months) were purchased from SIPEIFU (Beijing, China). *Slc25a26* knockout mice (C57 background) were obtained from Zhi-hua Wang Laboratory in the Wuhan University. All the mice were housed in SPF animal facility at the Huazhong University of Science and Technology.

2.2. Oocyte and Embryo Collection for Culturing and Microinjection. Fully grown GV oocytes were obtained from female mice by manual rupturing of antral ovarian follicles. For microinjection, denuded GV oocytes were collected in M2 medium (M1250, Easycheck, China) with 2.5 μM milrinone to inhibit spontaneous germinal vesicle breakdown (GVBD). Then, *Slc25a26* cRNA (700 ng/μl) were coinjected with *H2b-egfp* cRNA (200 μg/μl) into GV oocytes using a micromanipulator and microinjector (Eppendorf) under an inverted microscope (Eclipse TE200, Nikon). After microinjection, the oocytes were cultured in *in vitro* maturation (IVM) medium (M2115, Easycheck, China) with 2.5 μM milrinone for 8 h to allow translation of exogenous cRNA. Similarly, siRNA against *Slc25a26* (70 μM, sense: 5′-GCUG UUGGAUCCUUUCCUATT-3′; antisense: 5′-UAGGAA AGGAUCCAACAGCTT-3′) or negative control oligo was injected into GV oocytes and cultured in IVM medium with milrinone for 20 h to allow efficient knockdown. siRNA against mouse *Slc25a26* and the negative control oligo were synthesized by GenePharma (Shanghai, China). Then, microinjected oocytes were washed in IVM medium for several times, followed by culturing in IVM medium covered with mineral oil at 37°C in a 5% CO_2 incubator for *in vitro* maturation. To collect zygotes, 3-4-week-old female mice were superovulated by injecting 10 IU of pregnant mare serum gonadotropin (PMSG) followed 48 h later with 10 IU of human chorionic gonadotropin (HCG) then mating with male overnight. Zygotes were obtained from the oviducts after 16 h of HCG injection. Zygotes were injected with *Slc25a26* cRNA together with *H2b-egfp* cRNA and cultured in KSOM medium (M1450, Easycheck, China) covered with mineral oil at 37°C in a 5% CO_2 incubator for their development.

2.3. Plasmid Construction and cRNA Synthesis. Total RNA was extracted from mouse testis following the manufacturer's protocol using the TRI Reagent (Sigma, T9424). Total RNA was reverse transcribed into cDNA by Hifair 1st Strand cDNA Synthesis Super Mix for qPCR (gDNA digester plus) (11141ES10, YEASEN, Shanghai, China). *Slc25a26* gene was cloned from cDNA using nested PCR by Prime-STAR HS DNA Polymerase (R010A, TaKaRa) with 2 primer pairs (the first pair: forward, 5′-AAGTAG TTGCTCCATATCCCG-3′; reverse, 5′-TTGTAGCCAGT TTGCTTTCC-3′; the 2nd pair: forward, 5′-CTAGCTAGC CACCATGGACGCGCCGGGCT-3′; reverse, 5′-CTGC TAA CCGGTGGTGGGCTCTTCCTGCCCACC-3′). PCR products were digested with NheI and AgeI (NEB Inc., MA, USA) and ligated into PVAX1 vector with FLAG tag. cRNAs were *in vitro* transcribed and capped from linearized plasmids using mMESSAGE mMACHINE Kit (AM1344, Invitrogen) and Poly(A) Tailing Kit (AM1350, Invitrogen) according to the manufacturer's instruction. Synthesized RNA was aliquoted and stored at -80°C.

2.4. Immunofluorescence. Oocytes or embryos were fixed in 4% paraformaldehyde for 30 min and permeabilized in 0.5% Triton X-100 for 25 min at room temperature (RT). After blocking with 1% BSA for 1 h at RT, oocytes were incubated with primary antibodies at 4°C overnight. Primary antibodies used were as follows: anti-α-tubulin-FITC antibody (1 : 200; Sigma, F2168), anti-SLC25A26 antibody (1 : 150; Sigma, HPA026887), and anti-FLAG antibody (1; 200; AE063, ABclonal). Then, oocytes were washed in PBS 3 times and incubated with CoraLite594-conjugated Goat Anti-Rabbit IgG(H+L) (SA00013-4, Proteintech Group, Inc.) and CoraLite488-conjugated Affinipure Goat Anti-Rabbit IgG(H+L) (SA00013-2, Proteintech Group, Inc.) for 1-2 h at RT. After washing in PBS, oocytes were put into the antifade medium containing Hoechst 33342 on a glass slide and observed under a confocal laser scanning microscope (LSM 800, Zeiss, Germany). For mitochondria and endoplasmic reticulum staining, oocytes were cultured in M2 medium containing 200 nM Mito-Tracker Red CMXRos (C1035, Beyotime, China) or ER-Tracker Red (C1041, Beyotime, China) with a dilution ratio of 1 : 1000 for 30 min at 37°C. To assess mitochondrial membrane potential, oocytes were cultured in M2 medium with JC-1 (C2006, Beyotime, China) at 37°C for 30 min. After three times of washing, oocytes were mounted on antifade medium with Hoechst 33342 and examined under a confocal laser scanning microscope (LSM 800, Zeiss, Germany).

Reactive oxygen species (ROS) levels of oocytes were determined by Reactive Oxygen Species Assay Kit (S0033S, Beyotime, China). Generally, oocytes were incubated with fluorescent probe DCFHDA for 30 min at 37°C. Following washing, oocytes were placed into antifade medium containing Hoechst 33342 and observed under the laser scanning confocal microscope (LSM 800, Zeiss, Germany). For Annexin-V staining, oocytes were stained with the Annexin V-FITC (C1062L, Beyotime, China) for 20 min at RT in the dark. Then oocytes were washed three times and placed into antifade medium containing Hoechst 33342 and observed under the laser scanning confocal microscope (LSM 800, Zeiss, Germany). Immunofluorescence was carried out and processed on control oocytes and treatment in parallel for each antibody. The same confocal microscope settings were used to obtained images for comparison. Immunofluorescence signals were captured using Image J 1.43u software (National Institutes of Health (NIH)), and mean gray value of regions of interest was analyzed for the quantification of the fluorescent intensity.

2.5. Western Blotting Analysis. GV oocytes were lysed in 1 × SDS-PAGE Protein Loading Buffer (5 × SDS-PAGE Protein Loading Buffer (20315ES05, YEASEN, China) diluted with RIPA lysis buffer containing protease inhibitor) and boiled in 98°C water for 5 minutes. The lysates were then separated by 12% sodium dodecyl sulfate-polyacrylamide gel electrophoresis and transferred onto polyvinylidene difluoride membranes (Millipore, Darmstadt, Germany). Following blocking in 5% nonfat milk for 1 h at room temperature, the blots were incubated with anti-SLC25A26 (1 : 500 dilution, Sigma, HPA026887) and anti-GAPDH (1 : 1000 dilution, 60004-1-Ig, Proteintech, Wuhan, China) antibodies overnight at 4°C. After washing in TBST for 3 times, the blots were incubated with horseradish peroxidase-conjugated secondary antibodies for 1 h at room temperature. After washing in TBST, chemiluminescence was detected with ECL working fluid (Beyotime). The relative densities of protein bands were analyzed using ImageJ software.

2.6. Measurement of ATP Content. ATP determination was performed using an ATP Determination Kit (A22066, Invitrogen). In brief, 15 oocytes were lysed in 30 μl lysis buffer (20 mM Tris, 0.9% Nonidet P-40, and 0.9% Tween-20). Low-concentration ATP standard solutions (0, 0.1, 0.5, 1, 10, 50, 100, and 500 nmol of ATP) were prepared by diluting the 5 mM ATP solution. 10 μl samples or ATP standard solutions mixed with 200 μl standard reaction solution (1× reaction buffer, 1 mM DTT, 0.5 mM D-luciferin, and 0.2 μg/ml firefly luciferase) were made according to the experimental protocol of ATP Determination Kit, and bioluminescence was measured using a plate reader. An eight-point standard curve was produced in each assay, and ATP levels were calculated using the formula derived from the linear regression of the standard curve.

2.7. Determination of mtDNA Copy Number. 10-20 oocytes were loaded in a PCR tube with 30 μl lysis buffer (50 mM Tris-HCl pH 8.0,;0.5% Triton X-100, and 0.2 mg/ml proteinase K) and was incubated at 55°C for 2 h. Proteinase K was heat inactivated at 95°C for 10 min, and then, the samples were used for PCR analysis. Quantitative real-time PCR was performed using the ABI StepOne system and mouse mtDNA-specific primers are as follows: forward, 5′-AACC TGGCACTGAGTCACCA-3′ and, reverse, 5′-GGGTCT GAGTGTATATATCATGAAGAGAAT-3′.

2.8. Low-Input RNA Sequencing and Data Analysis. RNA sequencing library preparation of oocytes was carried out by the Smart-Seq2 method. Generally, samples (10 oocytes per sample) for the control and SLC25A26-OE groups were collected and directly lysed in the single-cell lysis components with RNase inhibitors. Then, the 1st cDNA strand was synthesized with oligo dT by reverse transcription and amplified by PCR. Following purification of amplified products, the library was constructed by DNA fragmentation, end repair, addition of "A" and joint, PCR amplification, and library quality control. Qualified libraries were loaded onto Illumina Hiseq platform for PE150 sequencing. Raw reads were processed with Cutadapt v1.16. Trimmed reads were mapped to mouse genome (GENCODE release M23) using STAR with default settings. Differential expression of genes for pairwise comparisons was assessed by DESeq2 v1.24.0. The TE transcripts program was used to obtain counts for transposable elements (TEs) with default parameters. Read counts of gene and TE transcripts were normalized to the total aligned counts. Differentially regulated genes in the DESeq2 analysis were defined as those which were more than twofold increased or decreased with adjusted $p < 0.05$. Volcano and heat map were generated by R.

2.9. RNA Extraction and Quantitative Real-Time PCR (qRT-PCR). A total of 25-30 oocytes/zygotes or 20 cleavage embryos or 15 blastocysts were collected, respectively. Total RNA was extracted using the TRI Reagent (Sigma, T9424) and reverse transcribed into cDNA by Hifair 1st Strand cDNA Synthesis Super Mix for qPCR (gDNA digester plus) (11141ES10, YEASEN, Shanghai, China). Each PCR reaction consisted of 10 μl of Hieff qPCR SYBR Green Master Mix (High Rox Plus) (11203ES03, YEASEN, Shanghai, China), 8.2 μl of water, 1 μl of cDNA sample, and 0.8 μl of gene-specific primers (5 μM; *Slc25a26* primers: forward, 5′-TCTGGGGCAACAGTGTGTAG-3′; reverse, 5′-TACTAA GTGTGTGCGGCGGT-3′; *mt-Cytb* primers: forward, 5′-ACCTCAAAGCAACGAAGCCT-3′; reverse, 5′-TGGGTG TTCTACTGGTTGGC-3′). Real-time PCR was performed by the StepOnePlus Real-Time PCR system (Applied Biosystems, USA). mRNA levels were normalized to *Gapdh*. The experiments were performed for at least three times.

2.10. Genotyping. Total genomic DNA extracted from mouse tails was used to determine the genotypes of mice by PCR. Mouse tails were dissolved in a DNA lysis buffer (25 mM NaOH; 2 mM EDTA) at 95°C for 1 h and then in neutralizing buffer (40 mM Tris-HCl, pH = 6.8). PCR was performed for 30-33 cycles at 95°C for 30 s, 60°C for 30 s, and 72°C for

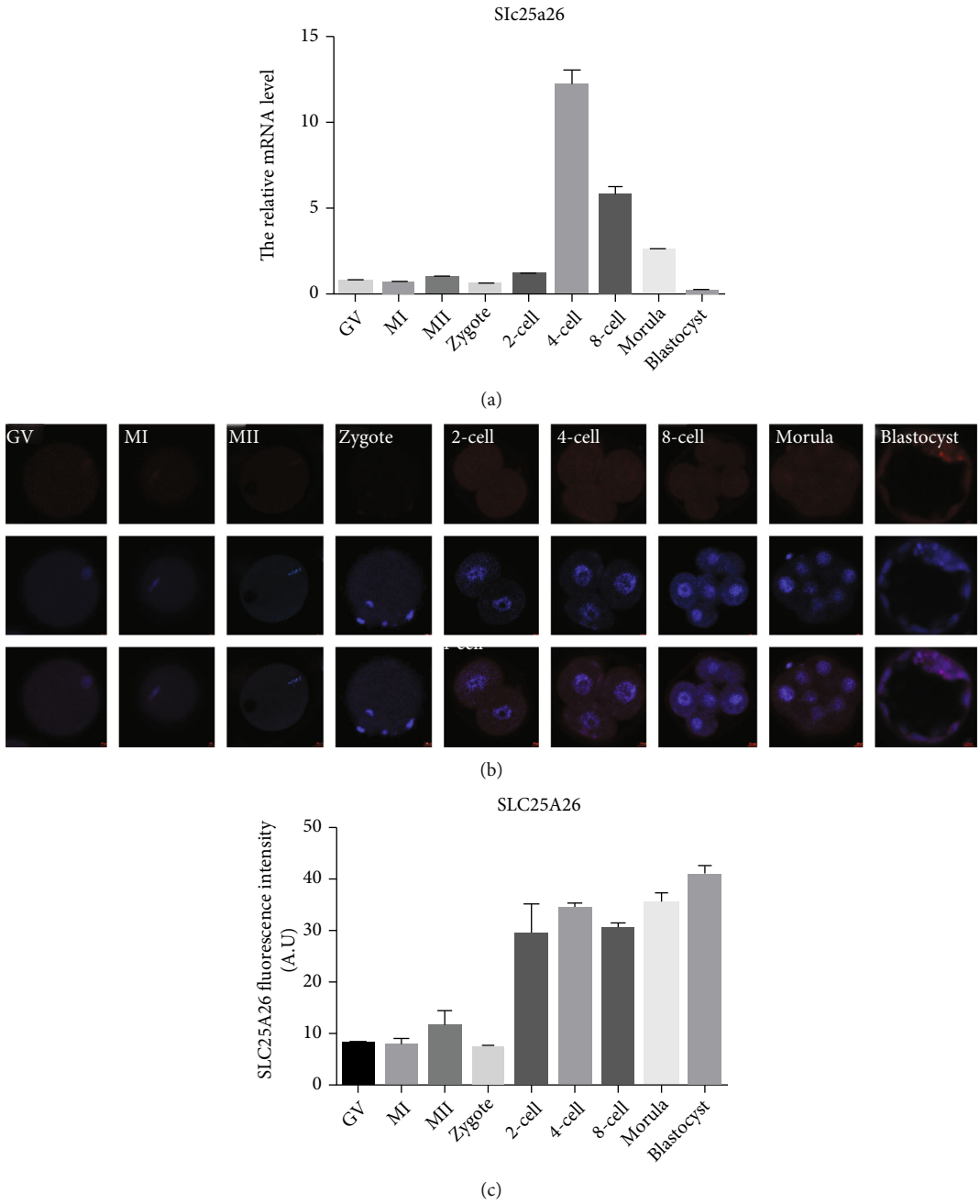

Figure 1: Expression pattern of mRNA and protein of *Slc25a26* during mouse oocyte maturation and embryo preimplantation development. (a) The mRNA levels of *Slc25a26* in GV, MI, and MII oocytes and mouse embryos at zygote, 2-cell, 4-cell, 8-cell, morula, and blastocyst stages were examined by qRT-PCR. 20–30 oocytes and embryos were collected for each group. (b) GV, MI, and MII oocytes and zygote, 2-cell, 4-cell, 8-cell, morula, and blastocyst stage embryos were immunolabeled with anti-SLC25A26 antibody to identify subcellular localization and expression of SLC25A26 during oocyte maturation and preimplantation development. Red, SLC25A26; blue, DNA. Bar = 10 μm. (c) The protein levels of SLC25A26 in GV, MI, and MII oocytes and embryos at zygote, 2-cell, 4-cell, 8-cell, morula, and blastocyst stages were measured with ImageJ for quantification of fluorescence intensities ($n = 8$ for each group). A.U. means arbitrary units. Data are presented as the mean ± SEM.

40 s, with a final extension at 72°C for 5 min using primers (knockout allele: forward, 5′-CCAGTGGATTGAAGAAGT TTTGAAGGAC-3′; reverse, 5′-AAGCTCCTTGTTGACT GGGTCATTC-3′; wild-type allele: forward, 5′-GAGGTA GAAGTGCAACTGAGCGAACA-3′, reverse, 5′-GTATCT GTACTGTTCCTGTGCATGGG-3′). DNA fragments were visualized by 2% agarose gel electrophoresis.

2.11. Analysis of Dissected Embryos. For the analysis postimplantation embryos, *Slc25a26* heterozygous males were

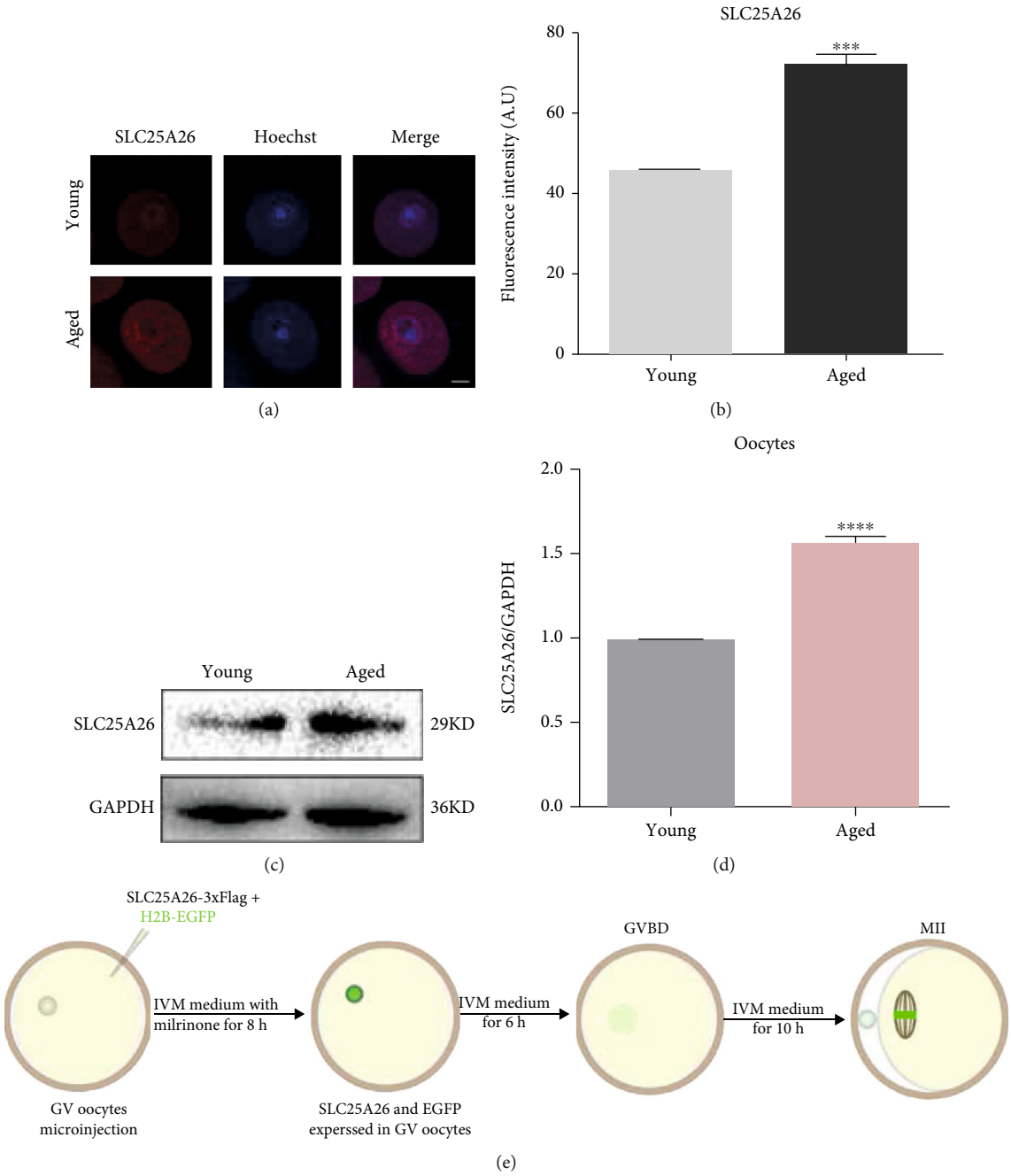

Figure 2: Continued.

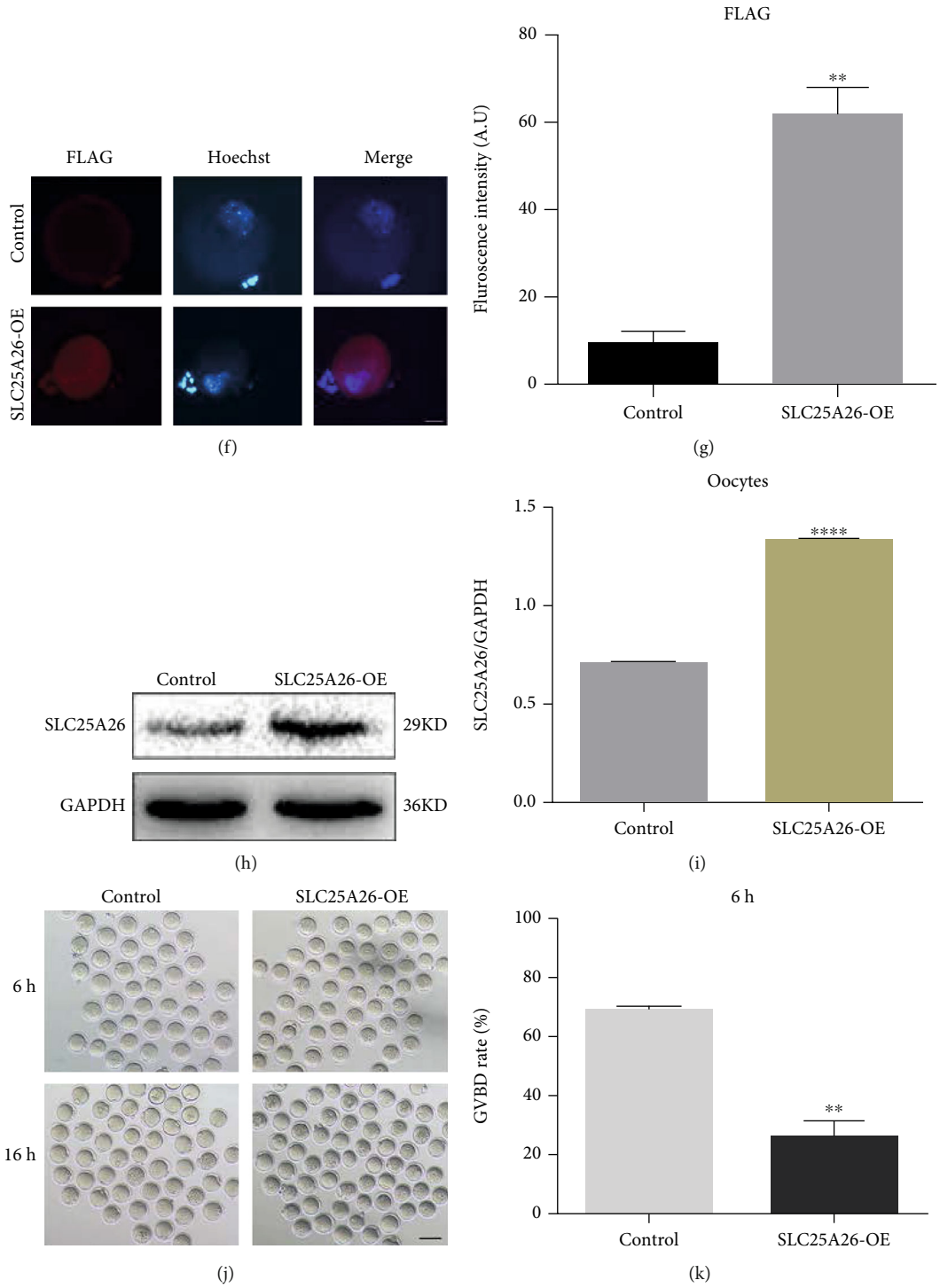

Figure 2: Continued.

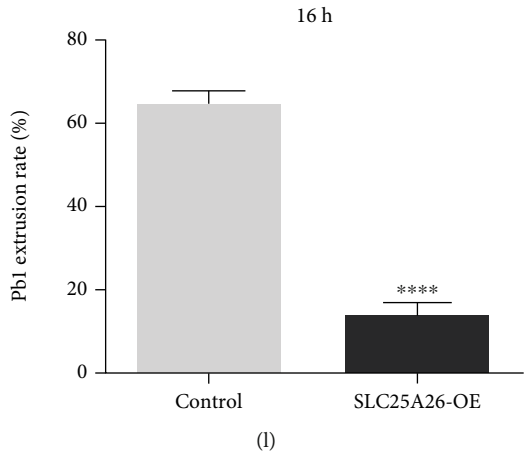

Figure 2: Effects of SLC25A26 expression on the meiotic progression of mouse oocytes. (a) Representative images of SLC25A26 protein staining in young and aged oocytes. Scale bar = 20 μm. (b) The fluorescence intensity of SLC25A26 signals was measured in young and aged oocytes. $^{***}p < 0.001$. A.U. means arbitrary units. (c) Representative western blotting images of SLC25A26 protein in young and aged oocytes. (d) The mean densitometric quantification of SLC25A26 protein level as measured in young and aged oocytes with ImageJ. $^{****}p < 0.0001$. (e) Schematic of overexpressing the SLC25A26 in GV oocyte by microinjection and its IVM culture. Efficiency of SLC25A26 overexpression (SLC25A26-OE) after mRNA injection was verified by immunofluorescence: (f) representative images of FLAG protein staining in control and SLC25A26-OE group. Scale bar = 50 μm. (g) The fluorescence intensity of FLAG signals was measured in control and SLC25A26-OE oocytes. $^{**}p < 0.01$. A.U. means arbitrary units. (h) SLC25A26 protein level was determined by western blot analysis. (i) The mean densitometric quantification of SLC25A26 protein level as measured in control and SLC25A26-OE oocytes with ImageJ. $^{****}p < 0.0001$. (j) Representative images of control and SLC25A26-OE oocytes. Scale bar = 100 μm. (k and l) Quantitative analysis of GVBD and Pb1 extrusion rate in control and SLC25A26-OE. $^{**}p < 0.01$ and $^{****}p < 0.0001$. Data are presented as the mean ± SEM.

mated with *Slc25a26* heterozygous females, and embryos were dissected from pregnant females at 7.5, 8.0, 8.5, 9.5, and 10.5 dpc (days post coitum). The day of plug formation was defined as embryonic day 0.5. After dissection, embryos were photographed with stereomicroscope linked to a camera.

2.12. Statistical Analysis. Data were presented as mean ± SEM. All experiments were replicated more than three times. Statistical comparisons were made with Student's *t* test. $p < 0.05$ was considered to be statistically significant.

3. Results

3.1. Changes of mRNA and Protein Levels of Slc25a26 during Mouse Oocyte Maturation and Preimplantation Development. The mRNA and protein levels of *Slc25a26* during oocyte maturation and preimplantation development were determined by qRT-PCR and immunofluorescence staining, respectively. The transcript of *Slc25a26* was at a low level in oocytes and early embryos before 4-cell stage, increased significantly at the 4-cell stage, then decreased gradually, and became weakest at blastocyst stage (Figure 1(a)). Immunofluorescence staining proved that SLC25A26 protein was mainly localized in the cytoplasm of oocytes and preimplantation embryos (Figure 1(b)). The fluorescence intensity of SLC25A26 appeared weak in oocytes and zygotes, was enhanced at the 2-cell stage, and had robust expression later on (Figures 1(b) and 1(c)). These results indicate that oocytes maintain a low level of SLC25A26 and SLC25A26 is induced after embryonic program is turned on.

3.2. Increased SLC25A26 Level in Naturally Aged Oocytes Impaired Developmental Competence of Mouse Oocytes. Firstly, we detected the SLC25A26 level in young and aged oocytes by immunostaining and western blotting. We identified significantly increased expression level in aged oocytes comparing to young oocytes (Figures 2(a), 2(b), 2(c), and 2(d)). To investigate the consequence of SLC25A26 protein accumulation in oocytes, we overexpressed SLC25A26 protein in GV oocytes by microinjection with *Slc25a26* cRNA, and *H2b-egfp* cRNA was coinjected to confirm success of microinjection (Fig. S1). The injected oocytes were then cultured in IVM medium containing milrinone to allow protein synthesis for 8 h and were then transferred to IVM medium for oocyte maturation (Figure 2(e)). The expression of exogenous SLC25A26 protein was verified by examination of FLAG tag and total SLC25A26 level (Figures 2(f), 2(g), 2(h), and 2(i)). After culturing for 6 hours in IVM medium, the ratio of GVBD was decreased in the SLC25A26 overexpression group compared with that in the control group ($p < 0.01$; Figures 2(j) and 2(k)). Moreover, the first polar body (Pb1) extrusion rate had significantly decline ($p < 0.0001$) due to SLC25A26 overexpression upon *in vitro* maturation for 16 hours (Figured 2(j) and 2(l)). These observations imply that SLC25A26 accumulation in mouse oocytes dampened developmental competence of oocytes.

To explore whether knockdown of *Slc25a26* could restore the quality of the aged oocytes, we injected siRNA

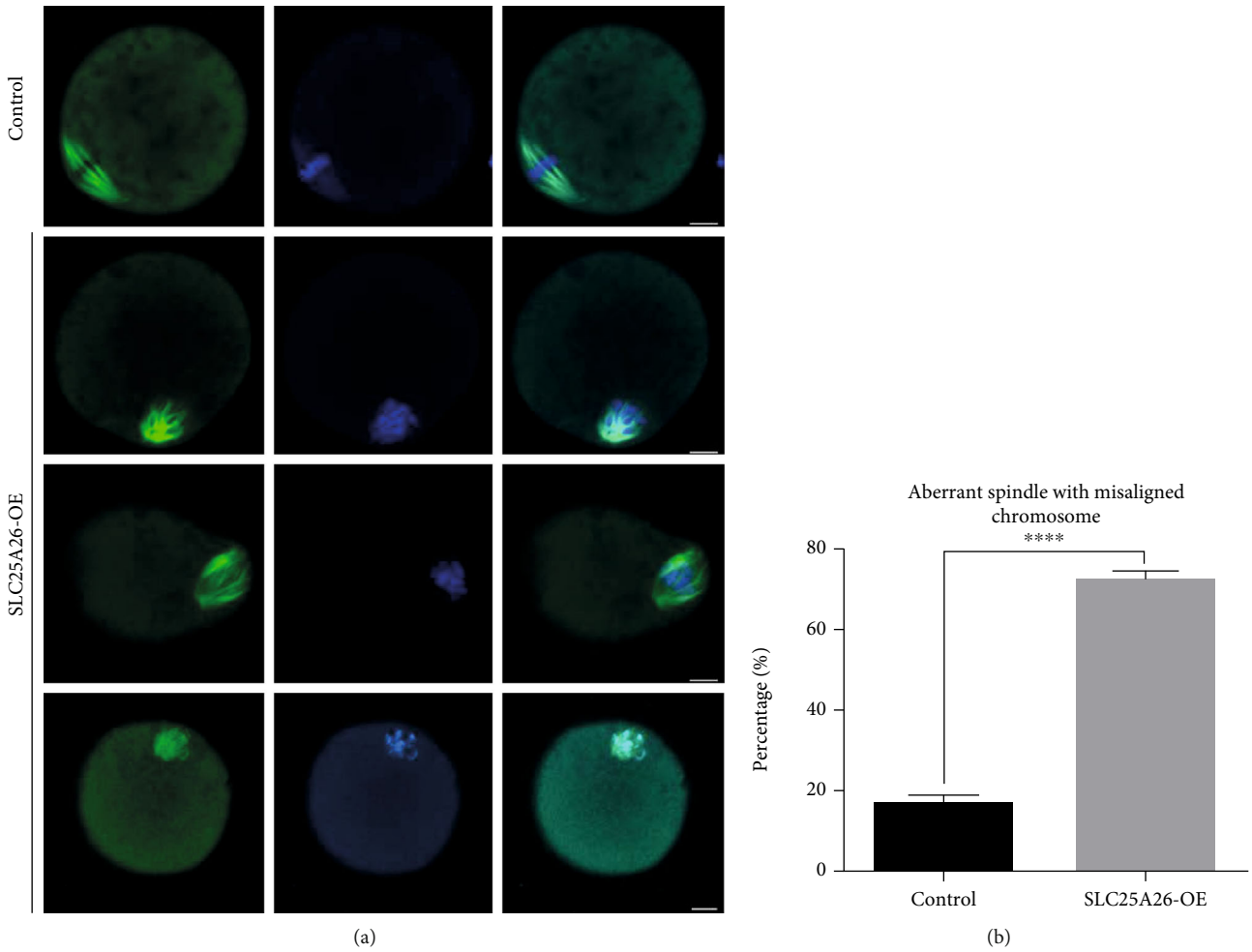

Figure 3: SLC25A26 overexpression induces spindle defects and chromosome misalignment in oocyte meiosis. (a) Control and SLC25A26-OE oocytes were stained with anti-α-tubulin-FITC antibody to visualize the spindle (green) and counterstained with Hoechst 33342 (blue) to observe chromosomes. Scale bar = 50 μm. (b) The rate of control and SLC25A26-OE oocytes with spindle/chromosome defects was recorded. Data are presented as the mean ± SEM. $^{****}p < 0.0001$.

against *Slc25a26* in aged GV oocytes (Fig. S2A). qRT-PCR was performed to validate decreased of *Slc25a26* transcript (Fig. S2B). However, we observed that there was no significant difference of GVBD rate and Pb1 extrusion rate between the aged oocytes and aged oocytes with *Slc25a26* knockdown (Fig. S2A, C). There are other misregulated factors that contribute to the decline of quality of aged oocytes, and knockdown of SLC25A26 is not enough to efficiently rescue maturation rate of aged oocytes.

3.3. Increased SLC25A26 Protein Level Damaged Spindle Organization and Chromosome Alignment in Mouse Oocytes. One of the important indicators of high-quality oocytes is normal spindle morphology with aligned chromosomes which is associated with efficient oocyte meiosis [19]. Impaired oocyte maturation indicated that SLC25A26 overexpression affected meiotic apparatus in oocytes. Therefore, we stained the oocytes with anti-α-tubulin-FITC antibody to visualize the spindle morphologies and costained with Hoechst 33342 to detect chromosome alignment. The immunofluorescence results showed that control metaphase-stage oocytes displayed a typical barrel-shaped spindle with well-organized chromosomes at the equator plate (Figure 3(a)). By contrast, a high percentage of disorganized spindle morphologies and misaligned chromosomes was observed in SLC25A26-overexpressed oocytes (Figures 3(a) and 3(b); $p < 0.0001$). We observed irregular shaped spindles, some with one spindle pole and clumped chromosomes in oocytes with elevated SLC25A26 level. Therefore, SLC25A26 accumulation impaired spindle formation and chromosome arrangement in mouse oocytes.

3.4. Elevated SLC25A26 Level Caused Mitochondrial Dysfunction in Mouse Oocytes. Due to SLC25A26's function in mitochondria, we then checked whether mitochondrial functions were affected upon *Slc25a26* overexpression. Because mitochondrial morphology and dynamics are tightly related to mitochondrial function, we labeled oocyte mitochondria with Mito-Tracker to visualize their distribution patterns. Normally, the majority of immature oocytes

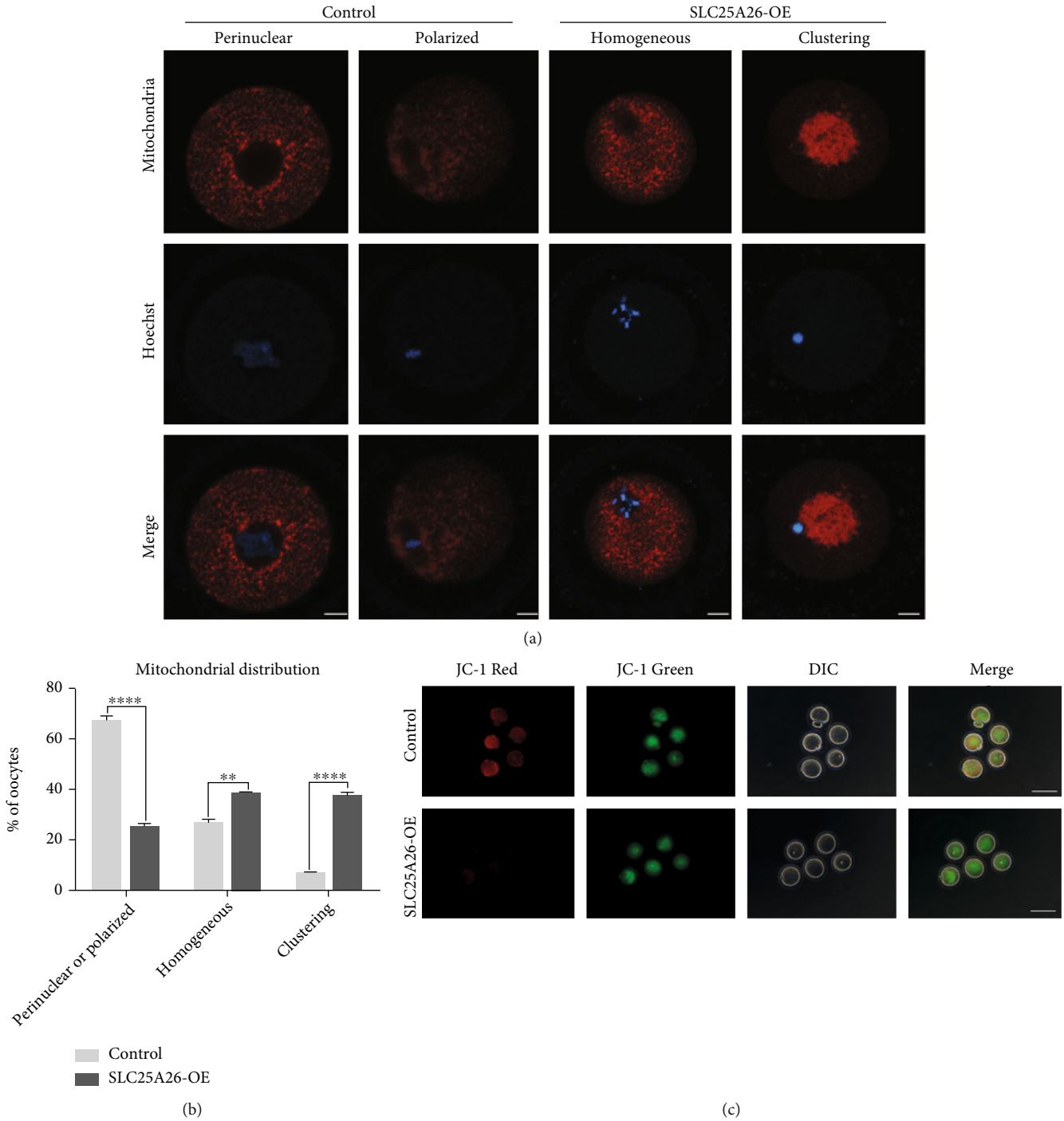

Figure 4: Continued.

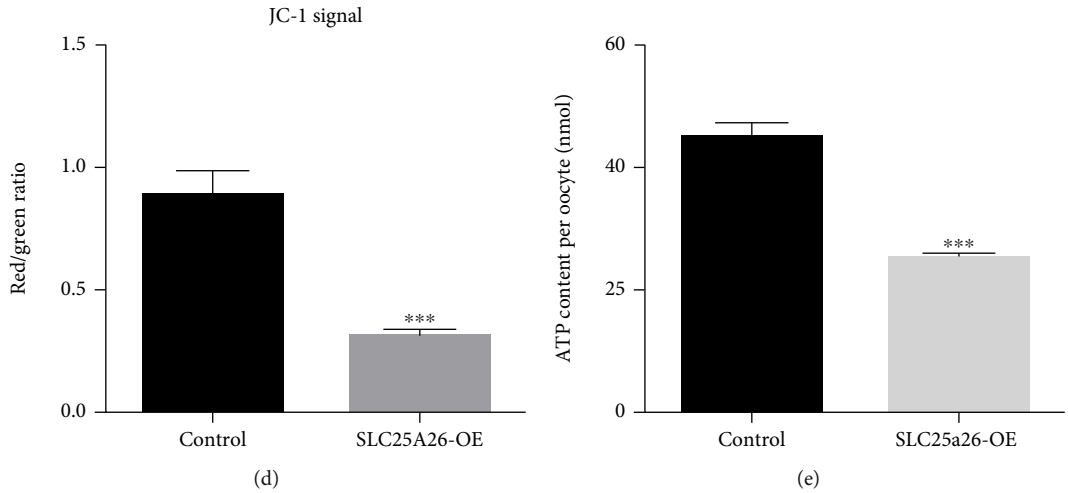

Figure 4: SLC25A26 overexpression disrupts mitochondrial redistribution, membrane potential, and ATP content in oocyte. (a) Representative images of mitochondrial distribution in control and SLC25A26-OE oocytes. Oocytes were stained with Mito-Tracker Red to show mitochondria. Scale bar = 10 μm. (b) Each mitochondrial distribution pattern rate was recorded in in control and SLC25A26-OE oocytes. $^{**}p < 0.01$ and $^{****}p < 0.0001$. (c) Mitochondrial membrane potential ($\Delta\Psi$m) was detected by JC-1 staining in control and SLC25A26-OE oocytes (red, high $\Delta\Psi$m; green, low $\Delta\Psi$m). Scale bar = 100 μm. (d) The ratio of red to green fluorescence intensity was calculated in control and SLC25A26-OE oocytes. (e) ATP levels were measured in control and SLC25A26-OE oocytes. Data are presented as the mean ± SEM. $^{***}p < 0.001$.

presented perinuclear distribution pattern with accumulation of mitochondria around nucleus, and MII oocytes displayed a polarized distribution pattern with mitochondria enriched around the spindle [20]. We found that the proportion of clustering and homogeneous mitochondria in oocytes were significantly increased when SLC25A26 was overexpressed (Figures 4(a) and 4(b); $p < 0.0001$ and $p < 0.01$), whereas the proportion of perinuclear/polarized distribution pattern was declined accordingly (Figures 4(a) and 4(b); $p < 0.0001$). We also detected mtDNA copy number in SLC25A26-overexpressed and control oocytes. However, there was no significant difference between the two groups (Fig. S3). The key function of the mitochondria is to produce ATP. Therefore, the ATP level is an ingenious indicator of mitochondrial function. We then measured the ATP content in oocytes and identified significantly reduced ATP content of SLC25A26-overexpressed oocytes compared with control oocytes (Figure 4(e); $p < 0.001$). Additionally, mitochondrial membrane potential ($\Delta\Psi m$) is critical to ATP production by ATP synthase and a measure of mitochondria viability [21]. We then assessed mitochondrial membrane potential by JC-1 staining. Mitochondria with high membrane potential presented red fluorescence and low membrane potential exhibited green fluorescence. For quantitative analysis, the ratios of red/green fluorescence intensity were calculated to present $\Delta\psi m$. Notably, the red/green ratio was significantly decreased in SLC25A26-overexpressed oocytes as compared to those of control (Figures 4(c) and 4(d); $p < 0.001$). These results showed that SLC25A26 accumulation in oocytes had a general disturbance of mitochondrial functions.

3.5. Accumulation of SLC25A26 Induced Oxidative Stress and Apoptosis in Mouse Oocytes. Mitochondria are the main producer and target of reactive oxygen species (ROS) [22, 23]. When mitochondria are injured in oocyte, oxidative stress response may be activated and promote apoptosis. Therefore, we detected ROS levels using DCFH-DA fluorescent dye staining and apoptosis by Annexin-V staining both in control and SLC25A26-overexpressed oocytes. As shown in Figures 5(a) and 5(b), the fluorescence intensity of ROS in SLC25A26-overexpressed oocytes was significantly increased compared to control ($p < 0.01$). As anticipated, Annexin-V staining showed no fluorescence signal in control oocytes. However, positive fluorescence signals were detected in SLC25A26-overexpressed oocytes (Figures 5(c) and 5(d); $p < 0.0001$), indicating the occurrence of early apoptosis. Our results showed that enhanced SLC25A26 activity induced oxidative stress and early apoptosis in mouse oocytes.

3.6. Effects of SLC25A26 Overexpression on Mouse Oocyte Transcriptome. To further explore the mechanisms for declined ability of oocyte maturation caused by SLC25A26, we performed ultra low-input RNA-seq analysis to characterize change of transcriptome of SLC25A26-overexpressed oocytes. Principal component analysis (PCA) showed variation of transcriptome between control and SLC25A26-overexpressed GV oocytes (Fig. S4). Notably, only a few genes had changed expression upon SLC25A26 overexpression, with 6 genes upregulated and 7 genes downregulated (Figures 6(a) and 6(b)). *Slc25a26* is one of the 6 upregulated genes, which is consistent with the overexpression purpose of our experiment. *C1qc*, *Ccl4*, *Ctss*, *Tmsb4x*, and *Scimp* were other 5 upregulated genes and *Pramel38*, *mt-Cytb*, *E330014E10Rik*, *Pomc*, *Prl*, *Nnat*, and *Gh* were 7 downregulated genes. Table 1 annotates the 12 genes with changed expression. Four upregulated genes (*C1qc*, *Ccl4*, *Ctss*, and

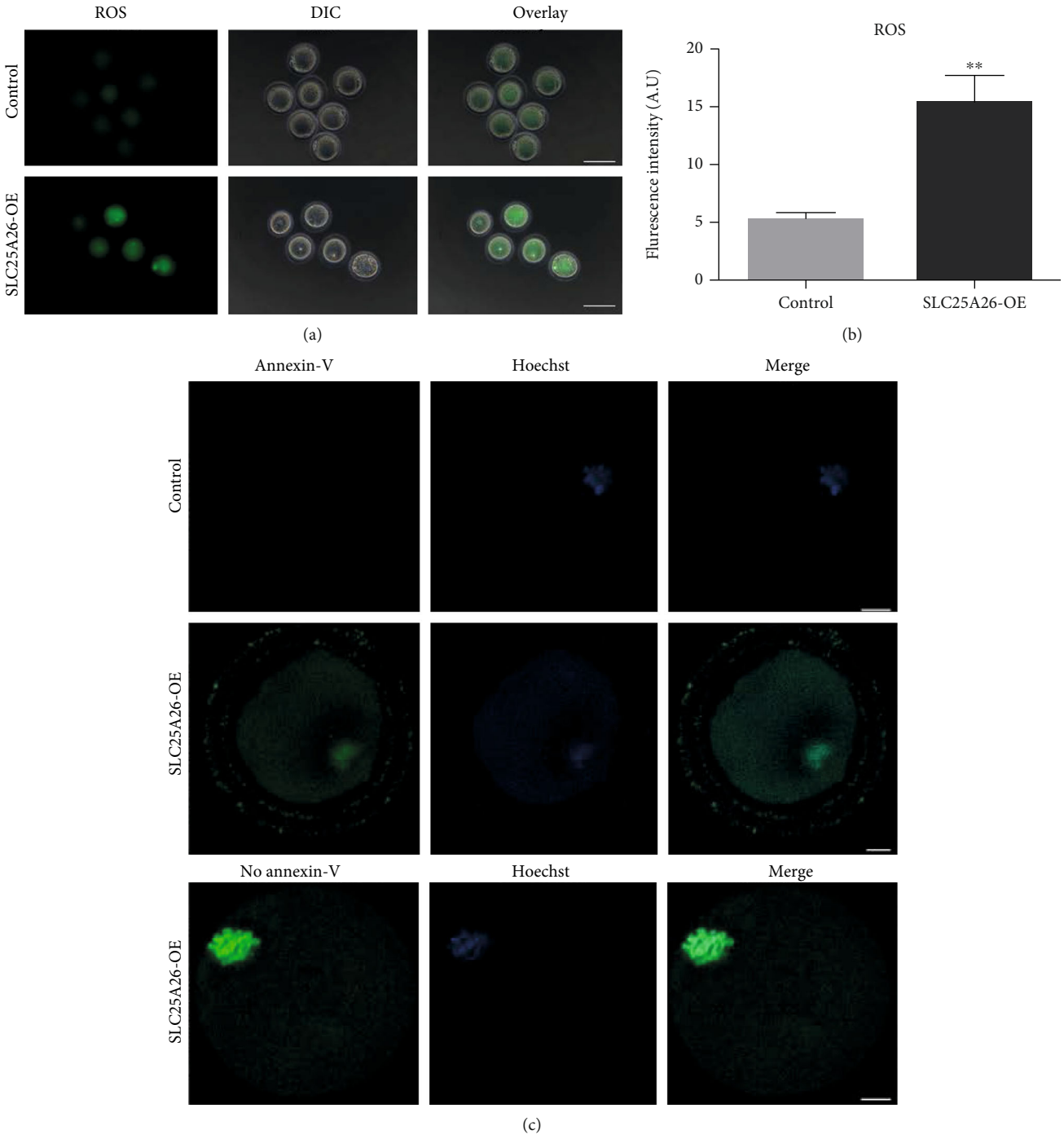

Figure 5: Continued.

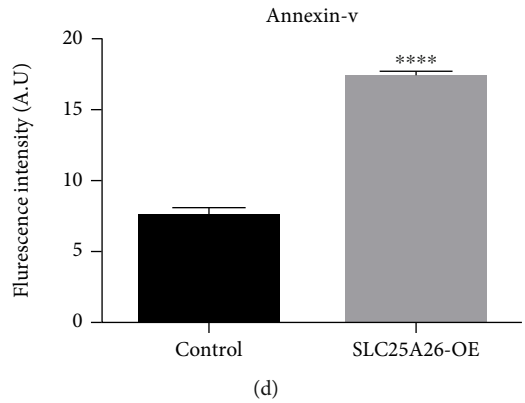

Figure 5: Effect of SLC25A26 overexpression on ROS accumulation and apoptosis in oocytes. (a) Representative images of ROS levels detected by DCFH staining in control and SLC25A26-OE oocytes. Scale bar = 100 μm. (b) The fluorescence intensity of ROS signals was measured in control and SLC25A26-OE oocytes. (c) Representative images of apoptotic status, assessed by Annexin-V staining, in control and SLC25A26-OE oocytes. Scale bar = 10 μm. (d) The fluorescence intensity of Annexin-V signals was measured in control and SLC25A26-OE oocytes. A.U. means arbitrary units. Data in (b) and (d) are presented as mean ± SEM. $^{**}p < 0.01$ and $^{****}p < 0.0001$.

Scimp) are related to immunity, and *Tmsb4x* function is associated with binding to and sequestering actin monomers (G actin) to inhibit actin polymerization. Among 7 downregulated genes, 3 genes (*Pomc*, *Prl*, and *Gh*) belong to hormones and 2 genes (*Pramel38* and *E330014E10Rik*) are associated with apoptotic process, cell differentiation, and transcription. Interestingly, *mt-Cytb* is a component of the ubiquinol-cytochrome c reductase complex (complex III or cytochrome b-c1 complex) that is a part of the mitochondrial respiratory chain. In addition, qRT-PCR was performed to validate decreased expression of *mt-Cytb* (Figure 6(c)).

Collectively, RNA-seq result indicated that SLC25A26 overexpression altered transcriptome of oocytes which may reflect impaired oocyte quality. We also analyzed the level of TEs and observed no obvious changes upon SLC25A26 overexpression (Fig. S5).

3.7. Aberrant Expression of SLC25A26 Disturbed Early Mouse Development. To evaluate the impact of SLC25A26 accumulation in preimplantation development, we overexpressed SLC25A26 in mouse zygotes by microinjecting *Slc25a26* cRNA. And H2b-egfp cRNA was coinjected to confirm success of microinjection (Fig. S6). Following microinjection, the expression of exogenous SLC25A26 protein was verified by immunostaining examination of SLC25A26 in 2-cell embryos (Figure 7(a)). The rate of blastocyst formation was evaluated at E4.5. Compared with the control group, the blastocyst formation rate of the SLC25A26 overexpression group was slightly decreased (Figure 7(b); $p < 0.05$). This result revealed that SLC25A26 accumulation had minor effect on preimplantation development.

To further identify developmental roles of *Slc25a26*, we examined phenotype of *Slc25a26* knockout mice. In the knockout mouse model, exon 2 of *Slc25a26* was deleted with Clustered Regularly Interspaced Short Palindromic Repeats/CRISPR-associated protein 9 (CRISPR/Cas9) technology (Fig. S7). Genotyping PCR products are shown in Figure 7(c) and strategy of genotyping is shown in Fig. S8. To obtain homozygous knockout mice, we mated heterozygous male mice with heterozygous female mice and noticed that although most obtained early embryos could develop to blastocyst stage, no homozygous pups were obtained, indicating developmental arrest at postimplantation stage. Therefore, we isolated embryos at 7.5, 8.0, 8.5, 9.5, and 10.5 dpc for phenotype examination. No obvious morphological changes could be seen in heterozygous embryos as compared to the wild type (Figures 6(d) and 6(e)), and *Slc25a26* knockout embryos (*Slc25a26*-/-) were also identified in 7.5, 8.0, 8.5, and 9.5 dpc embryos (Figure 7(d)). Notably, the 7.5 dpc embryos were seen as morphologically comparable to heterozygous or wild-type embryos. However, 8.0, 8.5, and 9.5 dpc embryos of *Slc25a26*-/- embryos had obvious developmental arrest compared with the wild-type control embryos. We also observed resorbed embryos in 10.5 dpc embryos (Figure 7(e)) where the genotype could not be precisely identified since the mother's decidual tissue could not be separated from the resorptions. No *Slc25a26*-/- embryos were found at these or further stages. The above results clearly indicated that *Slc25a26* deficiency sabotaged early mouse development.

4. Discussion

Mitochondrion is the major place for aerobic respiration which is the primary source of ATP through oxidative phosphorylation (OXPHOS). Beyond the production of ATP via OXPHOS, mitochondria participate in numerous cellular functions, involved in stress responses, apoptosis, and chromosome segregation [9]. Disturbances and deficiencies of mitochondrial function not only reduce quality of oocyte/embryo but also contribute to postimplantation failure, long-term cell dysfunction, and adult disease [9, 24]. According to mRNA and protein level of *Slc25a26* in our study, it seems that SLC25A26 is dispensable for development of oocytes and early stage of embryos. Interestingly, we found that SLC25A26 level was increased in oocytes from naturally aged mice which implied that enhanced expression

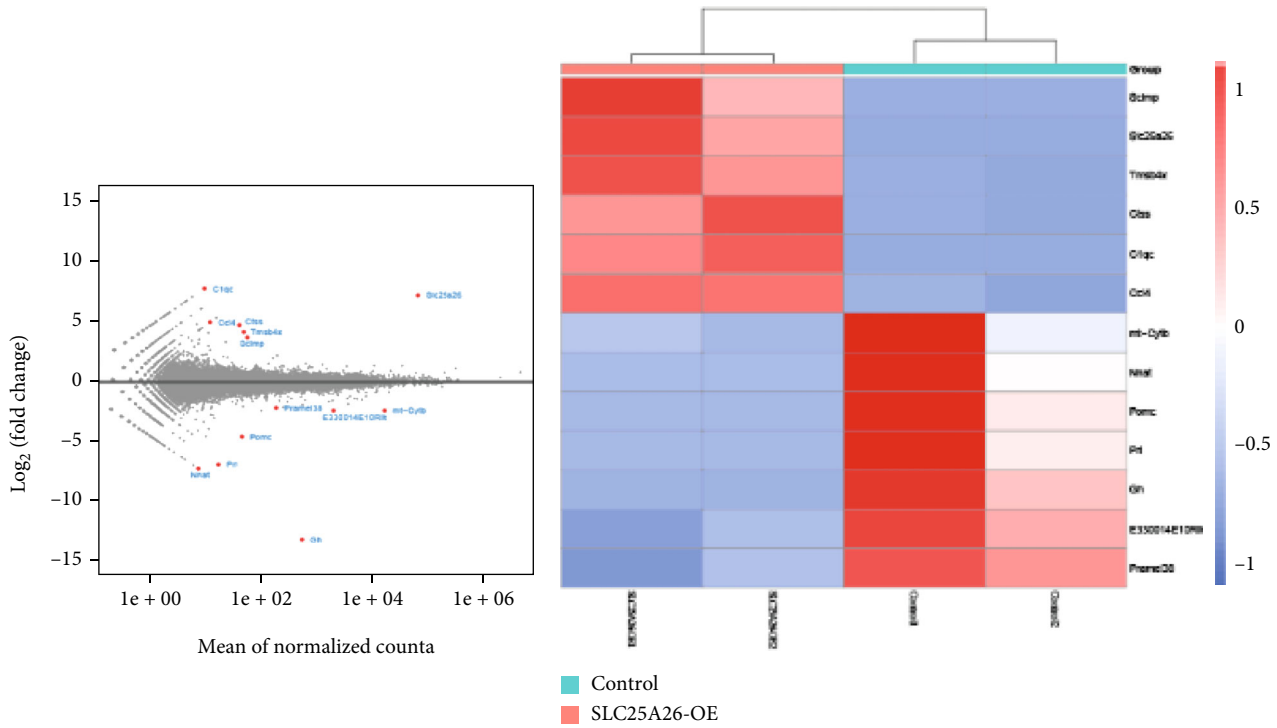

(a) (b)

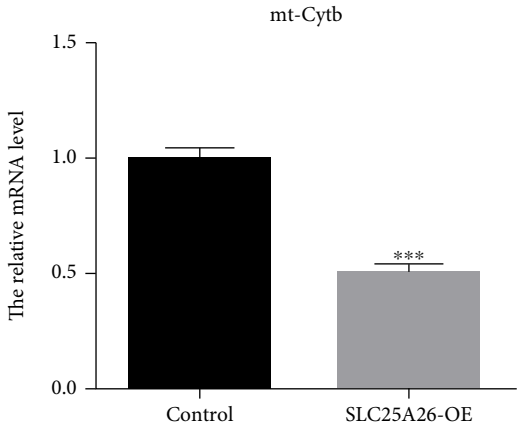

(c)

Figure 6: Continued.

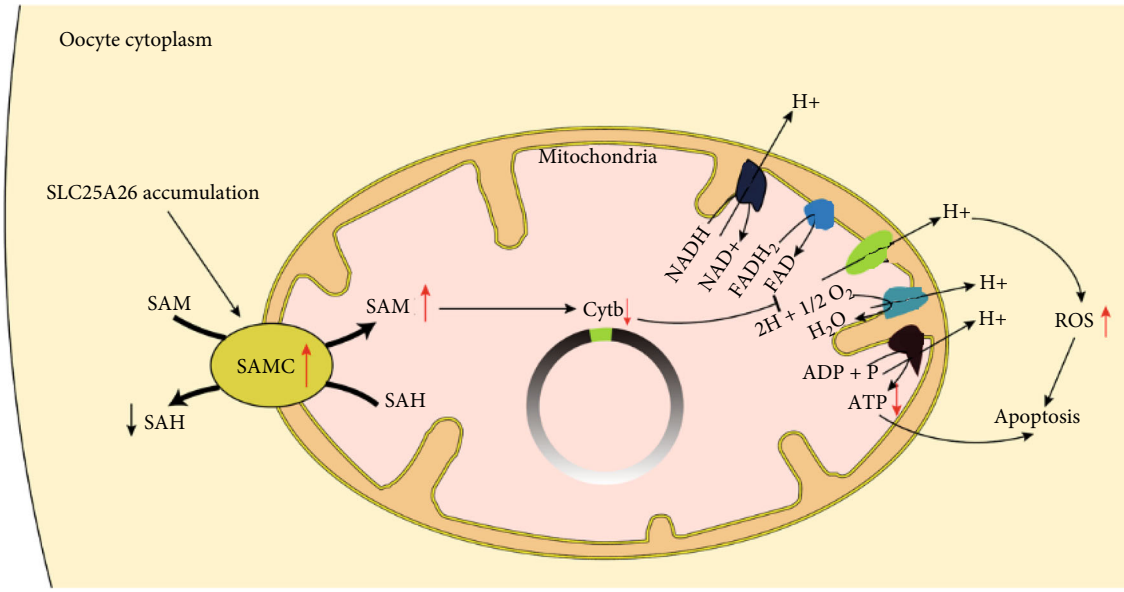

(d)

Figure 6: Transcriptome comparison between control and SLC25A26 overexpression oocytes. (a) An MA plot showing the RNA expression level. The changed genes were designated by red (up- or downregulated) in SLC25A26-OE relative to control oocytes. (b) Heatmap illustration displaying the 13 changed genes after SLC25A26-OE oocytes. (c) The relative mRNA level of *mt-Cytb* were examined in control and SLC25A26-OE oocytes by qRT-PCR. $^{***}p < 0.001$. Data are presented as the mean ± SEM. (d) Schematic pathways related to SLC25A26 overexpression. SLC25A26 (SAMC) overexpression leads to an increase of SAM level, which affects the synthesis of mt-Cytb (complexes III) of the respiratory chain and leads to insufficient synthesis of ATP. Downregulated mt-Cytb also caused elevated ROS.

Table 1: Misregulated genes upon SLC25A26 overexpression in mouse oocytes.

Gene symbols	Chr	Description and function (source: UniProt)
C1qc	4	Complement C1q subcomponent subunit C. Complement activation, classical pathway source, and innate immune response [51].
Ccl4	11	Chemokine (C-C motif) ligand 4. Cytokine, chemotaxis, and inflammatory response [52].
Ctss	3	Cathepsin S. Antigen processing and presentation of exogenous peptide antigen via MHC class II Source [53].
Tmsb4x	X	Thymosin beta-4. Binds to and sequesters actin monomers (G actin) and therefore inhibits actin polymerization [54].
Scimp	11	SLP adaptor and CSK interacting membrane protein. Lipid tetraspanin-associated transmembrane adapter/mediator that acts as a scaffold for Src family kinases and other signaling proteins in immune cells [55].
Pramel38	5	PRAME-like 38. Negative regulation of apoptotic process, cell differentiation and transcription, and DNA-templated. Positive regulation of cell population proliferation. Source: InterPro.
Mt-Cytb	MT	Mitochondrially encoded cytochrome b. Component of the ubiquinol-cytochrome c reductase complex (complex III or cytochrome b-c1 complex) that is part of the mitochondrial respiratory chain [56].
E330014E10Rik	5	RIKEN cDNA E330014E10 gene. Negative regulation of apoptotic process, cell differentiation and transcription, and DNA-templated. Positive regulation of cell population proliferation. Source: InterPro.
Pomc	12	Proopiomelanocortin. A polypeptide hormone precursor yielding several biologically active peptides involved in different cellular functions.
Prl	13	Prolactin acts primarily on the mammary gland by promoting lactation.
Nnat	2	Neuronatin participates in brain development.
Gh	11	Growth hormone is involved in growth control.

of SLC25A26 might impact oocyte quality. Indeed, our examination showed that SLC25A26-overexpressed oocytes exhibited lower GVBD and maturation rate. As expected, SLC25A26 overexpression in oocytes led to aberrant mitochondrial distribution, reduced $\Delta\psi m$ and ATP content, and increased production of ROS. All of these mitochondrial abnormalities can impair oocyte quality. For example, the difference in mitochondrial localization has been associated with developmental competence of oocytes [25]. Moreover, mitochondrial dysfunction has been associated with overproduction of ROS which leads to oxidative stress and reduced ATP [26–28].

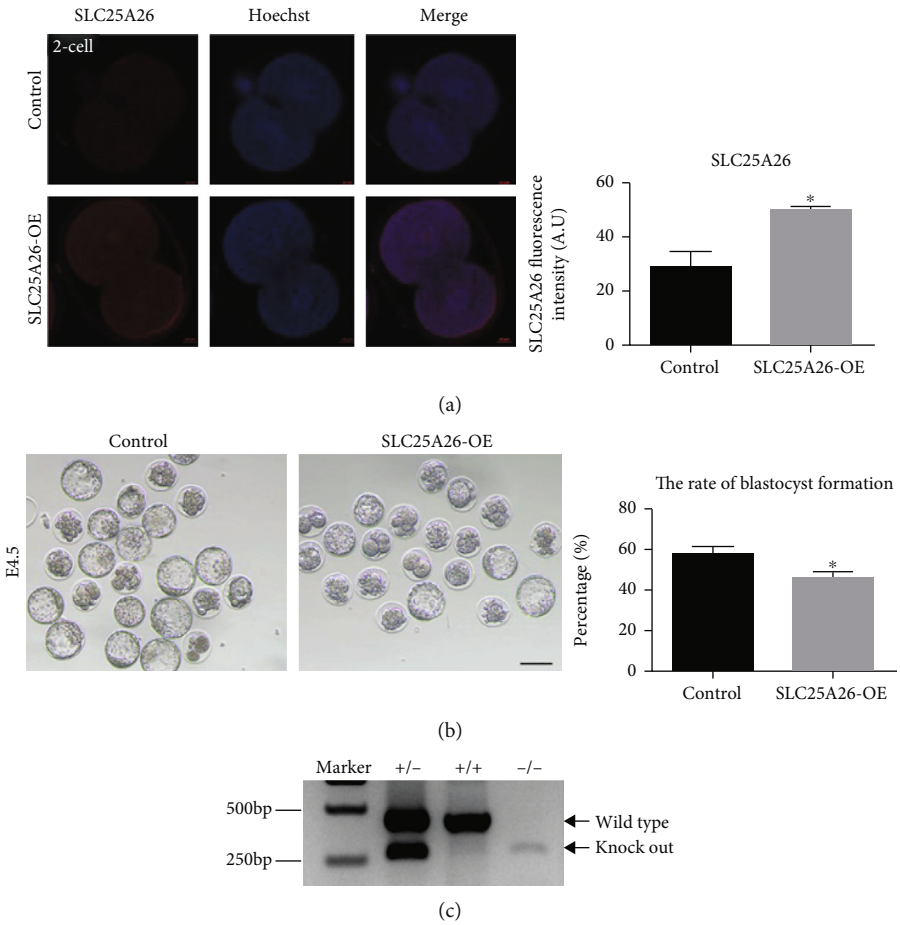

Figure 7: Continued.

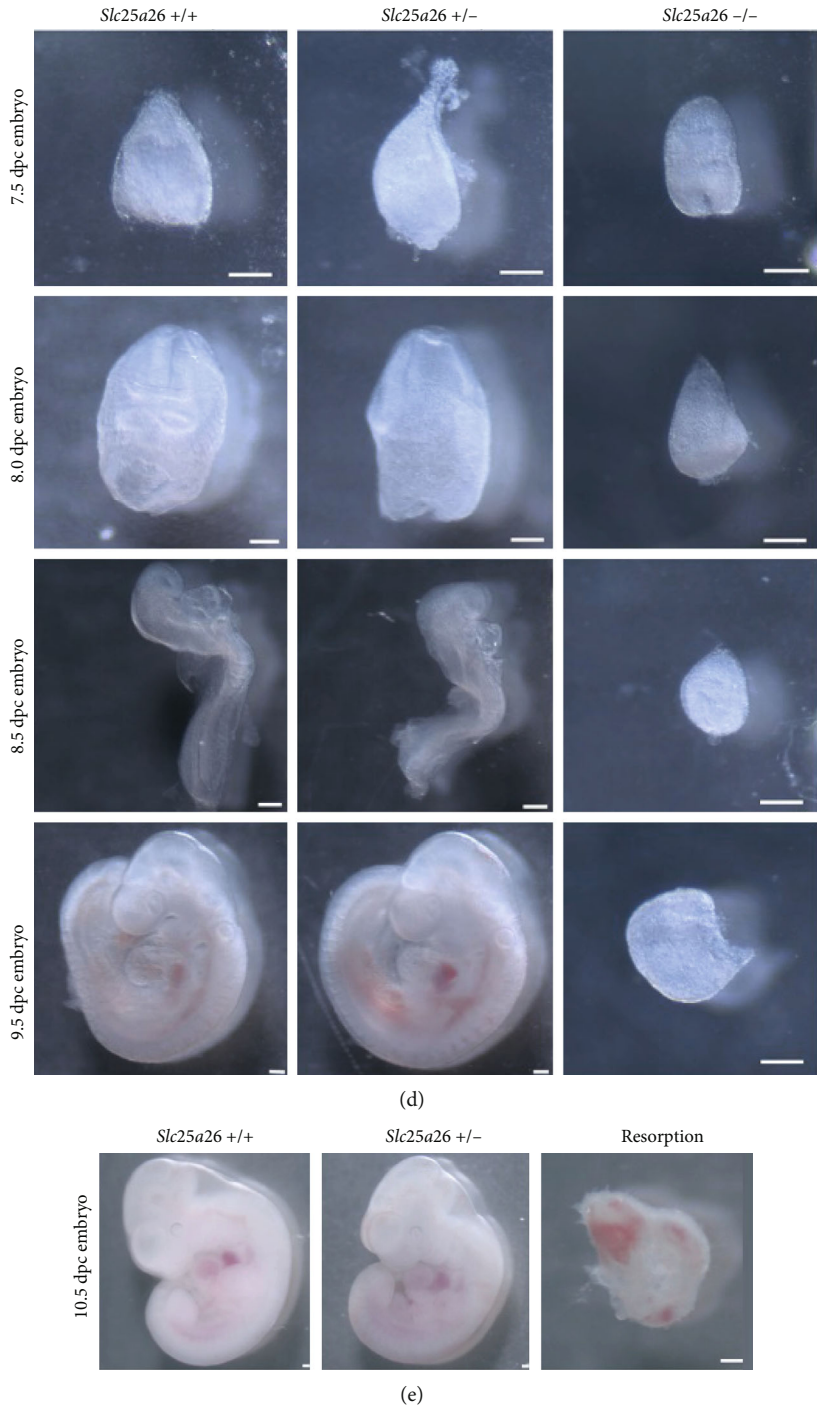

Figure 7: Effects of SLC25A26 overexpression on preimplantation embryos and SLC25A26 knockout on postimplantation embryo development. (a) Representative images of SLC25A26 protein staining in control and SLC25A26-OE 2-cell embryos. Scale bar = 10 μm. The fluorescence intensity of SLC25A26 signals was measured in control and SLC25A26-OE 2-cell embryos with ImageJ. A.U. means arbitrary units. Data are presented as the mean ± SEM. $^{*}p < 0.05$. (b) Representative image of E4.5 control and SLC25A26-OE embryos. Scale bar = 100 μm. And the blastocyst formation rate was recorded in control and SLC25A26-OE embryo after fertilization. Data are presented as the mean ± SEM. $^{*}p < 0.05$. (c) Representative image of genotyping PCR products visualized on agarose gel. The bands indicated by arrow were amplified from wild-type and knockout allele, respectively. (d) Representative image of embryos at 7.5, 8.0, 8.5, and 9.5 dpc obtained by crossing *Slc25a26* heterozygous mice. Wild-type (+/+), heterozygous (+/−), and knockout embryos are shown. Scale bar = 100 μm. (e) Representative image of embryos at 10.5 dpc. Wild-type (+/+), heterozygous (+/−), and resorption embryos are shown. Scale bar = 100 μm.

SLC25A26 is a member of mitochondrial carrier family, and its main function is to catalyze the import of SAM into mitochondria in exchange for intramitochondrial S-adenosine homocysteine (SAH) [16, 29, 30]. SAH was produced from SAM in the methylation reactions and only hydrolyzed in the cytoplasm [16, 29, 30]. The overexpression of SLC25A26 upregulated SAM entry into mitochondria forcing methionine to be converted to SAM. Thus, homocysteine was accumulated and GSH was depleted [15]. GSH is a detoxifying antioxidant that protects the cells from ROS as well as free radicals [31]; homocysteine is a toxic metabolite to tissues in high concentrations associated with abnormal gene expression and induced cell cycle arrest and cell apoptosis [15, 32–34]. Hyperhomocysteinemia (HHcy) impairs oocyte/embryo quality via deregulation of one-carbon metabolism and hypermethylation of mitochondrial DNA [35, 36]. The overexpression of SLC25A26 may be similar to SAMC overexpression in CaSki cells inducing abnormal homocysteine and GSH level which triggered ROS production and apoptosis [15].

Furthermore, through ultra low-input RNA-seq analysis, we observed a marked reduction of mtDNA-encoded cytochrome b, *mt-Cytb*, in SLC25A26-overexpressed oocytes. *mt-Cytb* is the only mtDNA-encoded subunit of the ubiquinol-cytochrome c reductase complex (complex III or cytochrome b-c1 complex) that is part of the mitochondrial respiratory chain [37, 38]. Mitochondrial respiratory chain (also called mitochondrial electron transport chain (ETC)), composed of four multiprotein complexes named complex I–IV, is a series of electronic carriers embedded in the mitochondrial inner membrane to form proton gradient used for the generation of ATP [38, 39]. Besides its involvement in ATP synthesis, the mitochondrial ETC promotes ROS production [40]. ETC I and III complexes are the major sources of ROS [41]. Many studies demonstrated that downregulated *mt-Cytb* caused elevated ROS and decreased ATP production [37, 38, 42, 43]. Oocyte meiotic maturation is an active energy demanding process, and decreased ATP content in oocytes were frequently found to be related to defective spindle assembly and chromosome alignment [44, 45]. Thus, impaired oocyte quality upon SLC25A26 overexpression may be due to disturbed DNA methylation in mitochondrial genome for decreased expression of *mt-Cytb*. Moreover, we observed altered expression of a few nuclear genes upon SLC25A26 overexpression, and this may be caused by indirectly impacted degradation activity of transcripts in oocytes, possibly through interrupted mitochondrial activity.

Additionally, we found that *Slc25a26* knockout mice displayed embryonic lethality at 10.5dpc, indicating an essential role of SLC25A26 for early embryo development. Accumulated evidence also showed that SLC25A26 plays an important role in human development. Clinical findings reported that SLC25A26 mutations were associated with a complex autosomal recessive multisystem disease COXPD28. Patients with SLC25A26 mutations ranged from neonatal mortality resulting from respiratory insufficiency and hydrops to childhood acute episodes of cardiopulmonary failure and slowly progressive muscle weakness [18, 46]. These articles elucidated that SLC25A26 mutations caused various mitochondrial defects, including those affecting RNA stability, protein modification, mitochondrial translation, and the biosynthesis of CoQ10 and lipoic acid [18, 46]. Knockout of *Slc25a26* in mice caused embryo-lethal phenotype which may be due to failure of the mitochondrial biogenesis during embryogenesis. The critical cellular roles of mitochondria are underscored by the observation that loss of mitochondrial fusion/fission results in embryonic lethality in mice [9, 47]. Mice deficient in either *Mfn1* or *Mfn2* interrelated mitochondrial fusion die around 11.5 dpc [48]. Another mitochondrial fusion-related factor *Opa1* knockout in mice caused embryonic lethality at 13.5dpc [49]. Knockout of dynamin-related protein 1 (*Drp1*) partly mediated mitochondrial fission leading to embryonic lethality at 11.5 dpc [50].

Above all, abnormal expression of SLC25A26 in oocytes and embryos can cause changes of SAM content in mitochondria, resulting in changed gene or protein methylation levels which could affect the expression of mitochondrial function gene like *mt-Cytb* and disturb mitochondria function, leading to reduced $\Delta\psi$m, ATP content, and increased production of ROS, thereby affecting oocyte quality and embryonic development. However, oocyte maturation is inseparable from the periovicular environment *in vivo*. It is worth exploring whether abnormal expression of *Slc25a26* in oocyte has crosstalk with granulosa cell *in vivo*, and whether there is abnormal expression of *Slc25a26* in granulosa cells of aged female because impaired cellular functions in granulosa cells can also impact quality of oocyte and early embryo.

5. Conclusion

In summary, accumulation of SLC25A26 in mouse oocytes damaged oocyte quality through impairing mitochondrial function and mitochondrial respiratory chain. And deficiency of SLC25A26 in mice resulted in embryonic lethality at 10.5 dpc. Therefore, proper level of SLC25A26 in oocyte/embryo is essential for normal oocyte maturation and early embryo development.

Abbreviations

GV: Germinal vesicle
GVBD: Germinal vesicle breakdown
SAMC: S-adenosylmethionine carrier
SAM: S-adenosylmethionine
ROS: Reactive oxygen species
OXPHOS: Oxidative phosphorylation
SAH: S-adenosine homocysteine
HHcy: Hyperhomocysteinemia
ETC: Electron transport chain.

Data Availability

RNA-seq data generated during this study has been deposited to GEO database: PRJNA773040.

Ethical Approval

All animal experiments were approved by the Tongji Medical College Committee on the Use and Care of Animals and were conducted according to the committee's guidelines.

Conflicts of Interest

The authors declare no conflict of interests in this paper.

Authors' Contributions

L-Q Z designed the project. G-P C and S-M G performed the experiments. Y-Y L helped with the experiments. G-P C, Y Y, and X H analyzed the data. G-P C and L-Q Z wrote the manuscript. All authors contributed to the article and approved the final manuscript.

Acknowledgments

We thank Professor Zhi-hua Wang in the Wuhan University for sharing with us the *Slc25a26* knockout mice. This work was supported by the National Natural Science Foundation of China (NSFC) [31771661 and 32170820], National Key R&D Program of China [2018YFC1004502 and 2018YFC1004001], and Program for HUST Academic Frontier Youth Team.

Supplementary Materials

Supplementary Figure 1: Slc25a26 cRNA and H2b-egfp cRNA were successfully microinjected into oocytes. Representative images of EGFP fluorescence signals in oocytes 16 hours after microinjection with Slc25a26 cRNA and H2b-egfp cRNA. Scale bar = 50 μm. Supplementary Figure 2: knockdown of Slc25a26 does not restore maturation rate of the aged oocytes. (A) Representative images of aged oocytes injected with control or siRNA against Slc25a26 (siSlc25a26). Scale bar = 50 μm.(B) Relative mRNA levels of Slc25a26 were detected in control and siSlc25a26 group. (C) Quantitative analysis of GVBD and Pb1 extrusion rate in control and siSlc25a26 group. $^{**}p < 0.01$. Data are presented as the mean ± SEM. Supplementary Figure 3: overexpression of SLC25A26 does not affect mitochondrial DNA copy number. Relative mtDNA copy numbers were detected in control and SLC25A26-OE oocytes. Supplementary Figure 4: PCA analysis of RNA-seq data from control and SLC25A26-OE oocytes at GV stage. Each dot represents one library, color-coded by oocyte group. Supplementary Figure 5: overexpression of SLC25A26 does not affect TE expression level. Comparison of normalized counts of TEs between control and SLC25A26-OE oocytes. Supplementary Figure 6: Slc25a26 cRNA and H2b-egfp cRNA were successfully microinjected into zygotes. Representative images of EGFP fluorescence signal in 4.5 dpc blastocyst microinjected with Slc25a26 cRNA and H2b-egfp cRNA. Scale bar = 50 μm. Supplementary Figure 7: generation of the Slc25a26 KO allele using CRISPR/Cas9. Schematic representation of the mouse Slc25a26 locus with exon 2 deletion. Supplementary Figure 8: strategy of genotyping. Wild type: ② PCR reaction obtains a single WT band (440 bp). Heterozygote: ① PCR reaction obtains a KO band (246 bp) and ② PCR reaction obtains a WT band (440 bp). Homozygote: ① PCR reaction obtains a single KO band (246 bp) and ② PCR reaction without product. *(Supplementary Materials)*

References

[1] L. Li, S. Zhu, W. Shu et al., "Characterization of metabolic patterns in mouse oocytes during meiotic maturation," *Molecular Cell*, vol. 80, no. 3, pp. 525–540.e9, 2020.

[2] Z. Du, H. Zheng, Y. K. Kawamura et al., "Polycomb group proteins regulate chromatin architecture in mouse oocytes and early embryos," *Molecular Cell*, vol. 77, no. 4, pp. 825–839, 2020.

[3] Y. Li, Y. Miao, J. Chen, and B. Xiong, "SIRT6 maintains redox homeostasis to promote porcine oocyte maturation," *Frontiers in Cell and Development Biology*, vol. 9, article 625540, 2021.

[4] X. Li, M. Gao, Y. He, B. Xiong, H. Liu, and L. Gu, "Intersectin-Cdc42 interaction is required for orderly meiosis in porcine oocytes," *Journal of Cellular Physiology*, vol. 234, no. 5, pp. 7492–7497, 2019.

[5] Y. L. Miao, K. Kikuchi, Q. Y. Sun, and H. Schatten, "Oocyte aging: cellular and molecular changes, developmental potential and reversal possibility," *Human Reproduction Update*, vol. 15, no. 5, pp. 573–585, 2009.

[6] J. E. Holt, S. I. Lane, and K. T. Jones, "The control of meiotic maturation in mammalian oocytes," *Current Topics in Developmental Biology*, vol. 102, pp. 207–226, 2013.

[7] X. Wu, F. Hu, J. Zeng et al., "NMNAT2-mediated NAD+ generation is essential for quality control of aged oocytes," *Aging Cell*, vol. 18, no. 3, article e12955, 2019.

[8] D. T. Baird, J. Collins, J. Egozcue et al., "Fertility and ageing," *Human Reproduction Update*, vol. 11, no. 3, pp. 261–276, 2005.

[9] A. J. Harvey, "Mitochondria in early development: linking the microenvironment, metabolism and the epigenome," *Reproduction*, vol. 157, pp. R159–R179, 2019.

[10] W. J. Kaelin and S. L. McKnight, "Influence of metabolism on epigenetics and disease," *Cell*, vol. 153, no. 1, pp. 56–69, 2013.

[11] S. Pauwels, M. Ghosh, R. C. Duca et al., "Dietary and supplemental maternal methyl-group donor intake and cord blood DNA methylation," *Epigenetics*, vol. 12, no. 1, pp. 1–10, 2017.

[12] J. Liu, W. Gao, Y. Pan, and G. Liu, "Metabolic engineering of Acremonium chrysogenum for improving cephalosporin C production independent of methionine stimulation," *Microbial Cell Factories*, vol. 17, no. 1, p. 87, 2018.

[13] D. W. Lin, B. P. Chung, and P. Kaiser, "S-adenosylmethionine limitation induces p38 mitogen-activated protein kinase and triggers cell cycle arrest in G1," *Journal of Cell Science*, vol. 127, no. 1, pp. 50–59, 2014.

[14] V. Iacobazzi, V. Infantino, A. Castegna, and G. Andria, "Hyperhomocysteinemia: related genetic diseases and congenital defects, abnormal DNA methylation and newborn screening issues," *Molecular Genetics and Metabolism*, vol. 113, no. 1-2, pp. 27–33, 2014.

[15] A. Menga, E. M. Palmieri, A. Cianciulli et al., "SLC25A26 overexpression impairs cell function via mtDNA hypermethylation and rewiring of methyl metabolism," *The FEBS Journal*, vol. 284, no. 6, pp. 967–984, 2017.

[16] G. Agrimi, M. A. Di Noia, C. M. Marobbio, G. Fiermonte, F. M. Lasorsa, and F. Palmieri, "Identification of the human mitochondrial S-adenosylmethionine transporter: bacterial expression, reconstitution, functional characterization and tissue distribution," *The Biochemical Journal*, vol. 379, no. 1, pp. 183–190, 2004.

[17] C. Jin, Y. Li, Y. Su et al., "Novel copper complex CTB regulates methionine cycle induced TERT hypomethylation to promote HCC cells senescence via mitochondrial SLC25A26," *Cell Death & Disease*, vol. 11, no. 10, p. 844, 2020.

[18] Y. Kishita, A. Pajak, N. A. Bolar et al., "Intra-mitochondrial methylation deficiency due to mutations in SLC25A26," *American Journal of Human Genetics*, vol. 97, no. 5, pp. 761–768, 2015.

[19] M. Zhang, X. ShiYang, Y. Zhang et al., "Coenzyme Q10 ameliorates the quality of postovulatory aged oocytes by suppressing DNA damage and apoptosis," *Free Radical Biology & Medicine*, vol. 143, pp. 84–94, 2019.

[20] J. Zeng, M. Jiang, X. Wu et al., "SIRT4 is essential for metabolic control and meiotic structure during mouse oocyte maturation," *Aging Cell*, vol. 17, no. 4, article e12789, 2018.

[21] D. B. Bartlett, C. A. Slentz, L. H. Willis et al., "Rejuvenation of neutrophil functions in association with reduced diabetes risk following ten weeks of low-volume high intensity interval walking in older adults with prediabetes - a pilot study," *Frontiers in Immunology*, vol. 11, p. 729, 2020.

[22] M. Dodson, Q. Liang, M. S. Johnson et al., "Inhibition of glycolysis attenuates 4-hydroxynonenal-dependent autophagy and exacerbates apoptosis in differentiated SH-SY5Y neuroblastoma cells," *Autophagy*, vol. 9, no. 12, pp. 1996–2008, 2013.

[23] J. Ramalho-Santos, S. Varum, S. Amaral, P. C. Mota, A. P. Sousa, and A. Amaral, "Mitochondrial functionality in reproduction: from gonads and gametes to embryos and embryonic stem cells," *Human Reproduction Update*, vol. 15, no. 5, pp. 553–572, 2009.

[24] E. Babayev and E. Seli, "Oocyte mitochondrial function and reproduction," *Current Opinion in Obstetrics & Gynecology*, vol. 27, no. 3, pp. 175–181, 2015.

[25] E. M. Ferreira, A. A. Vireque, P. R. Adona, F. V. Meirelles, R. A. Ferriani, and P. A. Navarro, "Cytoplasmic maturation of bovine oocytes: structural and biochemical modifications and acquisition of developmental competence," *Theriogenology*, vol. 71, no. 5, pp. 836–848, 2009.

[26] J. S. Bhatti, G. K. Bhatti, and P. H. Reddy, "Mitochondrial dysfunction and oxidative stress in metabolic disorders - a step towards mitochondria based therapeutic strategies," *Biochimica et Biophysica Acta - Molecular Basis of Disease*, vol. 1863, no. 5, pp. 1066–1077, 2017.

[27] A. V. Kudryavtseva, G. S. Krasnov, A. A. Dmitriev et al., "Mitochondrial dysfunction and oxidative stress in aging and cancer," *Oncotarget*, vol. 7, no. 29, pp. 44879–44905, 2016.

[28] H. Zhang, Z. Pan, J. Ju et al., "DRP1 deficiency induces mitochondrial dysfunction and oxidative stress-mediated apoptosis during porcine oocyte maturation," *Journal of Animal Science and Biotechnology*, vol. 11, no. 1, p. 77, 2020.

[29] C. M. Marobbio, G. Agrimi, F. M. Lasorsa, and F. Palmieri, "Identification and functional reconstitution of yeast mitochondrial carrier for S-adenosylmethionine," *The EMBO Journal*, vol. 22, no. 22, pp. 5975–5982, 2003.

[30] L. Palmieri, R. Arrigoni, E. Blanco et al., "Molecular identification of an Arabidopsis S-adenosylmethionine transporter. Analysis of organ distribution, bacterial expression, reconstitution into liposomes, and functional characterization," *Plant Physiology*, vol. 142, no. 3, pp. 855–865, 2006.

[31] C. X. Yin, K. M. Xiong, F. J. Huo, J. C. Salamanca, and R. M. Strongin, "Fluorescent probes with multiple binding sites for the discrimination of Cys, Hcy, and GSH," *Angewandte Chemie (International Ed. in English)*, vol. 56, no. 43, pp. 13188–13198, 2017.

[32] Y. Long, X. Zhen, F. Zhu et al., "Hyperhomocysteinemia exacerbates cisplatin-induced acute kidney injury," *International Journal of Biological Sciences*, vol. 13, no. 2, pp. 219–231, 2017.

[33] P. A. Outinen, S. K. Sood, S. I. Pfeifer et al., "Homocysteine-induced endoplasmic reticulum stress and growth arrest leads to specific changes in gene expression in human vascular endothelial cells," *Blood*, vol. 94, no. 3, pp. 959–967, 1999.

[34] T. Zou, W. J. Liu, S. D. Li, W. Zhou, J. F. Yang, and C. G. Zou, "TRB3 mediates homocysteine-induced inhibition of endothelial cell proliferation," *Journal of Cellular Physiology*, vol. 226, no. 11, pp. 2782–2789, 2011.

[35] B. Berker, C. Kaya, R. Aytac, and H. Satiroglu, "Homocysteine concentrations in follicular fluid are associated with poor oocyte and embryo qualities in polycystic ovary syndrome patients undergoing assisted reproduction," *Human Reproduction*, vol. 24, no. 9, pp. 2293–2302, 2009.

[36] L. Jia, Y. Zeng, Y. Hu et al., "Homocysteine impairs porcine oocyte quality via deregulation of one-carbon metabolism and hypermethylation of mitochondrial DNA†," *Biology of Reproduction*, vol. 100, no. 4, pp. 907–916, 2019.

[37] H. Li, X. Zhang, F. Wang et al., "MicroRNA-21 lowers blood pressure in spontaneous hypertensive rats by upregulating mitochondrial translation," *Circulation*, vol. 134, no. 10, pp. 734–751, 2016.

[38] Z. Sun, W. Zhang, X. Xue et al., "Fluoride decreased the sperm ATP of mice through inhabiting mitochondrial respiration," *Chemosphere*, vol. 144, pp. 1012–1017, 2016.

[39] A. Pal, A. Pal, S. Banerjee, S. Batabyal, and P. N. Chatterjee, "Mutation in cytochrome B gene causes debility and adverse effects on health of sheep," *Mitochondrion*, vol. 46, pp. 393–404, 2019.

[40] A. Amaral, B. Lourenco, M. Marques, and J. Ramalho-Santos, "Mitochondria functionality and sperm quality," *Reproduction*, vol. 146, no. 5, pp. R163–R174, 2013.

[41] J. P. Mazat, A. Devin, and S. Ransac, "Modelling mitochondrial ROS production by the respiratory chain," *Cellular and Molecular Life Sciences*, vol. 77, no. 3, pp. 455–465, 2020.

[42] R. Singh, B. Purkait, K. Abhishek et al., "Universal minicircle sequence binding protein of Leishmania donovani regulates pathogenicity by controlling expression of cytochrome-b," *Cell & Bioscience*, vol. 6, no. 1, p. 13, 2016.

[43] R. Zhou, R. Wang, Y. Qin et al., "Mitochondria-related miR-151a-5p reduces cellular ATP production by targeting CYTB in asthenozoospermia," *Scientific Reports*, vol. 5, p. 17743, 2016.

[44] H. Li, L. You, Y. Tian et al., "DPAGT1-mediated protein N-glycosylation is indispensable for oocyte and follicle development in mice," *Adv Sci (Weinh).*, vol. 7, no. 14, p. 2000531, 2020.

[45] S. Giacopazzi, D. Vong, A. Devigne, and N. Bhalla, "PCH-2 collaborates with CMT-1 to proofread meiotic homolog interactions," *PLoS Genetics*, vol. 16, no. 7, article e1008904, 2020.

[46] Y. Ji, S. Wang, Y. Cheng et al., "Identification and characterization of novel compound variants in SLC25A26 associated with combined oxidative phosphorylation deficiency 28," *Gene*, vol. 804, article 145891, 2021.

[47] S. Hoppins, F. Edlich, M. M. Cleland et al., "The soluble form of Bax regulates mitochondrial fusion via MFN2 homotypic complexes," *Molecular Cell*, vol. 41, no. 2, pp. 150–160, 2011.

[48] H. Chen, S. A. Detmer, A. J. Ewald, E. E. Griffin, S. E. Fraser, and D. C. Chan, "Mitofusins Mfn1 and Mfn2 coordinately regulate mitochondrial fusion and are essential for embryonic development," *The Journal of Cell Biology*, vol. 160, no. 2, pp. 189–200, 2003.

[49] V. J. Davies, A. J. Hollins, M. J. Piechota et al., "Opa1 deficiency in a mouse model of autosomal dominant optic atrophy impairs mitochondrial morphology, optic nerve structure and visual function," *Human Molecular Genetics*, vol. 16, no. 11, pp. 1307–1318, 2007.

[50] J. Wakabayashi, Z. Zhang, N. Wakabayashi et al., "The dynamin-related GTPase Drp1 is required for embryonic and brain development in mice," *The Journal of Cell Biology*, vol. 186, no. 6, pp. 805–816, 2009.

[51] A. Mangogna, B. Belmonte, C. Agostinis et al., "Prognostic implications of the complement protein C1q in gliomas," *Frontiers in Immunology*, vol. 10, p. 2366, 2019.

[52] N. L. Cheng, X. Chen, J. Kim et al., "MicroRNA-125b modulates inflammatory chemokine CCL4 expression in immune cells and its reduction causes CCL4 increase with age," *Aging Cell*, vol. 14, no. 2, pp. 200–208, 2015.

[53] A. Steimle, K. Gronbach, B. Beifuss et al., "Symbiotic gut commensal bacteria act as host cathepsin S activity regulators," *Journal of Autoimmunity*, vol. 75, pp. 82–95, 2016.

[54] I. Scheller, S. Beck, V. Göb et al., "Thymosin $\beta 4$ is essential for thrombus formation by controlling the G-actin/F-actin equilibrium in platelets," *Haematologica*, 2021.

[55] J. E. Curson, L. Luo, L. Liu et al., "An alternative downstream translation start site in the non-TIR adaptor Scimp enables selective amplification of CpG DNA responses in mouse macrophages," *Immunology and Cell Biology*, vol. 100, no. 4, pp. 267–284, 2022.

[56] M. Hirose, A. Künstner, P. Schilf et al., "A natural mtDNA polymorphism in complex III is a modifier of healthspan in mice," *International Journal of Molecular Sciences*, vol. 20, no. 9, p. 2359, 2019.